MANUFACTURING OF CONTINUOUS FLOW EQUIPMENT.

by

Mr. Martin Strydom

A dissertation submitted in fulfilment of the requirements for the award of the degree of

Master of Science

Chemistry

at Nelson Mandela University

December 2017

Promoter: Prof. Paul Watts

PREFACE

The experimental work for this thesis was carried out between March 2016 and October 2017 in the North Campus Research Laboratory under the supervision of Prof. Paul Watts. The research was funded by the National Research Foundation (NRF).

Martin Strydom

DECLARATION

I **Martin Strydom** hereby declare that this thesis is my own. It is being submitted Master of Chemistry at the Nelson Mandela University, Port Elizabeth and it has not been previously submitted for assessment in any other Institution.

ACKNOWLEDGEMENTS

- Special thanks to Professor Paul Watts for guidance throughout the process and his secretary Carla Venter for administrative assistance.
- Mr Coos Bosma for statistical advice.
- Dr Arno Janse van Vuuren, at the Centre for High Resolution Transmission Electron Microscopy at Nelson Mandela University South Campus, for valuable advice and microscopy services.
- Mr Glen Henning of Edge Engravers for his laser engraving/ablation services.
- Mr Jeremy Cizek senior artisan at the Mechanical Engineering Department for valuable construction advice.
- Thanks to the South African National Research Foundation for the Scarce Skills Masters Bursary which supplemented my living costs during this study.
- Nelson Mandela University's Research Capacity and Development Scholarship for supplemental funding.
- My parants, Kirstin Burger and church for support and wisdom during this study.
- Jesus, my Lord and Saviour, for the ability to complete this work.

EXECUTIVE SUMMARY

For the work of this thesis a proof of concept microreactor and pump have been designed. Open source technology was used where possible to reduce the manufacturing cost. The pump is a pseudo HPLC/Syringe pump hybrid which adopts designs from both pumping systems. It works by charging two volumes of liquid into the primary chamber while the secondary chamber discharges. When the charge of the primary chamber is complete half of the liquid is pumped into the secondary chamber and the other half gets discharged. This has the benefit of sharing a common drive to reduce cost. The pump did function; however, the 3D printed parts did not have sufficient rigidity to offset mechanical stress, thus flexing occurred. The micro-reactor that was developed, was unique to commercial units. It was not chemically or thermally bonded but clamped with a gasket sealing the channels. This provides the advantage of unblocking inert material in the reactor. The reactor disk that was clamped was a super alloy, namely, Hastelloy C276. The reactor was tested against two commonly used reactors, namely, Chemtrix3227 and Little Things Factory (MS+VS). A simple synthesis of ethyl acetate has been used as a model reaction for comparing. The test reactor did not perform as well as the commercial counterparts, however probable causes have been identified for potential future work. Both the pump and the reactor worked as a proof of concept system, however further development is required for commercialisation.

Keywords: *Micro-reactor, continuous-flow-synthesis, microfluidics, open-source-equipment, Arduino, ethyl acetate, esterification, HPLC pump,*

LIST OF ABREVIATIONS

ABS	:	*Acrylonitrile Butadiene Styrene*
ADC	:	*Analog to Digital Convertal*
API	:	*Active Pharmaceutical Ingredient*
ARV	:	*Anti Retroviral*
CAD	:	*Computer Aided Design*
CAM	:	*Computer Aided Machining*
CFD	:	*Computational Fluid Dynamics*
CNC	:	*Computer Numerical Control*
COP's	:	*Cyclic Olefin Co-Polymer*
EDM	:	*Electrical Discharge Machining*
FDM	:	*Fused Deposition Molding*
FIB	:	*Focussed Ion Beam*
HIV	:	*Human Immunodeficiency Virus*
HPLC	:	*High Performance Liquid Chromatography*
LCD	:	*Liquid Crystal Display*
LOAC	:	*Lab-on-a-Chip*
PCB	:	*Printed Circuit Board*
PDMS	:	Polydimethylsiloxane
PEEK	:	*Polyether Ether Ketone*
PID	:	*Preportional Integral Derivative*
PLA	:	*Polylactic acid*
PLC	:	*Programmable Logic Controller.*
PMMA	:	*Poly(methyl methacrylate)*
PTFE	:	*Polytetrafluoroethylene*
SAR	:	*Split-and-Recombine*
SEM	:	*Scanning Electron Microscopy*
SLA	:	*Stereolithography*
SLS	:	*Selective Laser Sintering*

List of figures.

List of tables.

Table of Contents

1. Introduction

1.1 Overview of problem

Since chemistry was conceived, the practical techniques remained the same; Fundamentally transferring chemicals into a container (flask or tank) and wait for the reaction to finish. The sheer simplicity of this method has been carried through to modern synthetic approaches and played a significant role in the advancement of chemistry. However, this way of synthesis, known as batch chemistry, has its limitations when considering kinetics and thermodynamics as well as scale up to manufacturing. Microfluidics and continuous flow synthesis has received much attention recently to overcome these limitations and improve current synthetic reactions. (1) But one of the main limitations of these techniques is that lab infrastructure is typically equipped for batch processes, hence increasing the difficulty of implementation. In addition, microfluidics is often considered as an expensive and impractical technique to use. To truly take advantage of microfluidics and continuous flow synthesis the infrastructure should be adapted from its start to accommodate this technology.

Southern African nations, especially South Africa, is plagued with alarmingly high Human Immunodeficiency Virus (HIV) infection rates as well as other associated diseases such as Tuberculosis and Malaria. South Africa has the highest percentage population of people living with HIV and that are on Antiretrovirals (ARV) treatment. Due to poor pharmaceutical, social and government infrastructure the control of these diseases remains a challenging task. Local pharmaceutical production of these ARV drugs has decreased significantly. From 1995 to 2010, 37 active pharmaceutical ingredients (API) plants have closed, resulting in ~ 6500 job losses along with a significant economic impact. During this same period the imports in the pharmaceutical sector, which is the fifth largest importer in South Africa, increased by R9.8 billion a year. In 2016 alone, the import costs were $1.9 billion. (R25 billion assuming current exchange rates), Thus the trend is clearly to rely more on imports, which has economic and sociological consequences. (2) Another concerning trend is that of increased sales in pharmaceuticals, which is largely due to urbanization and improved healthcare capacity. This creates a higher demand for affordable pharmaceuticals which could worsen the reliance upon imported active pharmaceuticals (API's).

Pharmaceutical packing and formulation takes place within South Africa, with Aspen being the major company. However, active pharmaceutical ingredients (API's) manufacture is limited, thus, as stated, South Africa relies heavily on importing. However, it should be mentioned that some manufacturing does in fact take place, such as at Fine Chemical Cooperation (Cape Town) which is a branch of Aspen, but local manufacturing is not in a position to sustain the demand for API's.

1.2 Advantages of continuous flow and microreactor chemistry

The above mentioned are core problems in the local economy. Although it may be solved by traditional batch chemistry, continuous flow processes combined, offer advantages which are not as easy as with macroscale chemistry. (3) Faster mixing rates are available, which can be attributed to molecular diffusion having a larger contribution in a microscale volume. Quicker mixing rates reduces the rate limiting step for many reactions and therefore increase chemical throughput. Increased surface to volume ratios are also reported, which is beneficial for multiphase reactions. Both liquid-liquid and liquid gas reactions have shown superior performance in microreactors . (4) Due to the smaller nature and increased surface to volume ratio, excellent temperature control can be achieved. Some reactions which would be considered explosive at room temperature in batch, have been shown to be safe in microreactors. One such example is the nitration of Toluene, which has been shown to have higher conversions than batch as well as increased safety. (5) Since the reactor is fluidically sealed it provides for high pressure and elevated temperature conditions. To do this in batch, extremely strong reactor walls are required to cope with the pressures. This dramatically increases the cost. Since the surface area is small in a microreactor the total pressure exerted on the reactor will be minimal. (6) When considering the transition from research and development to scaling up batch chemistry processes often needs modifications to cope with different environments. This significantly increases the development time. Microreactors provide the ability to number up instead of scale up, which essentially provides identical results. Therefore a new synthetic route can be done in a fraction of the time. (7)

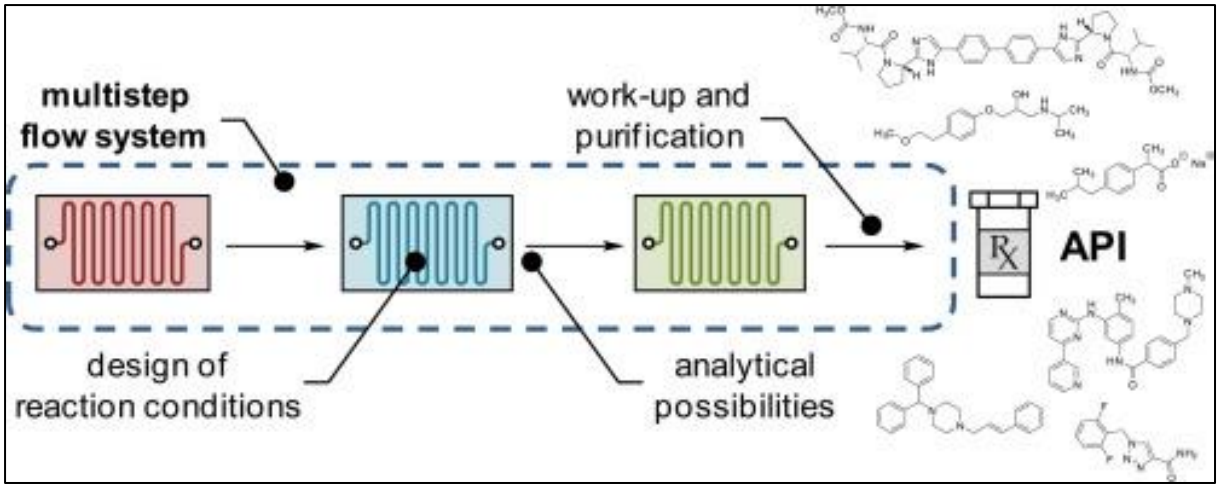

Figure 1:Generalised representation of a multistep microreactor setup.(8)

As shown in Figure 1, one of the key advantages of great commercial value is the ability for multistage syntheses. Usually in batch a workup stage is required which takes extra solvents and auxiliaries, which effectively makes the total synthetic route more expensive. Often continuous flow gives the ability to go directly from one reaction to the next, assuming chemical compatibility is achieved. Most routes employ a hybrid approach. (8)The multistage reactions also have another beneficial consequence, the decrease in waste material will make the continuous flow process greener then batch.

Although continuous flow synthesis and microfluidics have many advantages, its drawbacks are the prohibitive cost due to European manufacturing as well as blocking of the channels. Solving these two issues will make this technology ideal for local use.

The challenges of the South African healthcare sector could be a significant opportunity. Due to the pharmaceutical industry being relatively unchallenged one can take advantage of developing it to take advantage of continues flow- as well as microfluidic synthetic approaches. This will create a flexible infrastructure that can be quickly adapted to suit the supply and demand of the present challenges. This could potentially make South African API synthesis competitive with international competitors. Hence the need for low cost equipment for researchers.

1.1 Requirements for microfluidics and continuous flow chemistry

One of the defining features that separates microfluidics from batch is that the flow takes place in a plug. The plug continuously moves through miniscule channels and tubing, in which the liquid is never stationary. For the plug to move, active pumping is required due to high backpressures from capillary forces. Therefore, the equipment needed is, essentially, an adequate pump, tubing, fittings and the reactor with it's appropriate heating source. Further information about the pumps can be found in section 1.7. Various examples of the reactor's design can be found in section 1.1 and section 2.1

1.3 Properties of microfluidics

Microfluidics involves the manipulation of fluids within the micrometre scale. Differences exist when compared to batch synthesis. Microreactors have a small Reynolds number, which means that the viscous forces play a larger role than the kinematic forces or inertial forces when compared to batch.

$$Re = \frac{\rho u^2 (inertial\ forces)}{\mu \frac{u}{L} (viscous)} \qquad \textit{Equation 1.}$$

Re: Reynolds number

ρ = density (kg/m3)

u = velocity based on the actual cross section area of the duct or pipe (m/s)

μ = dynamic viscosity (Ns/m^2)

L = characteristic length (m)

v = μ / ρ = kinematic viscosity (m^2/s)

Smaller Reynold numbers will tend to have laminar flow while larger Reynold numbers will have turbulent flow. The transitional flow takes place between 2300 and 4000 Re.As the dimensions get smaller the viscous component increases and hence Re decreases. Due to the size of microfluidic devices the viscous forces dominate, which affords a laminar flow. However large pressure drops are also present, which complicates the movement of liquids. The dominance of laminar flow greatly

simplifies the mathematics. However conventional mixing techniques are not as feasible. This is due to mechanical and physical limitations. Channel roughness has shown to increase the Re number. Roughness in channels, in laminar flow, does affect the Re number slightly however the effect is more pronounced with larger Re numbers. A circular channel has lowest wetted surface contact hence the flow will have a lower Re number. Higher surface wettability per volume slightly increases the Re number. (9) However, on a micro-scale the viscous forces dominate.

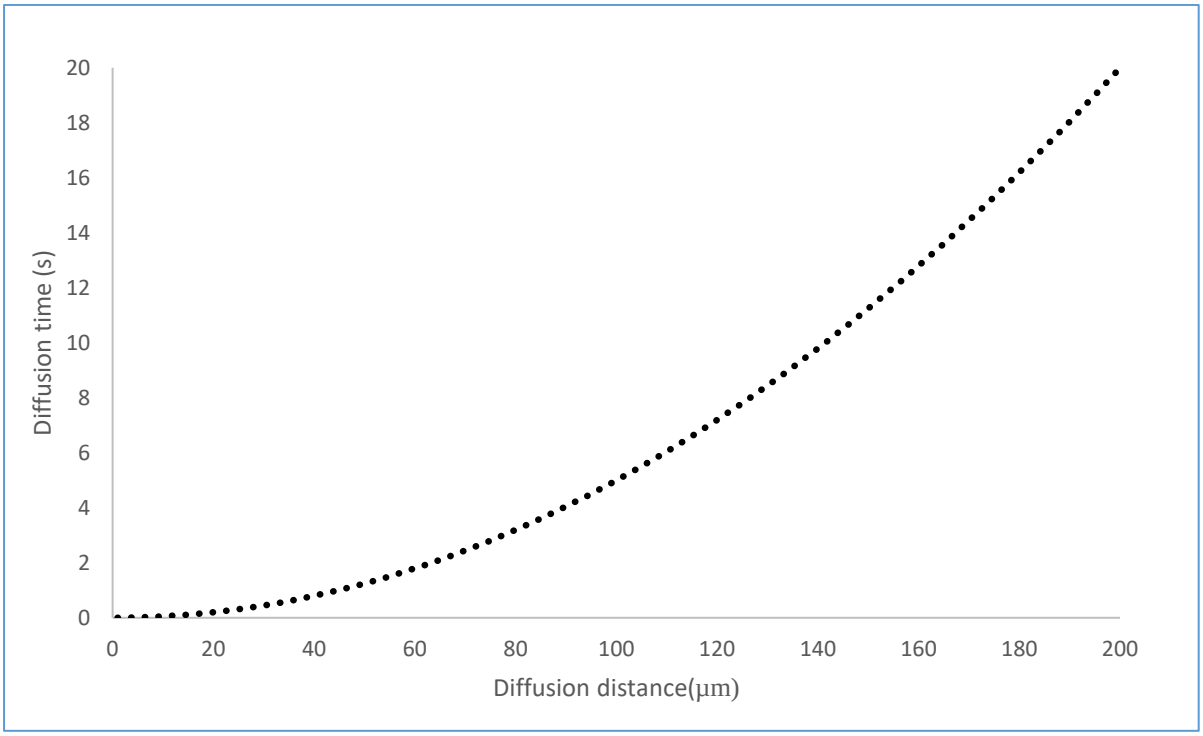

Figure 2: Molecular mixing rates at the microscopic range. (10)

Another identifying feature of microfluidics which resolves the mixing issue is fast molecular diffusion rates. Due to small dimensions, complete molecular diffusion can be accomplished within a realistic time. Complete molecular mixing can be achieved within seconds. Unmixed reagents equates to losing reaction time, which is extremely important in microreactors due to its small volume. Large containers require the formation of eddies, small droplets, that need to be generated mechanically. This requires a lot of energy and time to achieve complete mixing. However, microfluidics does this passively due to the liquids running parallel in the micrometre scale. Figure 2 shows the relationship between diffusion time and the distance of diffusion. (10) As the distance increases the diffusion time increases exponentially.

The laminar flow of microreactors has been exploited especially in multiphase reactions which affords superior surface to volume ratios. Therefore, smaller channels would cause a reaction to be limited by its chemical kinetics instead of mixing or diffusion kinetics. There is a limitation on how small the channels can get.

Darcy Weisbach equation:

$$\frac{\Delta p}{L} = f_D \cdot \frac{\rho}{2} \cdot \frac{< v >^2}{D}$$ Equation 2: Turbulent flow.

$$\frac{\Delta p}{L} = \frac{128}{\pi} \cdot \frac{\mu Q}{D^4}$$ Equation 3: Laminar flow.

Where:

μ = dynamic viscosity (kg/(m*s), N·s/m^2 or kg/(m·s))

Q = volumetric flow rate (m^3/s)

∆p = pressure drop (Pa/m)

L = length of channel (m)

D = hydraulic diameter (m)

<v> = mean flow rate (m/s)

Pressure drop is the difference in pressure between two connected points in fluid carrying space. The laminar flow form of the Darcy Weisbach equation is used for microfluidics due to miniscule channel sizes. Three variables affect the pressure drop. Namely, the diameter and length of the channel as well as the flow rate. As the hydraulic diameter declines the backpressure increases to the fourth power, consequently one should take great care when picking the diameter size to keep the reactor design within reasonable specifications. Both the length of the channel as well as the flow rate of the channel follows a linear relationship, therefore the channel's most important aspect is the hydraulic diameter. The dynamic viscosity won't change, assuming the temperature and pressure remains the same.

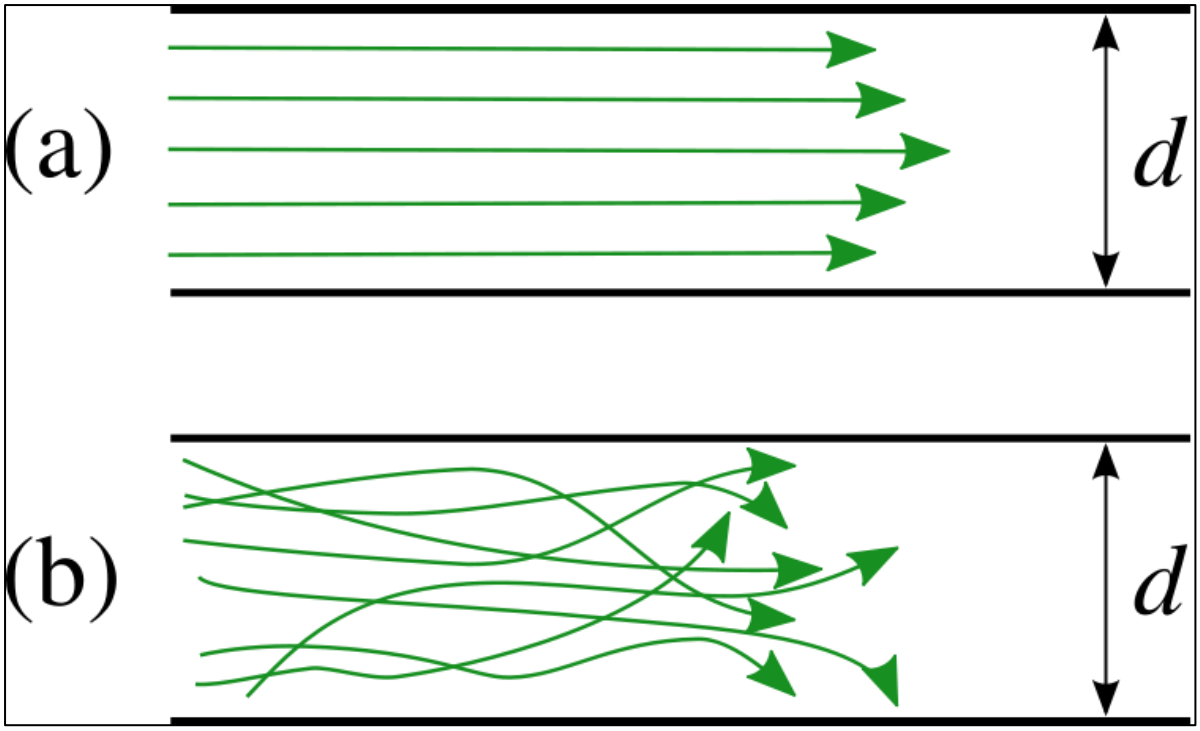

Figure 3:a: Laminar vs. b: Turbulent flow. (public domain)

As mentioned, diffusion time is exponential with regard to distance. But pressure drop increases exponentially with decreasing channel sizes. This interplay has severe practical consequences if it is not considered during the design of microreactors. Too high a backpressure would put strain on the pump, fittings as well as the reactor. This would require extra considerations of the design which in effect would make the system more expensive. On the other extreme, with the channels being larger, the molecular diffusion time will be too long. This will cause the reactor to be inefficient and the kinetics would be limited by the mixing time. In optimum reactor design the kinetics should be limited by the chemistry and no other factors. There is a work around reducing the pressure drop while maintaining the mixing ability. A short region of the channel can be dedicated to mixing. The idea behind this is to create disturbances in the laminar flow which will increase the surface to surface interaction of the two liquids. Other approaches use the geometry of the mixing structure to promote advection. It should be noted that the time spent in the mixing structure should be less than the chemical reaction time for optimization purposes. Unmixed components could have side reactions that could affect overall yield in reactions. (11)

1.1 Types of mixers

Mixing structures can be characterised into active and passive structures. Passive structures are limited by laminar flow. Laminar flow, without any mixing, structures only relies on molecular diffusion where only mixing is considered. During turbulent flow the plug gets sheared, which acts as a mixing structure. However, getting the flow turbulent in microfluidic levels requires extreme flow rates and pressures which is not always practical. Passive mixers manipulate the flow to reduce the diffusion distance hence shortening the time for complete diffusion. This in effect would cause the stream to spend less time in the mixing structure assuming the volume is less, and flow rate remains the same. Therefore, mixing structure should be designed for a specific flowrate range which the volume of the structure would increase with flowrate. Passive mixing structures can be single stream, more efficient multiple stream structures, using hydrodynamic focussing, promoting chaotic advection using indentations and spines. (12, 13)

1.3.1 T-Mixer

Figure 4: Simplified T-mixer design. Red and blue shows the two unmixed streams and purple shows the completed mixed stream. The mixing increases as time progresses.

T-mixers and Y-mixers are the simplest of the mixing structures. It involves the two streams getting joined with the joined parallel streams running in one channel. The concurrent streams rely on molecular diffusion to mix the streams. Y-mixers have been shown to give better results, 0.99 compared to 0.6. The drawback is that the Y mixer requires more space due to convex angles on the surface.(14)These mixers have been optimized by roughening the surface on the inside and reducing the mixing channel's dimensions to facilitate molecular diffusion. (15) It should be noted that the T-mixers and Y-mixers are quite inefficient when compared to other more elaborate designs. The T-mixer design can be improved greatly. Such designs include; circular micromixers, chessboard micromixers, super focus mixers and bifurcation type feeds. (16) Multilayer mixers provide the greatest mixing coefficients. However, costs increase due to multilayering that is often required to achieve the complexity.

1.3.2 Split and Recombine

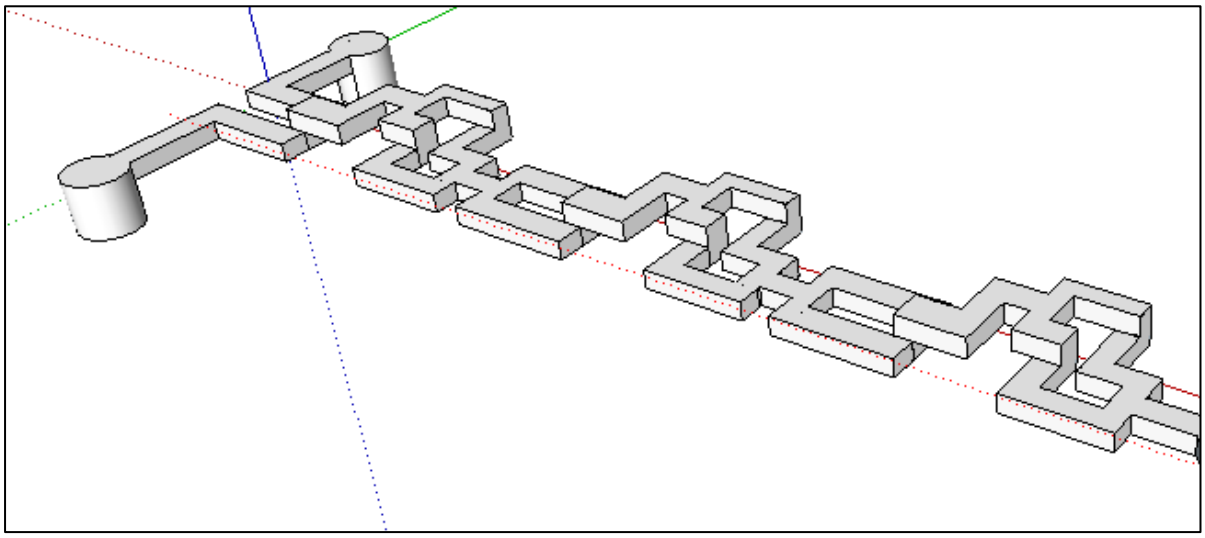

Figure 5: Multi-layered SAR micromixer (Generated via. Google SketchUP) Stream gets split in two and recombined in the opposite orientation.

Split and Recombine (SAR) mixers offer the most superior performance of the passive mixers. The stream is split into two streams; the streams are then rearranged to afford a 2 fold increase in its streams. Then the streams are recombined to give an n^2 amount of streams where n is the amount of original streams. SAR mixers have shown to be more efficient at smaller Reynold numbers, hence it is ideal for microfluidics. (17) By halving the distance by doubling the streams one increases the molecular diffusion rate exponentially. Another major advantage of these mixers is that the pressure drop is minimized due to the diameter of the channel being larger. The only pressure drop is due to change in direction which is low for laminar type flow.

1.3.3 Packed bed mixer

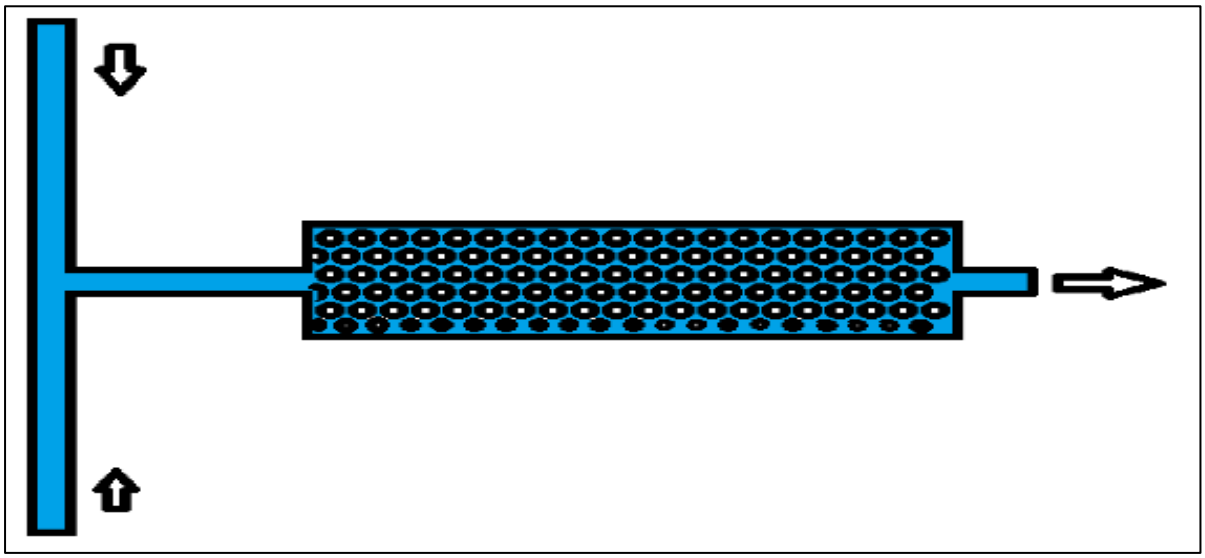

Figure 6:Packed bed micro reactor mixer. Individual beads, inert of catalytic, are packed into a cavity. This creates multiple routes for flow which increases mixing rates.

Apart from SAR mixers which exploit multi-dimensional flow there are also various other mixers which take advantage of this effect. Such a design is the packed bed microreactor. Packed bed microreactor mixers have been developed in which the mixing cavity is filled with an inert material such as glass beads (which could also be a heterogeneous catalyst in some cases). This creates flow in various random directions and greatly increased the mixing ability. The streams are recombined in a different order as initially pumped into the reactor, thus increasing the magnitude of molecular diffusion rate. The size of the filling material should be considered due to extreme backpressure. Another possible issue is the packing material moving into the channel. The advantage is that this design is that it is 2 dimensional. (18)

1.3.4 Two-split and Three-split mixers

Apart from the two-dimensional T-mixer the zigzag mixer is also a very common 2D mixing system. The zigzag mixer starts as a t-mixer which converges into a zig-zag channel pattern. This increases advection around the edges of the pattern. This additionally increases the length of the channel within the same distance, which makes this design compact. The main issue with this mixing structure is that the mixing rate is linearly proportional to length. So, the flowrate range is more limited when using this structure. Another approach to improve the zig zag is to adapt it to a two split- or three split rhombic design.

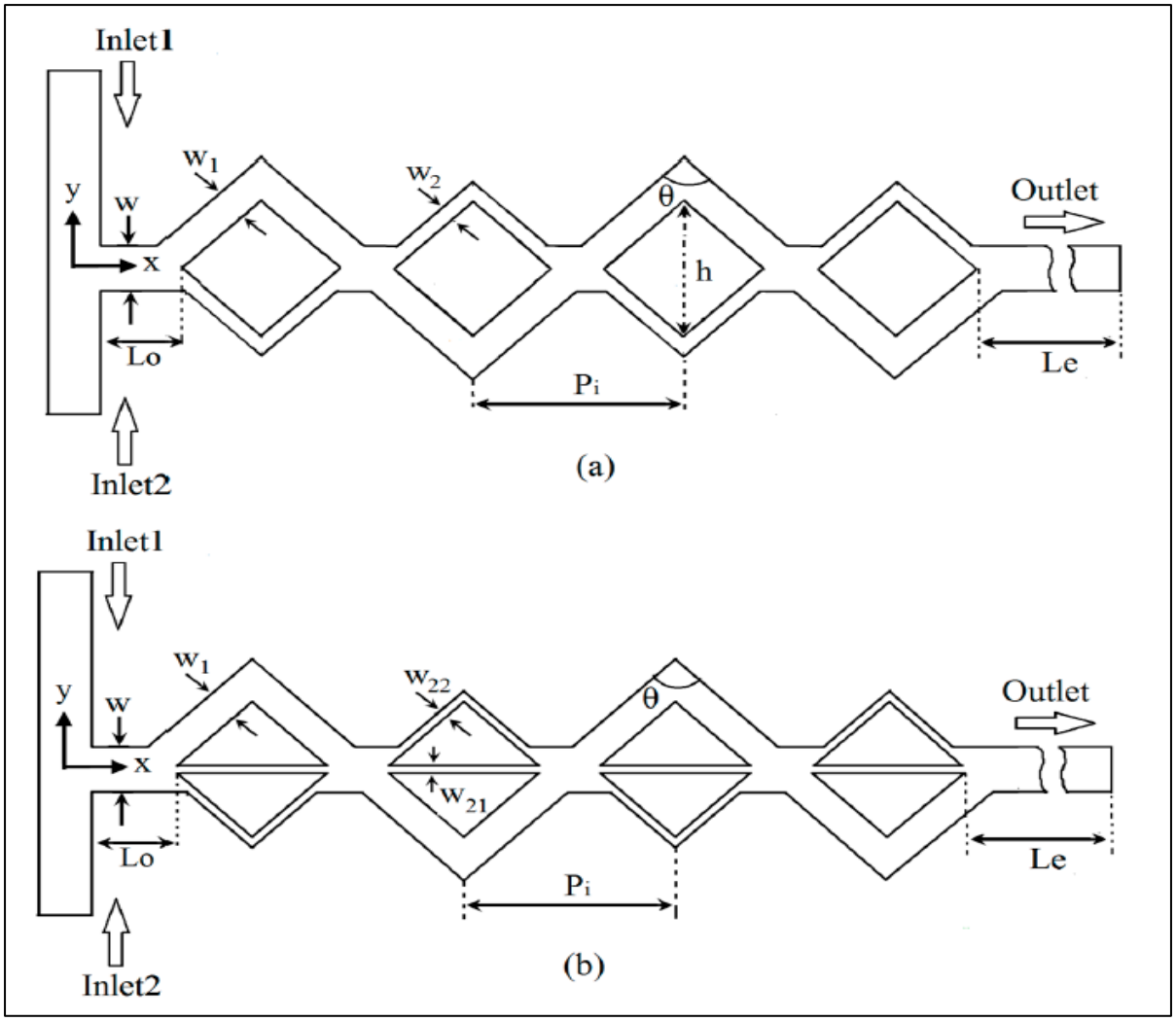

Figure 7:a:) Two-split rhombic mixer, b:) Three-split rhombic mixer. (19)

To get around the multilaminar issue with single layer mixers, injection micromixers, have been developed. This greatly reduces the manufacture complexity; hence this is the easiest method for manufacturers. However, these are not considered as effective as multi-layered laminate micromixers. Injection micromixers take a single channel, split it into sub streams and recombine the channels into a single channel. This increases surface contact with the reactor and reduces the mixing path of the reagents to increase molecular diffusion. However, when the sub streams are combined into the main stream the mixing rate is reduced. Therefore, the mixing of the streams is only increased while in the mixing structures. This is a disadvantage when compared to laminar SAR mixers. Diverse designs of single layer mixers have been developed. Two such designs being the two-split and three split mixers (Figure 7a & b). It consists of a T split followed by repetitive rhombic structures. These structures are placed in an asymmetric geometry. It is believed that the asymmetry

contributes towards the mixing rate. The larger channels are varied across the plane to assist in larger advection rates. A study done by Hossain and Kim investigated the difference between the three-split and two split mixers and found that the three-split provided superior mixing rates. The 3-split mixer outperformed the two-split from 1.4 to 1.6 mixing coefficient ratios at various Re Values, therefore the 3-split mixer has a better performance.

1.4 Channel designs

1.4.1 Theoretical

Apart from the mixing structure another important aspect to consider is the channel design. There are numerous factors when considering the reaction chamber/channel, with the dimensions being the most important. Another factor to consider is the reactor material; however, the dimensions will be covered first. As mentioned earlier the pressure drop is greatly influenced *via* the dimension of microfluidic devices. Generally, the smaller one can go, the better the mixing and heat transfer will be; however, this is severely limited *via* practical implications. The most predominant being pressure drop. Pressure drop influences reactor lamination sealing as well as fitting designs. Therefore, one should pay extreme attention when considering the dimensions. Another important consideration is reactor volume. Reactor volume can be roughly equated to channel height x channel width x channel length. An increase in volume increases the residence time. The residence time depends on the reactor volume that is exposed to the reagent and the time that volume, or plug, spends in the reactor. Hence a faster residence time would require a higher flowrate and a slower residence time a lower flowrate.

$$\tau = \frac{m}{f} \qquad \textit{Equation 4}$$

τ : Residence time (s)

m = Quantity of fluid in the system (unit of volume)

f = Flowrate of the system (unit of volume/time)

Based on reaction kinetics the chemist would choose the volume of the reactor for a specific reaction. For slower reactions, this would be more feasible. However, when considering faster reactions, a smaller volume would be more convenient. While the desired product resides in the channel undesirable side reactions may occur. Therefore, one should choose the correct volume based on the reaction.

When considering the reaction kinetics, heat transfer also needs to be considered. Heat tends to dissipate, however, the dissipation rate depends on surface exposure. The best way to contain heat, assuming the exterior is cooler, is to reduce the surface area, and, consequently the most insulating vessel would be a perfect sphere. Whereas to dissipate heat using the same assumptions the liquid must be spread out in an infinite film that contacts the reactor wall. Considering that batch chemistry uses round bottom flasks it is the most inefficient shape to equilibrate heat with its environment. Nevertheless, microreactors offer superior heat transfer due to their miniscule nature. This is solely due to distance of fluid to the reactor wall. Further improvements can be made by optimizing the channel shape. Ideally the channels should be as wide or high as possible to increase the heat transfer. However, one should keep in mind how it would affect the backpressure when designing a system.

1.5 Manufacturing techniques

Reactor material selection is essential when designing a microreactor, the reactor can only handle what the material can handle. As a chemist, the most logical material is glass, however, due to its crystalline nature shaping it is challenging.

Glass reactors are commonly used in microfluidics. Brands such as Chemtrix, Little Things Factory and Dolomite have established themselves in the market. Volumes from microliters to millilitres are common for these reactors.

1.5.1 Etching

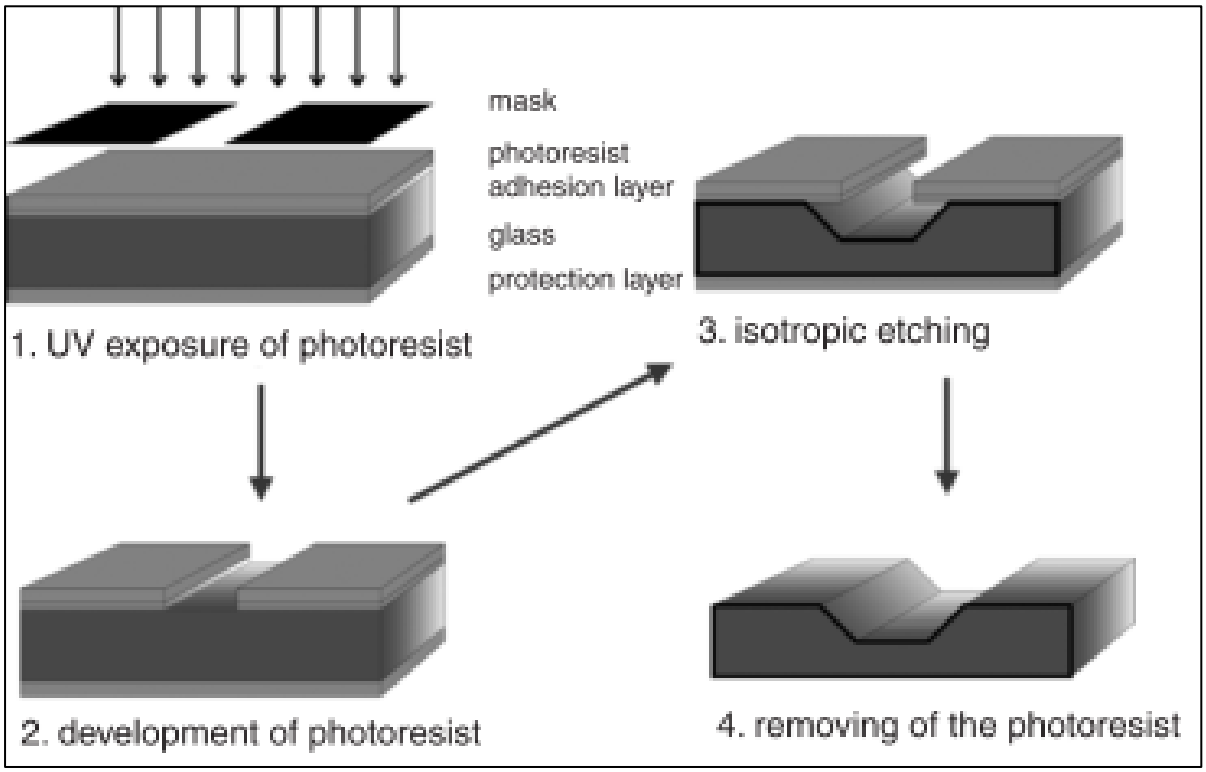

Figure 8: Isotropic wet etching procedure of glass. (20)

The most common method of producing micro-channels in glass is isotropic wet etching. The semiconductor industry played a pivotal role in these technologies where high definition resists can be optically applied with extreme precision onto surfaces. Various glass etching techniques have adopted these technologies. This technique entails applying a negative resist/photoresist layer onto a glass surface and the exposed area gets corroded isotropically through a chemical medium. After the etching the mask is removed. (21)

Using conventional wet etching methods, one drawback is that for amorphous structures the etching direction and rate is isotropic. This in effect causes under etching where the etchant begins to etch under the resists. This also creates an anisotropic shape that is severely limited with depth to width ratio. The depth to width ratio of this etching method is limited to 1:1. However the width to depth ratio of these channels can be extremely high, therefore the reactor volume is limited by the surface area of the reactor. This is one of the drawbacks of microreactors. Higher volumes will mean more chemical throughput for slower reactions.

Newer technologies enable the glass to be anisotropically etched by modifying the chemistry of the exposed channels. An example of such technology is FOTURAN where the glass is doped with unstable aluminium, silver and caesium ions. The unstable ions are oxidized via UV light which in effect makes the exposed glass less resistant towards etching. (20)

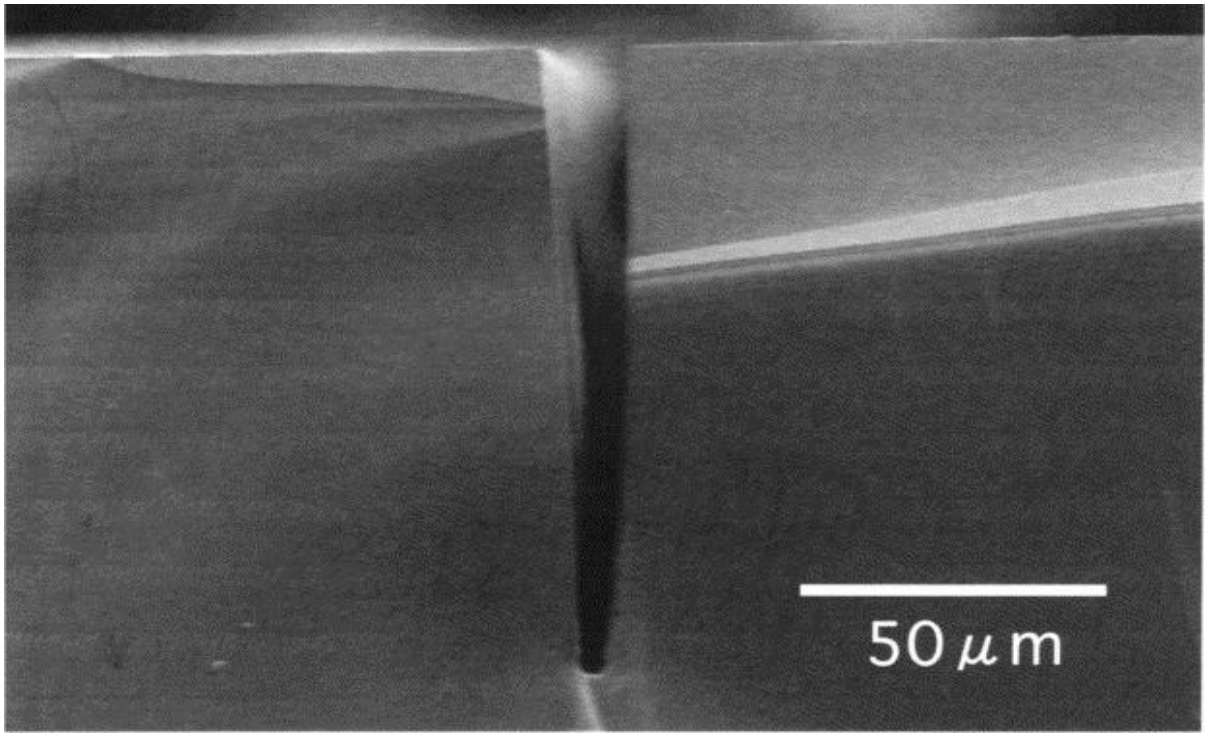

Figure 9: DRI etched channel in Pyrex glass. (21)

The etchant of glass, hydrofluoric acid, is extremely toxic to biological systems, therefore this is the main drawback of this technique. Another drawback is that the process is slow, rates of 3μm/min have been reported, but this can be overcome by scaling up, such as in the case of semiconductors where multiple IC's are etched onto a single silicon wafer. Other, less toxic derivatives are available; however, the etching rate is far less aggressive, which makes the process extremely time consuming. More recent etching techniques include plasma etching which is not only limited to glass, but other materials such as diamonds have been etched this way. One variant is Deep Reactive Ion etching (DRIE) where a gas is ionized, and the exposed surface is etched. Excellent aspect ratios can be obtained through this method, however the infrastructure setup is expensive and maximum etching rates are ~1μm/min.

The mask is generally applied only on 2 dimensions, thus only 2 dimensional structures can be etched. Therefore, the reactor needs to be fluidically sealed. Since glass is relatively chemically inert, bonding two layers of glass to each other needs extreme conditions. A common issue with this is delamination as well as air pockets that get stuck in between the layers. For this reason, glass microreactors are relatively expensive.

Although etching is the commonly used method of producing micro channels in glass, milling has also been used to cut micro channels. However milling rates are extremely reduced and expensive diamond tips need to be used due to the hardness and crystallinity of glass. (22)

Apart from glass, polymer reactors are used also. These reactors' main downfall is chemical resistance. Apart from poly-ether-ether-ketone(PEEK) and polytetrafluoroethylene(PTFE) and polysulfone, the polymers aren't feasible for harsh reaction conditions. Therefore, these reactors usually find their niche in biological applications where mild chemical environments are used. Apart from chemistry, microreactors also find their application in biological applications. These technologies are usually marketed under Lab on a chip, however some chemical processes are also included under this. Two main polymers are usually employed while making these chips. The first poly(methyl methacrylate) (PMMA) and second cyclic olefin polymers (COPs). Both provide excellent optical transparency as well as hydrophobic surfaces which makes them ideal for water based solutions. COP's are more desirable than PMMA due to its superior hydrophobicity and optical transparency. However, COP's glass transition temperatures are much higher which makes it more difficult to work with.

One of the advantages of polymer reactors is the ease of manufacturing. It is generally softer than glass and more ductile and hence it is more resistant against cracking. These plastics can be divided up into thermosets and thermoplastics. Thermoplastics are more common due to their adaptive nature and ease of manufacture. Various techniques exist to manufacture polymer reactors, and a few will be mentioned.

1.5.2 Milling

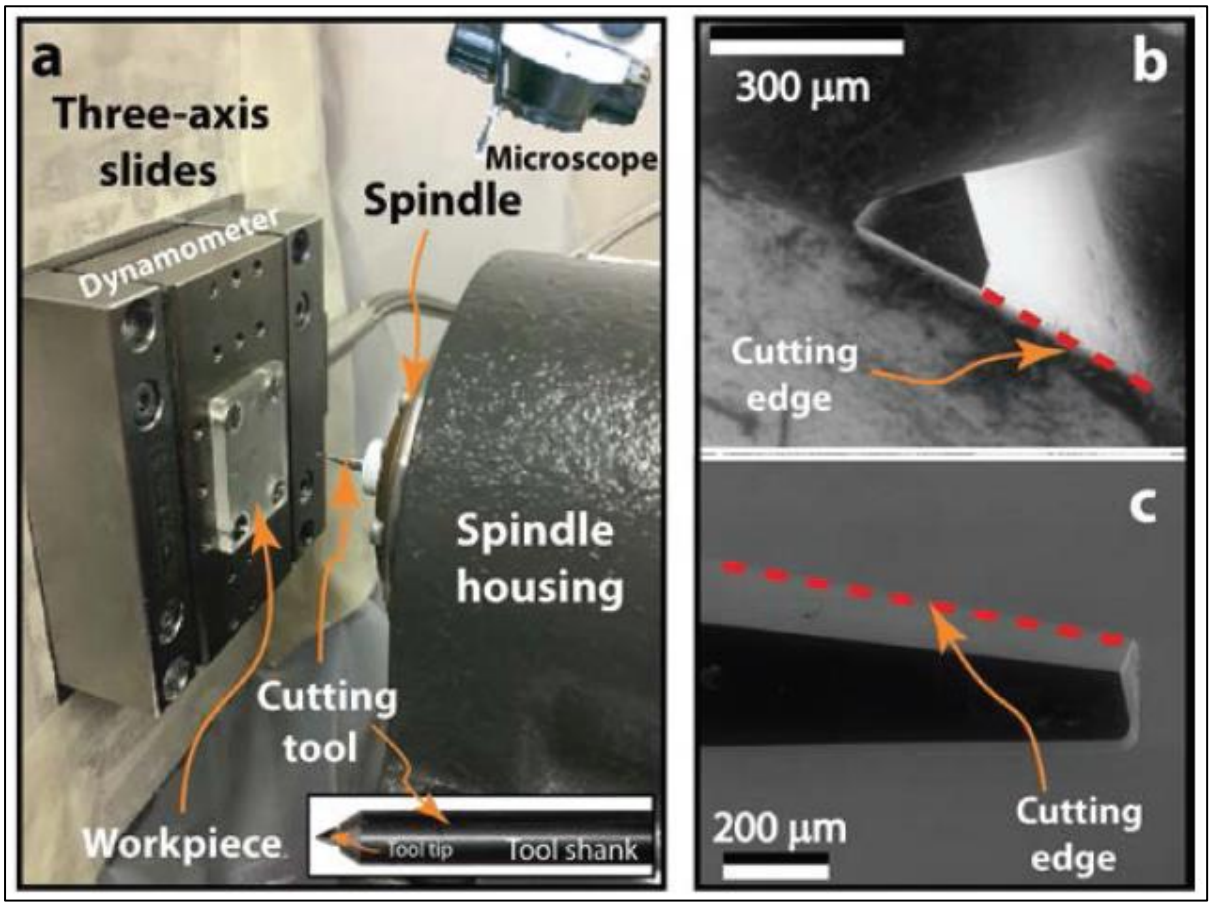

Figure 10: Micromill setup of PMMA. b:) front of 450µm daimond tipped cutting bit c:)Side of 450µm cutting bit. (23)

Direct methods of manufacture include micro milling and laser ablation. Micro milling removes the materials to form the structure via a spindle with an extremely fine cutting bit. The motion is controlled via a computer numerical control (CNC) system which affords remarkable accuracy. (23) Micro milling can be applied to most materials; however, care should be taken what tool head is selected. Imperfections which are negligible with macro milling becomes of extreme importance when working in micrometre scale. It should be mentioned that there differences exist from macro CNC mills compared to micro mills. Micro mills require speeds up to 150krpm's where conventional mills are lower. Another issue that is that hard to cut materials are difficult to machine due to the finite material strength at smaller scales. The positive side of micro milling is that the rigidity of the mechanics doesn't have to be as high and temperature related artefacts are not present if done correctly. If the infrastructure is set up this is also one of the most affordable machining methods. Since this technique is relatively new when compared to metals, the process usually

is done through trial and error, but currently modelling is being developed to optimize process conditions. (23) The mechanics of micro mills are able to have resolutions below 1µm, therefore the upper limit is the tool size to determine the radial resolution. Mechanical manufacturing of these tools is limited. But modern manufacturing methods such as focussed ion beam (FIB) milling coupled with a SEM have drastically reduced the size and variability of the tool heads. A FIB uses a focused stream of Ga^{2+} ions that corrodes the metal piece. The resolution is excellent and with the proper stage, interesting shapes may be machined.The drawback of this method is that the equipment is extremely expensive, the ion source is expensive, and it is very slow for machining tools.

1.5.3 Electric Discharge Machining

An alternative to produce the microtools is to use micro wire Electric-Discharge-Machining (EDM). Wire EDM (WEDM) is where a conductive wire is fed that is connected to a high voltage electric source. When the wire gets sufficiently close to the workpiece a discharge takes place over a dielectric medium which corrodes the wire as well as the workpiece. WDEM is a direct manufacturing method, therefore upscaling is often difficult when compared to where a negative form cathode is used. This will be discussed later in this section. Tool heads down to 20µm diameter have been made using this technique with reasonable quality. While Tungsten carbide can be used for both polymer and metal reactors, diamond tipped bits show superior performance when burring and melting is considered. This may be due to less irregularity on the surface of the bit.

1.5.4 Laser ablation

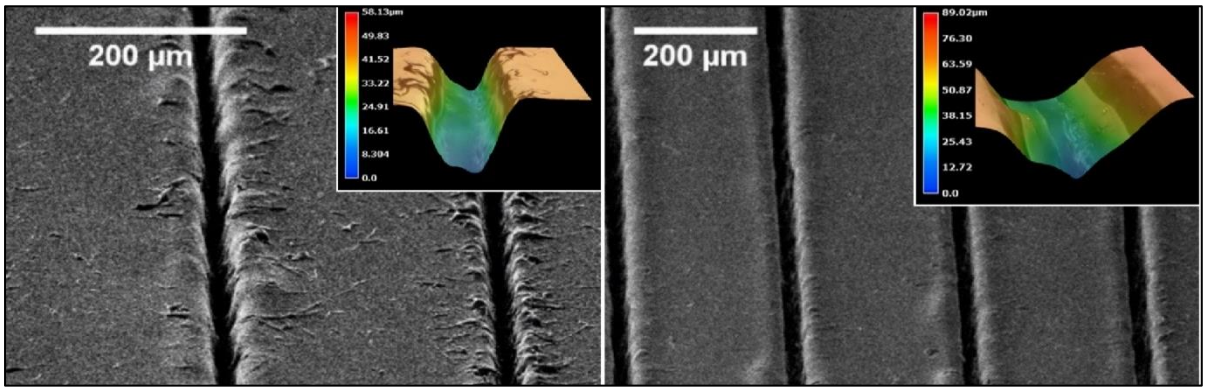

Figure 11: SEM of laser engraved surface of COC-polymer. Low fluence engraving (Left) affords a deeper shape than high fluence engraving (Right). (24)

Apart from the physical milling of microchannels in polymer substances laser milling/ablation has found its application in microchannel manufacturing also. Laser ablation is where material is removed through vaporisation, that is commonly known as phase explosion. It has been shown that laser ablation has been able to do surface modification in the micrometre as well as nanometre scale. It has not just been shown to be able to remove material, but also to do texturing and create nanoparticles on the surface of the substrate. Since laser ablation is a direct method, it provides the versatility of quickly prototyping new reactors without injection molding, or hot embossing, which is inefficient for prototyping. But the main drawback is that scaling up would be more difficult. The use of laser ablation has been well documented in literature or various materials. However, when considering the use of polymers, it is much more susceptible to oxidation due to its organic nature. The fluence of the beam is the amount of energy delivered to a specific area.

$$Fluence = \frac{Energy(J)}{Area(cm^2)} \qquad \text{Equation 5}$$

Hence a higher fluence means that more material is removed. The material removed is also proportional to the number of passes over the same area. In Figure 12 it can be observed that the relative sizes change as the passes increase. Depending on the beam's width the channel's diameter will be limited. Thus, the minimum width of the channel is the beams with.

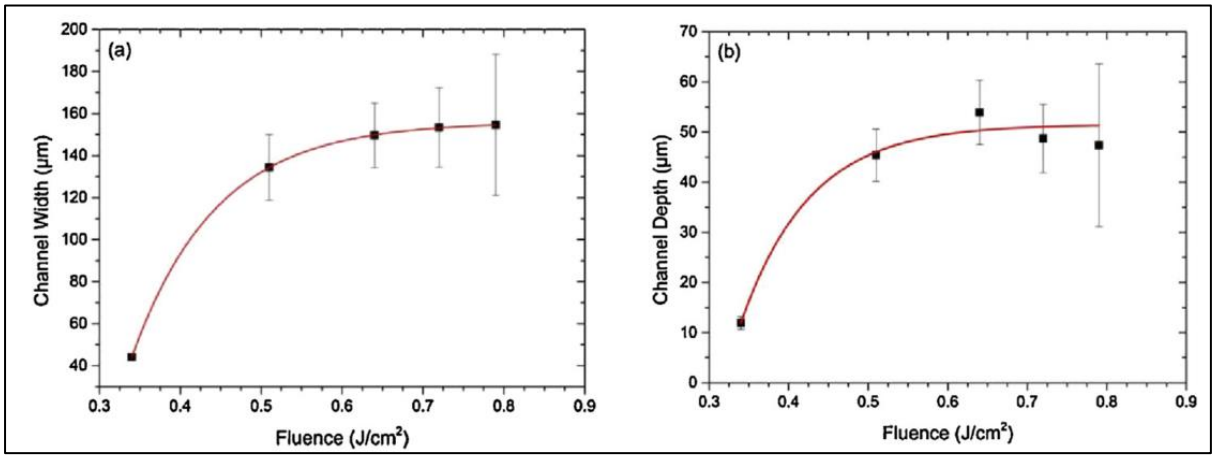

Figure 12: Channel dimensions vs. Fluence. (25)

The predictability of the channel's when using laser ablation follows a logarithmic function. It can be seen in Figure 12 that the variation increases as the fluence increases, which can be seen in Figure 12. This results in a Gaussian shape that forms on the channels cross sectional view. This is due to the absorbance mechanism. As the incidence rotates away from 90°, which is the highest absorption of energy, the reflected light increases which reduces the rate of ablation. As fluence increases the Gaussian profile of the channel widens. Results have shown that the width of the channels is much more predictable than the depth. The ideal channel diameter would be square, because this increases the surface to volume ratio. Two possible strategies can be employed to reduce the variability in dimensions. The first option is to improve the beam quality. Various definitions of beam quality exist, but in simple terms, it is how uniform the wavefunction is and tightly and parallel in the light is travelling. Ideally the intensity should be uniform throughout the beam which will cause the ablation to be uniform and hence the channel will be squarer in its cross-sectional view.

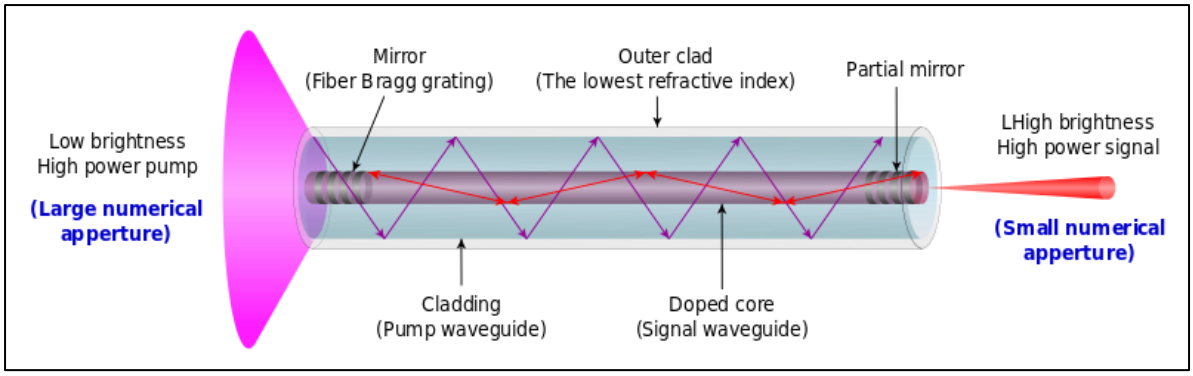

Figure 13: Double clad pumped fibre optic laser.

Fibre lasers have a reputation for having excellent beam quality. The active medium in these lasers are a fibre optic strand which is doped with various lanthanide series elements. Another approach is using a smaller beam and using a zig-zag toolpath. The idea of this is to distribute equal fluence over the surface. The equal distribution of fluence will most likely increase the cross sectional square shape. As mentioned earlier laser ablation is not only limited to polymers, but ceramics, metals and crystals have been extensively studied.

1.5.5 3D printing

Both micro-milling and laser ablation have been extensively studied in microreactor technology as direct methods. A newer technology in direct manufacturing is 3d printing. The main difference when comparing 3D printing with micro milling and laser ablation, is that 3D printing is additive in nature. Micromilling and laser ablation is subtractive. There are 3 branches in 3D printing. Namely; Fused Deposition Molding(FDM), Stereolithography(SLA) and Direct Laser Sintering(DLS).

Figure 14: FDM 3D printing farm (Public Domain)

The first 3d printers were designed in the mid 80s. Since the technology was patented the development was relatively slow. However, in recent years where the patent had expired the technology proliferated tremendously. One common movement is the RepRap movement where open source technology has been developed which took the machines from simple proof of concept designs to manufacturing lines in the form of ‘3D printing farms’. The prices of these machines also fell dramatically, which opened the market to hobby enthusiasts. Industry is slowly shifting in this direction to the adaptability of the method. It can be compared with microreactors where number up is employed instead of scale up.

1.5.5.1 Fused Deposition Molding (FDM) Printing.

FDM printing is the most common. FDM printing involves the use of a filament that consists of a thermoplastic. A geared extruder extrudes the filament through a hot end that deposits the molten polymer based on a predefined location. The most common plastic for FDM printers are acrylonitrile butadiene styrene (ABS) andpolylactic acid(PLA). However, new filaments are constantly being developed. The most notable being PEEK. Currently only INDAMATEC reasonable quality PEEK filament and PEEK also has a much higher glass and melting temperature, which makes the material hard to work with in context of 3d printing. Therefore, PEEK printed parts are quite expensive. Currently, September 2017, PEEK is about 41 times as expensive as ABS plastic. Another material that might show promise in FDM printing is high-density-polyethylene (HDPE). It is available as a filament and provides excellent chemical resistance. However, this material is known to be difficult to work with. For FDM prints to be successful, layers need to bond to each other. Thus, both layers need to be melted and then cooled until the next layer is applied. Typically layer heights for fine 3d printing are currently at 100µm and below. Since channels are typically in this range the deviation in extrusion width will be high. Another problem that might arise is the melting of the microchannel at higher temperatures. Therefore, if this is attempted, the cooling filament width and extrusion pressure must be finely tuned. Another issue with the quality of FDM printing is the variability in filament diameter and roundness. Both properties affect the material flow. As a result, deviation from these two properties will translate into nonconformities in the X and Y axis of the part. Apart from these issues numerous studies have shown that FDM printing can be used to make certain reactors. Such functions include; Immunosensors, Nanoparticle synthesis, Pathogenic bacteria detection and various others. (26) Most of these reactors were constructed using PDMS.One advantage of FDM printing is the ability for rapid prototyping. When considering custom mechanical parts 3D printing gives the user the ability to quickly test proof concept ideas. The use of FDM 3D printers has been employed by Dolomite microfluidics. But their application is primarily geared towards biological, lab on a chip design. Currently the only polymer on which the system operates is COP's. Currently FDM printed reactors for corrosive chemistry are limited by the print quality of PTFE and PEEK. Thus, further development in the plastics printing

qualities will open a whole new window to new microreactor design possibility. Especially where multidimensional structures which can easily be constructed.

1.5.5.2 Stereolithography (SLA) Printing

Another printing method, namely SLA, solves various structural quality issues when compared to FDM printing. SLA printing works through a laser or a DLP light source that cures a photosensitive polymer or uses a photo initiator. The part is built up layer by layer in a similar fashion to FDM printing and the part is moved up and down on the resin container to equilibrate the consistency of the resin. Various polymers exist that can be cured through various wavelengths. This technique was first developed in the 70s and evolved in the semiconductor industry. For this reason, extremely fine detail can be easily obtained with accurate dimensions. Recently there has been a trend to commercialise these printers for private use, resin prices are steadily dropping and becoming more compatible with FDM printers. Apart from the prices of the resins dropping, more complex functional groups are being developed.Such examples are given in Figure 15.

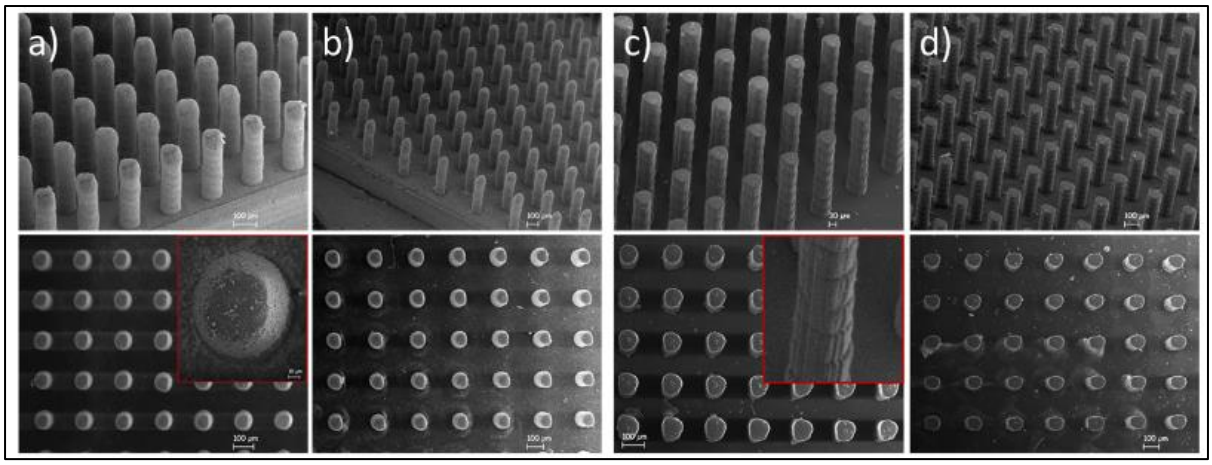

Figure 15:SEM images of SLA printed columns using a PFPE monomer with a urathane co-polyumer (C&D) and an acrylate PFPE co-polymer resin(A&B). Column width: 100um, Column height: 400um, Column spacing: 200um. (27)

Recent research in stereolithography has shown significant improvement in the production of omni-phobic surface structures using stereolithography. Fluoro groups, $-CF_2$ and $-CF_3$, have successfully been used in SLA printers. This quality of these prints far outweighs the quality of FDM and micro milled polymer parts. Recently a polycondensate UV curable resin has been developed, PFPE urethane dimethacrylate oligomer, commercially known as Fluorolink MD700 that has shown excellent structural qualities. Although chemical resistance studies are limited, the

surface wettability is extremely low which suggests it might have excellent chemical resistance. (27) As mentioned. the resolution for SLA printing far exceeds the resolution of current FDM printers. As can be seen in Figure 15 the parts are structurally independent when compared to FDM printing.

Lab on a chip (LOAC) systems have been constructed using SLA printed. Since biochemical studies has driven microfluids more than pure chemical studies therefore the bulk of the research has been focussed on water based solutions. This limits the application of these devices in corrosive chemistry reactions. It should be mentioned this method does not fall under direct structuring due to the whole layer being printed. FDM would be considered as a direct structuring method.

1.5.5.3 Selective Laser Sintering (SLS) Printing.

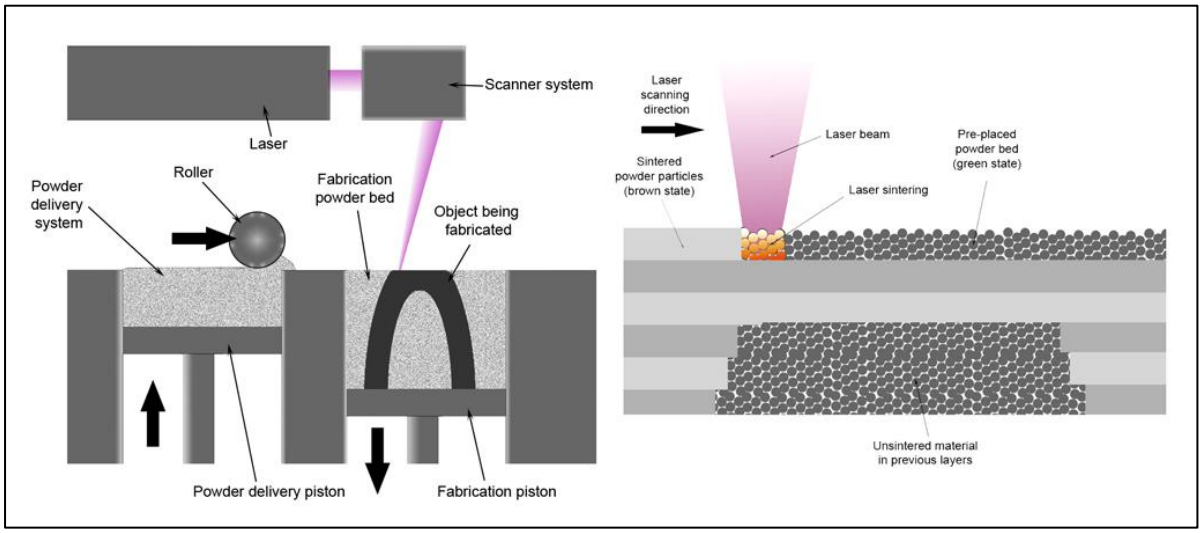

Figure 16:SLS 3d printing. (CC BY-SA 3.0Materialgeeza). The laser sinters layer by layer, while a roller applies a new layer of powder between each layer. The powder also acts as a support which reduces work flow time.

Another type of 3D printing is selective laser sintering(SLS). This technology is a newer technology compared to SLA and FDM printer. The principle of operation is that a laser sinters a powder layer by layer. Between each layer a raking system evenly distributes a fresh layer of material. FDM- and SLA printing requires support material for overhanging pieces in a part, this increases the material cost and reduces part quality, however SLS solves this by providing support in form of the powder. Individual islands can be printed and linked up at higher layers later in a print. This reduces material cost and increases overhang quality. Another advantage of SLS printing is its vast material options. Polymers, ceramics and metals has been

printed. Drawbacks of this technique are that the equipment is very expensive, and the bed needs to be held at an elevated temperature to facilitate the sintering process and the surface finish is highly porous. Therefore, post processing is required for an improved finish. SLS stainless steel microreactors has already been commercialised.

All the manufacturing methods until now have been direct structuring methods. As mentioned these methods are more suited for prototyping. However, when the prototype is ready for scaling up for commercial purposes, then using direct methods is not the best route. Various other methods are available for scaling up purposes.

1.5.6 Injection Molding

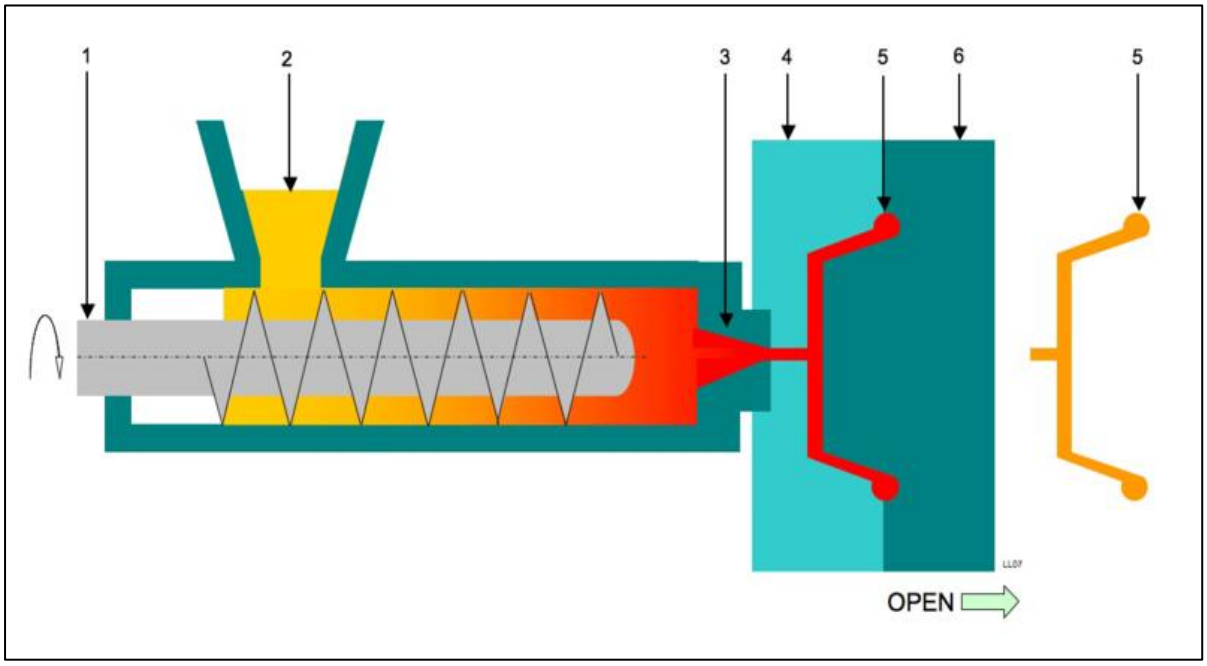

Figure 17: Injection mold machine representation. Plastic is fed into a hopper (1), where an auger (2) extrudes the plastic through the nozzle (3) into the mold(4,6). The plastic then sets in the mold cavity (5). (Public Domain Laurens van Lieshout)

One of the most common methods of large scale production of parts is injection molding. This is done after prototyping where a mold is produced for large scale production. The mold usually is a negative milled shape that is chemically inert. The shape of these molds needs careful consideration because the production of these molds tends to be very expensive. The return on investment for this technique is the volume of production. A well-designed injection mold can get millions of cycles. Thermoplastics are primarily used in injection molds due to their mailability at higher

temperatures, this affords the machines to heat, cool and reheat the extruder without any problems. Cooling thermoset plastics within mechanical parts would cause machine breakdown. Apart from thermosets and thermoplastics, thermoelastomers have also been used successfully. Another useful property of thermoplastics is their capacity for recycling. Waste thermoplastics can be re-pelleted and reused therefore this is the preferred method.

Injection molding has developed sufficiently to allow the process of micro injection molding. In conjunction with this, Computational Fluid Dynamics (CFD) has aided in mold design where polymer flow in the mold is optimized so one can achieve excellent quality. Recent research has also shown that injection molding coupled with ultrasonic waves has revealed excellent results. This occurs where the polymer is in powder form and the ultrasonic waves creates friction between the particles that melts it. Initially this process caused chain degradation which led to the mechanical properties of the polymer changing, but further optimisation has solved this issue.

The advantage of this method is that the heating is generated internally which reduces excess heat produced. In effect the throughput of production is increased, not to mention the energy savings. Additionally, the melt flow is increased due to sonic waves reducing chain to chain interactions. However, there are some drawbacks to this technique. The main one being cavitation and the formation of internal pressure gradients. (28)

There are two problems in injection molding of microreactors. The first is the injection phase. The reason for this is the same as mentioned earlier. Smaller sizes mean a higher backpressure of the injection process. Therefore, the injector needs to compensate for the increased backpressure generated by the small dimensions of the mold. Molten polymers also tend to have a higher viscosity which increases the backpressure. Incomplete injection will lead to cavitation in the mold. The second problem is the ejection of the part. Smaller parts are more prone to mechanical damage and difficult to remove from the mold. T micro features formed in the molding process increases the surface to volume which causes the part to stick more to the mold. Additionally, as the hot polymer cools it contracts which causes it to cling around circular objects such as through holes. (29)

Since injection molding is the end route for large scale production, it might be useful in certain market conditions to have a medium scale production method. Because microreactors are a relatively small industry compared to batch, an investor might require a stepping stone to start a new product. One such possibility is hot embossing. The development process still requires prototyping, however the upscaled manufacturing method differs slightly from injection molding, or in this case micro injection molding.

1.5.7 Hot embossing

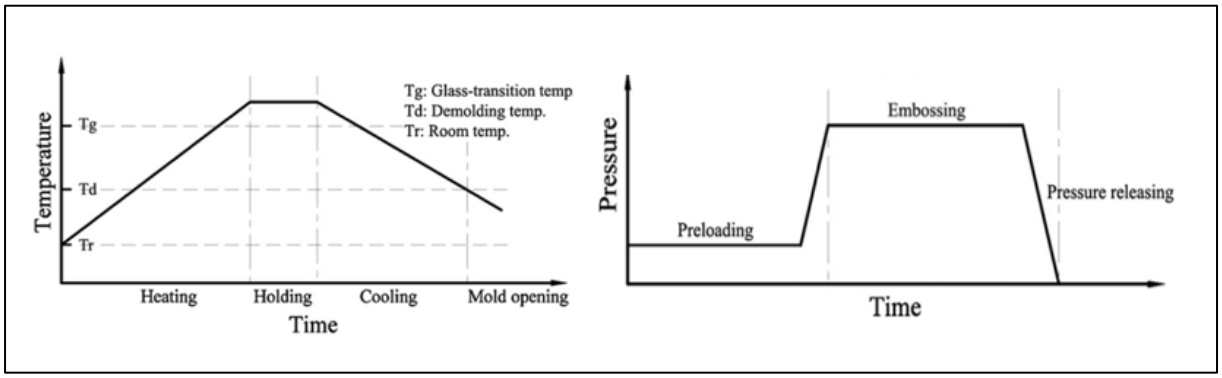

Figure 18: Process cycle of hot embossing. Pressure and temperature are two variables that affect hot embossing quality and time. As can be seen in the Temp vs. Time curve the limiting factor is the change in temperature. (30)

A stamp of the negative milled topographical microstructures is used in this process. It should be mentioned that laser ablation is also used to produce the stamp. The stamp is usually an inert piece of metal that is resistant towards corrosion for a long life. The process is divided up into three stages. In the first stage the stamp is heated, 20°C to 30°C, above the glass transition temperature of the workpiece. At the second the stamp is compressed on a pre-processed polymeric work piece at a certain pressure. At this stage the structures are transferred onto the workpiece. The final stage is cooling and demolding. Two variables affect the quality of the part namely; pressure and temperature. The factors that affect the process cycle are heating and cooling. Various processes have been developed to reduce this. One such example is induction heating of the stamp that only heats the surface of the stamp which reduces excess heat transfer to the system. Excessive heat build-up in the system means that cooling will take longer. (30)

1.6 Materials

1.6.1 Polymers

The above-mentioned methods for large scale production are primarily used for polymer products. Polymers are relatively easy to work with which makes them an attractive option for manufacturing, especially in large scale production. These methods have a been researched for acrylic as well as COP's. As mentioned earlier these polymers are highly susceptible to organic solvents, acids and base solutions. For microreactors to be used in organic chemistry, corrosion resistance should be of a primary concern since reactors cannot afford to fail due to degradation in complex multistep reactions.

Glass affords the best chemical resistance of all materials, but its machinability is difficult when considering methods other than etching. Etching also involves extremely toxic chemicals, as mentioned.

Although polymers have evolved to cater for certain microfluidic applications, there are still limitations when considering more corrosive chemistry. For polymers high corrosive chemistry is limited to PEEK and PTFE. While PEEK has a higher tensile strength, it is degraded by concentrated sulfuric acid. In contrast PTFE it is more inert towards corrosion, but it is susceptible towards cold flow hence a lower tensile strength.

Table 1:Mechanical properties of PEEK and PTFE. (31)

Property	**PEEK**	**PTFE**
Melting point (°C)	343	327
Density kg/m^3	1320	2200
Glass transition (°C)	143	Disputed.
Young's Modulus (GPa)	3.36	0.5
Coefficient of friction.	0.34	0.03-0.05
Tensile strength (MPa)	90-100	25-35
Thermal Conductivity (W/m·K) @20°C	0.25	0.25
Machinability	Exceptional.	Good.

Since PEEK is a better structural performance plastic due to its high glass temperature and higher tensile strength and superior machinability it will be ideal for a reactor material. The main drawback is its price. The University of Florida has developed a composite of PEEK filled PTFE where the structural strength of PEEK complements the low coefficient of PTFE. This possibly could find its use in microfluidics. But no research could be obtained about its micro machinability. (32)

As pointed out, one of the main advantages of microreactors is the superior heat transfer compared to batch chemistry, therefore to truly take maximum advantage one should invest in a material of superior thermal conductivity.

Table 2:Thermal conductivity of materials. (33)

Material	**Thermal Conductivity @ 25°C (W/m·K)**
Glass	1.05
PEEK	0.25
PTFE	0.25
Iron	25
Acrylic	0.2
Bronze	110
Aluminium	205
Copper	401
Polystyrene foam (Styrofoam)	0.033
Stainless steel	16
Hastelloy C276	9.8

Table 2 shows the thermal conductivity of various materials. Polymers has the lowest values, followed by glass and the highest being metals. When considdering heat conductance alone, metals are better for microreactors. But the drawback of metals is its machinability, and corrosian resistance. Copper and aluminium are relatively easy to machine due to their soft nature. However their main drawback is their susceptibliity to chemical corosion.

1.6.2 Metals

Metal alloys have been developed that provide excellent chemical corrosion. Stainless steel for instance, offers excellent resistance against oxidation. The high chromium levels in the alloy form a thin oxide layer that protects the iron against oxidation. Aluminium has the same effect where aluminium oxide acts as the thin layer. However, iron oxide flakes expose the metal surface. Stainless steel is susceptible to pitting corrosions when high concentrations of strong anions, especially chlorides, are present. However the corrosion rate is far less than that of pure iron. Stainless steel 316 has been used in continouos flow reactors as mentioned.

Newer generation superalloys have nearly perfect chemical resistance, oxidation and reduction characteristics. One such example is Hastelloy C276 which is a newer generation of Hastelloy C. It is a Nickel Molybdenym Chromium wrought alloy. It contains very little carbon and iron, thus flaking is non existent.

Table 3: Element composition of Hastelloy C273

Metal	Ni	Mo	Cr	Fe	W	Mn	V	Nb
Weight %	57	15-17	14.5-16.5	4-7	3.5 - 4.5	1	0.35	2.5

It has been used extensively in high corrosive chemical applications where versatility is needed. It also affords excellent stability at high temperatures. For even higher temperature metals Incolnel is avialable which finds its use in aerospace, but its high Iron content makes it more susceptible to chemical corrosion. Hastelloy C276 has been used for various components in the chemical industry such as reaction vessels, tubing and HPLC pump heads.

However C276 has two drawbacks. The first problem is that the metal is extremely expensive, partly due to patent rights as well as manufacturing complexity. The second issue is that the metal is very difficult to work with, therfore parts that are manufactured in C276 are extremely expenisve. Since physical contact machining is difficult with this material another option is non contact methods. One method of particular interest is laser ablation. Microtexturing of C276 has shown to alter its

interaction with aqueous liquids, especially hydrophobicity. Higher hydrophobic properties would reduce metal wetting and reduce corrosion potential. (34)

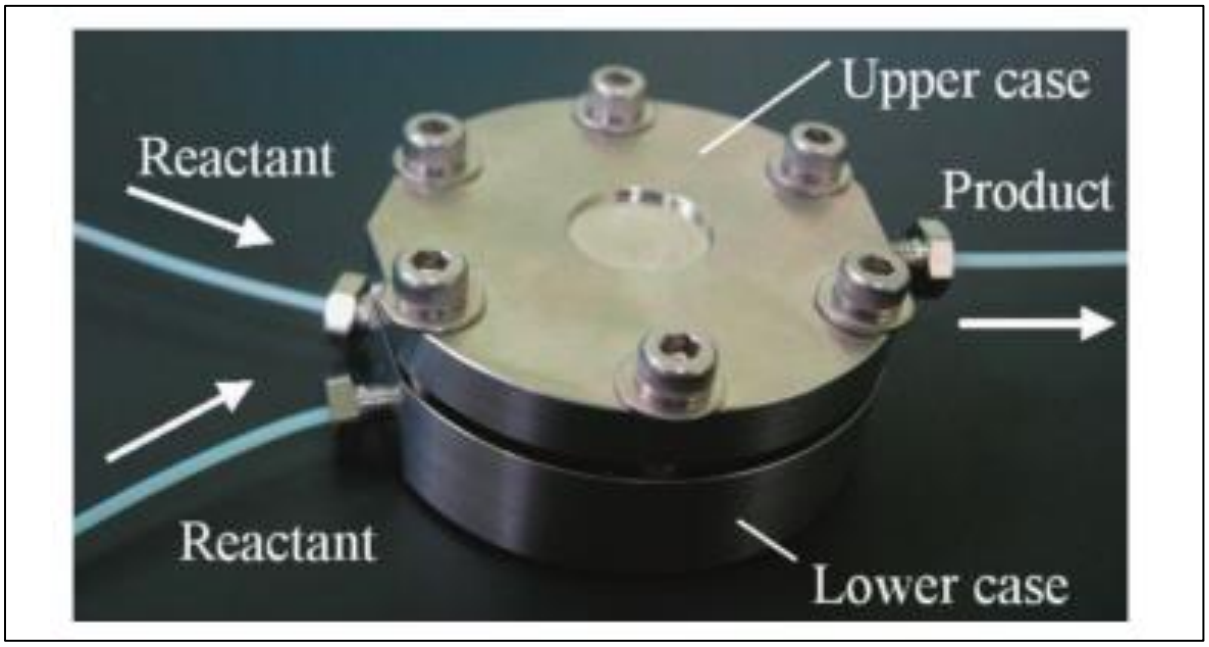

Figure 19: Hastelloy C276 clamp system sandwiching a glass chip reactor. (35)

But since microreactors are small, very little material is required to manufacture them. Therefore, Hastelloy C276 may be used as a practical material. Since it is more expensive, it's operation lifetime should be longer to offset the higher cost. As mentioned a common issue with microreactors is reactor blockage. Severe blockages may even cause the reactor to be scapped. This is especially true when the channels are extremely small, such as Chemtrix Labtrix reactors. Glass reactors are usually fused which makes unblocking reactors in some cases impossible. Some microreactors have a sandwich style clamp where if a blockage occurs, the clamp can be removed and blockage physically removed. Figure 19 shows a glass disc microreactor clamped in a Hastelloy C276 disk. Although, blockages can still occur. This can be corrected. (35) An ideal reactor would have the ability to be resistant towards blockages without signifcantly effecting reactor volume.

1.7 Pumps

Another essential part of microfluidics apart from the reactor is the pump. As stated, microreactors can have considerable backpressure, therefore a pump of sufficient pressure is required at low flow rates. Additionally, the pump should also have excellent chemical corrosion resistance as well as excellent reliability. Due to the sequential nature of microfluidics if one pump is not functioning the entire system would be considered useless. Although fixed volume pumps have their use in research and development, such as non-continuous flow syringe pumps, it is not suited for scaling up. When scaling up, the pump should be able to operate indefinitely.

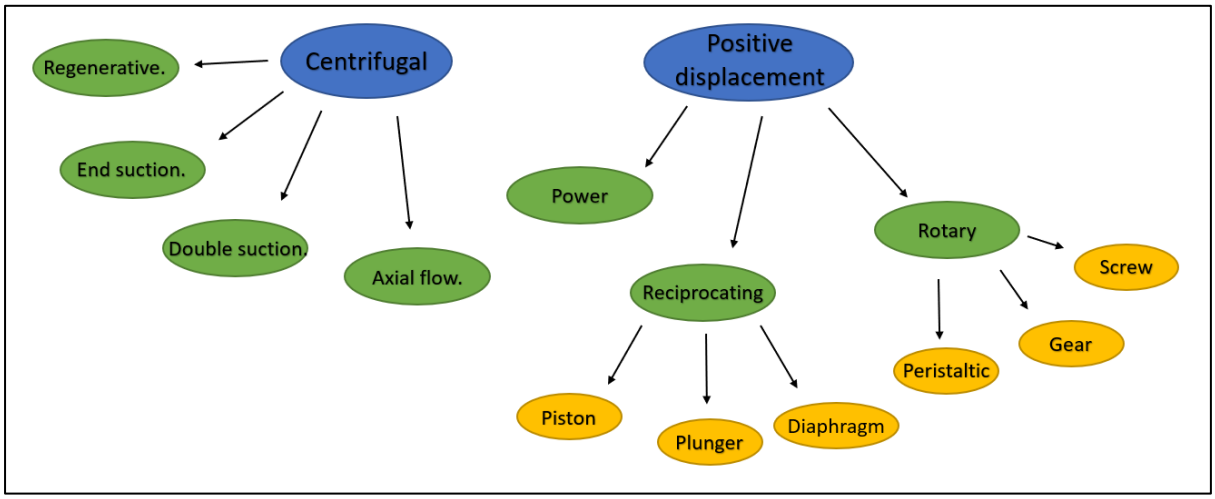

Figure 20: Classification of pumping systems. (Adapted from Engineering Toolbox)

Figure 20 shows the classification of different pump systems that exist. It should be mentioned that this figure is not exhaustive of every system in existence. But its purpose is to show a broad overview and a closer view of systems that are applicable to the scope of this study.

1.7.1 Centrifugal vs. Positive Displacement

Centrifugal pumps will be covered first. As the name suggests centrifugal pumps generate their work power through rotation. The gas or liquid is accelerated and the kinetic energy causes the pressure difference according to the Bernoulli principle. The low pressure causes free flow of matter into the inlet. Because there is no barrier for the fluid to flow back to its low-pressure position it is difficult to obtain high pressures when compared to positive displacement pumps. However, the advantage of this effect is that an extremely high-volume transfer is possible if the pressure gradient is sufficiently low. In the field of microfluidics accurate flowrates are a key component to successful synthesis. Two factors influence the flowrate in centrifugal pumps, namely viscosity and pressure. Higher viscosity fluids will create resistance toward flow, which in turn will reduce the kinetic energy of the fluid. This will lead to less pressure and consequently a lower flowrate. Since the pressure is proportional to the kinetic energy in a centrifugal pump, lower pressures mean that the flowrate will be lower. (36)

Table 4:Centrifugal- vs. Positive displacement pump properties.

Property	Centrifugal	Positive displacement.
Limiting factor for volume.	Pressure.	Displacement.
Pressures	Moderate	High.
Driving force	Acceleration of matter.	Compression of matter.
Flowrate determining factor	Viscosity and pressure	Volume displacement
Efficiency	Moderate	High

While centrifugal pumps are used in the chemical industry, their purpose is for fast transfer of liquids. Positive displacement pumps are used where higher precision of flowrate and higher pressures are required. Positive displacement pumps deliver the same amount of volume irrespective of the resistance of flow.

1.7.2 Gear- and screw pumps

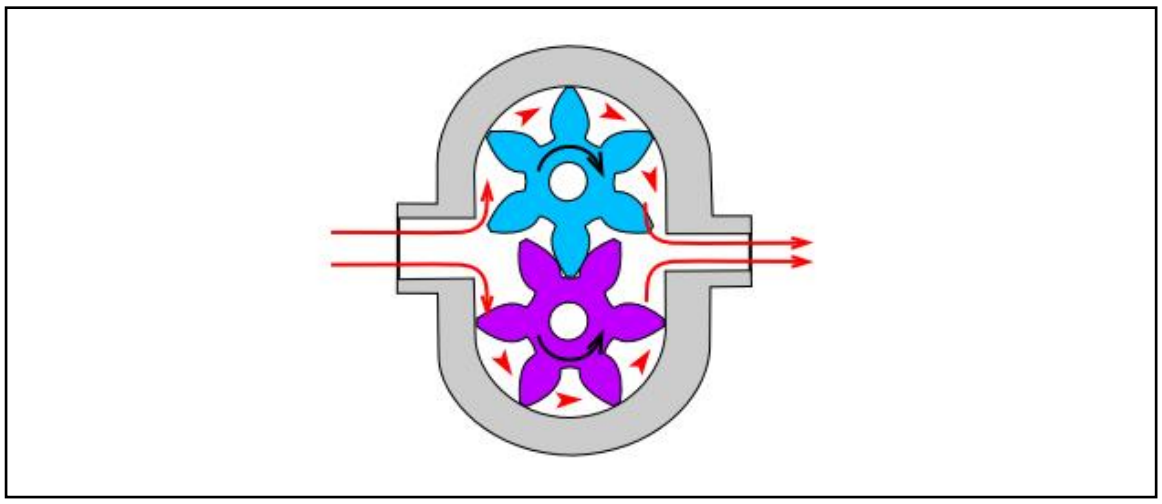

Figure 21: Positive displacement gear pump. (Public licence)

A branch of positive displacement pumps is rotary pumps. It is commonly confused with centrifugal pumps. It can be further divided up into gear pumps or positive displacement screw pumps. A gear pump consists of two parallel shafts that are synchronized when turning. Gears are attached to the shaft where the teeth of the adjacent gears form a seal with each other. Cavities on the external edges of the gears are where the mass flow takes place. The teeth form a dynamic seal with the edge of the motor housing. There should be a positive pressure at the inlet to have a large enough feed stock for the pump. However at normal atmospheric conditions it is usually not an issue. This only becomes an issue when the pump is operated at extreme conditions. One of the drawbacks of this pump is that no solids can be pumped. The solids will get crushed in the gears and damage the sealing ability. If the solids do not crush the whole pump will stall and function will be lost. Problems have also been reported with the gear teeth pump housing interface. Since the parts are moving, complete sealing is difficult to achieve thus a slight flow is observed in the reverse direction due to pressure difference. Although great improvements have been made in this technology, the backflow issue has not been completely solved. This problem has been circumnavigated by using a correctional closed loop system. (36) Advantages of the screw pump include its ability to pump extremely viscous liquids to pressures up to 210 bars which far exceeds basic microfluidic requirements.

Another positive displacement pump which works similarly to a gear pump is a screw pump. These pumps also can pump viscous liquids and at elevated temperatures.

Various sub designs are present within this class. A common design is that of a double screw pump where two screws run parallel. The teeth of the screws seal with the adjacent screw to form compartments. As the screws rotate, new compartments form on the inlet, while the compartments collapse on the outlet. The collapse of the filled compartments contributes towards the pressure. The sealing of double screw pumps takes place in the screw; therefore, the sealing is dynamic and less efficient. Therefore, these pumps have found their use in pumping viscous fluids which have an increased backpressure. Another difficulty with this pump is internal friction, therefore it is more suited for petrochemical uses. The screws also tend to be relatively expensive and as the parts get smaller the prices increase due to difficulty of manufacturing. Consequently these pumps are not commonly used in microfluidics.

1.7.3 Peristaltic pumps

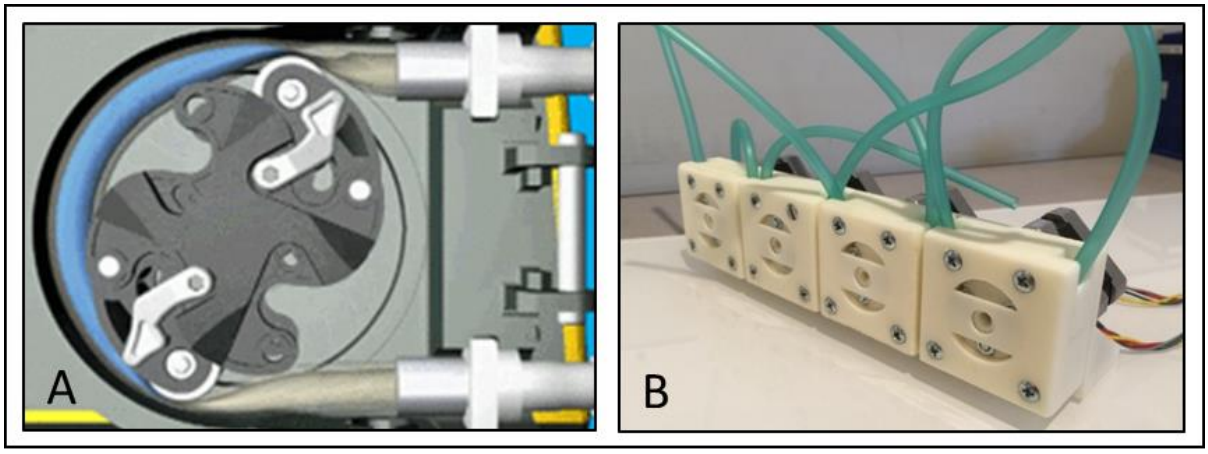

Figure 22: A: Representation of a peristaltic pump, fluid gets pushed through a tube in a clockwise manner. The fluid enters at the bottom and leaves at the top. (Wiki Public Domain author Njmcca), B: OpenSource peristaltic pump designed by Ryan Dibisch under CC3 licence. (Creative Commons)

However, one rotary pump has found its use in microfluidics; namely peristaltic pumps. The design of these pumps has been inspired by biological systems such as the esophagus and the intestines. Some advantages of these pumps are that there is no liquid wetting of the mechanical parts, hence a closed system, and constant pressure with little pulsations as well as precise control of flowrate. It works by inserting a flexible pipe in a housing where rollers push the liquid in a direction. Apart from microfluidics these pumps have been extensively used in the medical industry to infuse medication intravenously. Recent developments for these pumps includes a linear peristaltic pumping of fluids via a micro cam system. The materials used for

this pump are not suited for corrosive chemicals, since its application is aimed at lab on a chip technology. (37) The classification of rotary to linear peristaltic pumps shifts from rotary to a reciprocal diaphragm pump. Peristaltic pumps tend to be relatively inexpensive due to their uncomplicated design. Additionally, open source technology has allowed for these motors to be 3D printed at a fraction of the cost with reasonable accuracy. Although these pumps have many advantages, there are some disadvantages worth discussing. The primary problem with these pumps is degradation of the tubing. The rollers apply mechanical force which causes the tube to bend at its edges. Over time this will create a memory effect at the edges and the internal volume will reduce due to the deviation from its circular shape. The worst-case scenarios will result in the rupture of the tubing. Some of this can be negated by proper material selection. However, PTFE is not suitable since it has a cold flow effect where memory is loss due to mechanical forces. Therefore, less chemical inert elastomer tubing must be used which limits some chemistry in corrosive microfluidic application.

1.7.4 Reciprocating pumps

Reciprocating pumps are best suited for microfluidics, they deliver precise amounts of liquid and can be pumped at a high pressure. Three types of reciprocating pumps exist. Namely, diaphragm-, piston- and plunger pump.

1.7.4.1 Diaphragm pumps

Diaphragm pumps consist of an alternative diaphragm which guides fluid through a pulling and pushing flood with a one-way flow system such as check valves. The check valves are one-way valves that only allow fluid in a one-way direction. Hence, the membrane will pull the fluid through the inlet check valve and push the fluid through the outlet valve. These pumps are particularly efficient at pumping air due to large mass flow. They are commonly used in air compressors, vacuum pumps and in hydraulic pumps. Another feature which makes them attractive, is that they can handle slurries if the one-way valves (such as butterfly vavles) are properly selected.

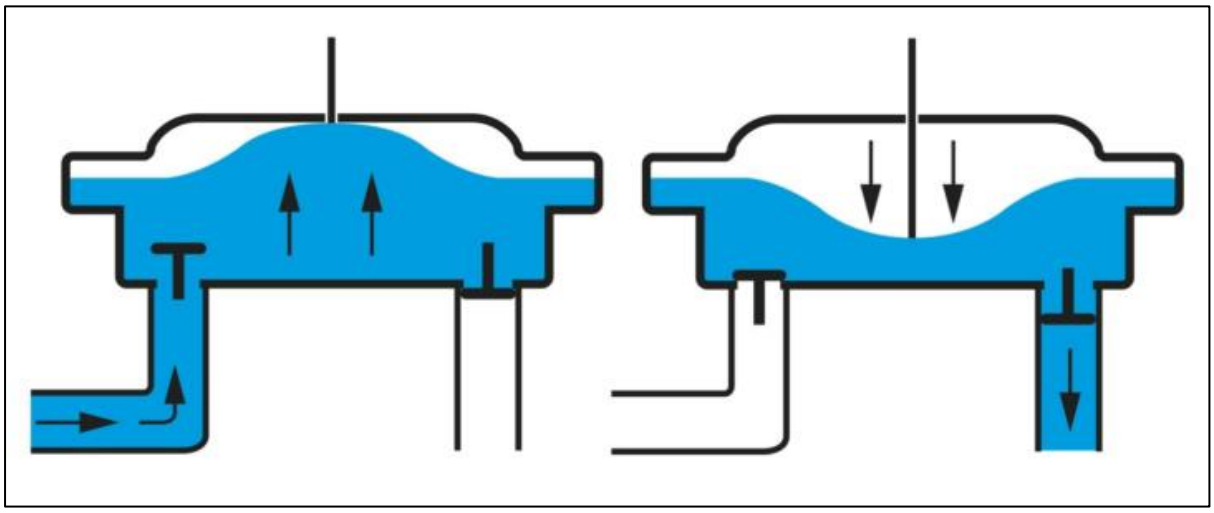

Figure 23: Pump cycle of a single channel diaphragm pump. (38)

Butterfly valves are such an example which allows the flow of slurries. They can achieve high pressures when designed well. When considering using diaphragm pumps in a microfluidic application, there are some drawbacks. The first drawback is that the flowrate is not constant. This will translate into regions of unequal stoichiometric concentrations within the microreactor. Consequently, the conversion rate will be limited through non- optimum concentration ratio's. Dual chamber pumps exist where the pull stroke pushes the adjacent fluid forward while the other chamber is being refiled.

The second problem with diaphragm pumps is the valve system. When using check valves, they require a cracking pressure to let fluid through. For vacuum pumps the lowest pressure that can be achieved is therefore the cracking pressure of the inlet check valve. The third problem is the lifetime of the membrane. Since the part gets stretched over time, it loses its integrity. Elastomer diaphragms can be used to offset this, but they tend to be more sensitive towards chemical corrosion.

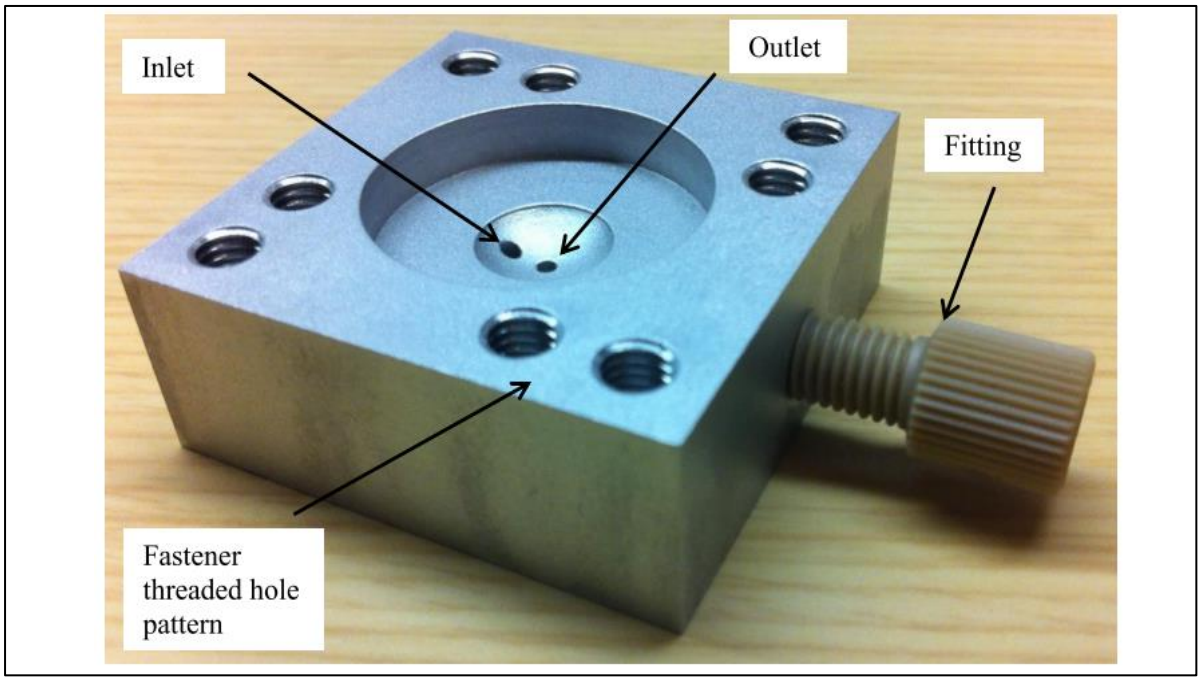

Figure 24: Pump head of a valve-less diaphragm pump. Full design would have multiple heads in series with a timed cam/piston system.(39).

As can be seen in Figure 24 a pseudo-diaphragm pumps has been developed by MIT's mechanical engineering department, which uses the membrane itself as a valve. (39) Since check valves tend to fail frequently and are relatively expensive this pump eliminates the need for check valves. A single cylinder has been developed that is driven by a piston which shows promising results at lower flowrates. However, a carefully constructed timed cam system is required for this pump to function, which would require an advanced manufacturing infrastructure.

1.7.4.2 Piston and Plunger Pumps.

Although diaphragm pumps show promise in microfluidics their two counterparts, piston- and plunger pumps, have dominated the field of microfluidic pumps. The exceptional HPLC pump as well syringe pumps fall under these classes and their use has solidified their place in microfluidics.

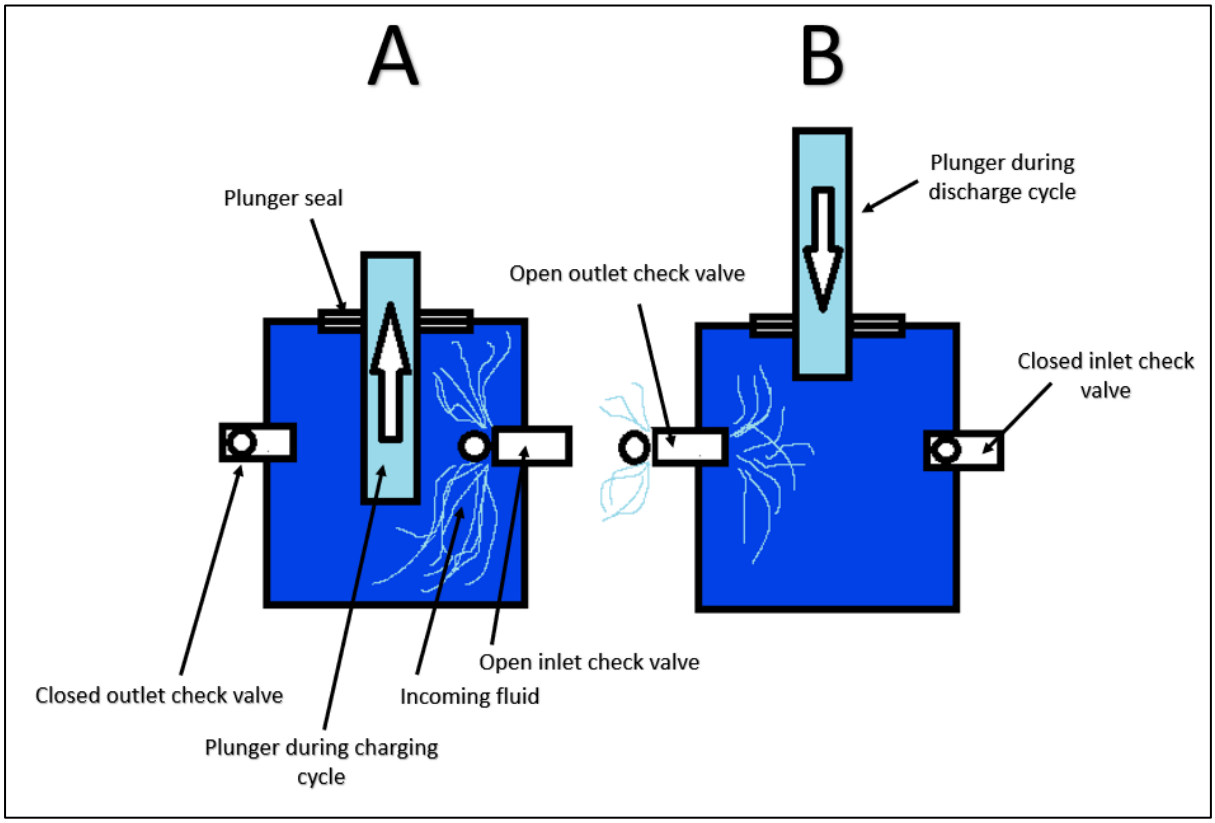

Figure 25: working of a single action plunger pump. a: Shows the charging cycle, the plunger pulls out while the inlet valve open due to lower pressure and the outlet closes. The flow is non-existent in this part of the stroke. (Generated via. PowerPoint)

As seen in Figure 25a plunger pumps have a stationary seal which is embedded in a pump head. The plunger, usually a smooth rod, oscillates in the pump head, this creates the positive displacement. The advantages of these pumps are that it refills the pump head automatically and that it can dispose fluid at high pressures. Single head plunger pumps have an oscillating flow profile that depends on the stroke function of the plunger. During the charging phase forward flow will stop. And during the discharge cycle there is flow. Thus, if this pump is going to be used in microfluidics the other reagent's pump's stroke should be synchronous. Figure 27 shows the problem; however, this problem has been partially solved through duplex- and even further with multiplex plunger/piston pumps.

Duplex pumps and power pumps have more than one piston or plunger that works in a synchronistical manner to offset pulsations which is a common issue with reciprocating pumps. They can either be double action, charge and discharge for a single piston, or power pumps, such as in the case of plungers driven by a cam system.

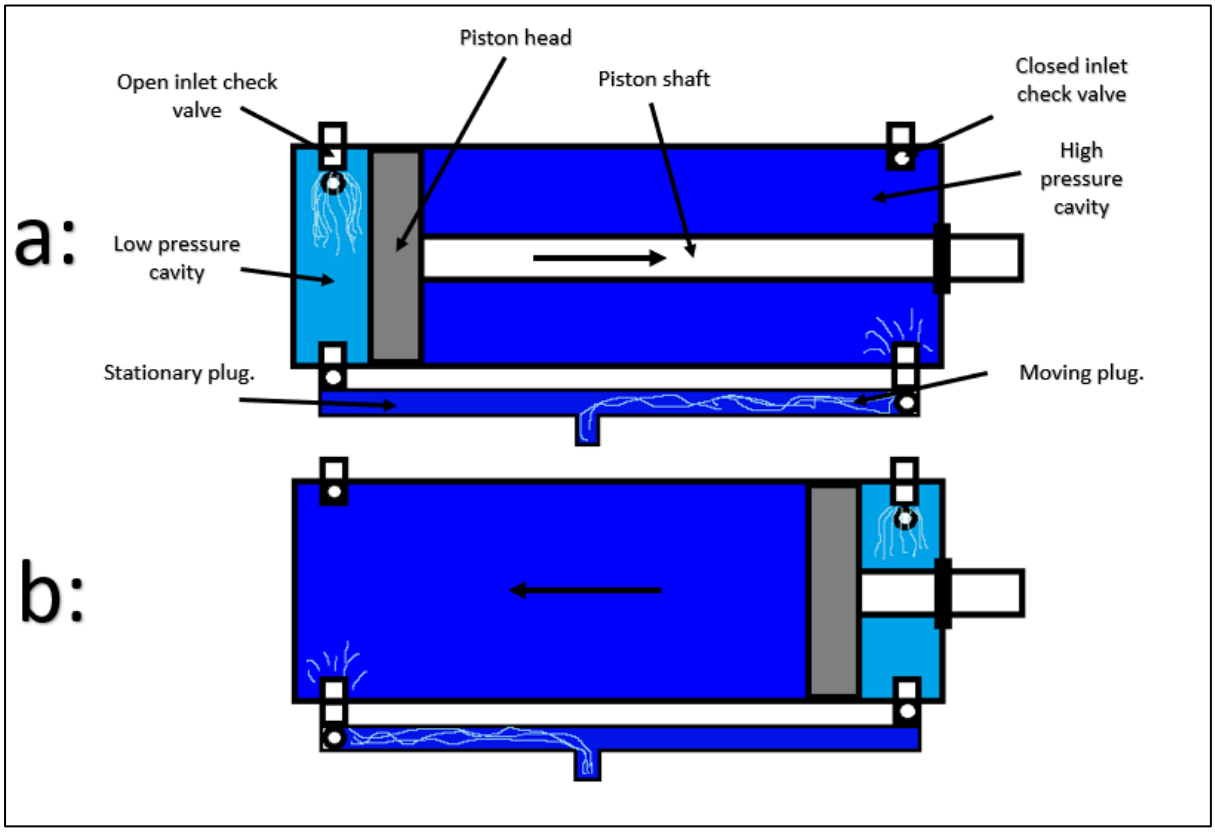

Figure 26: Schematic of a double action piston pump. The pump requires four one-way valves which work in unison to achieve a semi constant flow. A single driver is used to drive both cavities for their charge and discharge cycles. The arrow indicates the direction of the plunger's movement. (Generated via PowerPoint)

Figure 26 shows the pump cycle of a double action pump. It should be mentioned that this pump is the equivalent of a dual head reciprocating pump which has a sinusoidal cam system. As one of the cavities is charging, the other one is discharging. The inlets use the same stream and the outlets flow into the same exit stream. These pumps also have their limitations when constant flow is required. Usually the piston is driven by a rotating gear that will give the movement a sinusoidal function. At the top and bottom of the wavefunction the stroke will reverse, and a sudden stop will follow on peak of the wavefunction with in instantaneous reverse. This becomes especially problematic at lower flowrates.

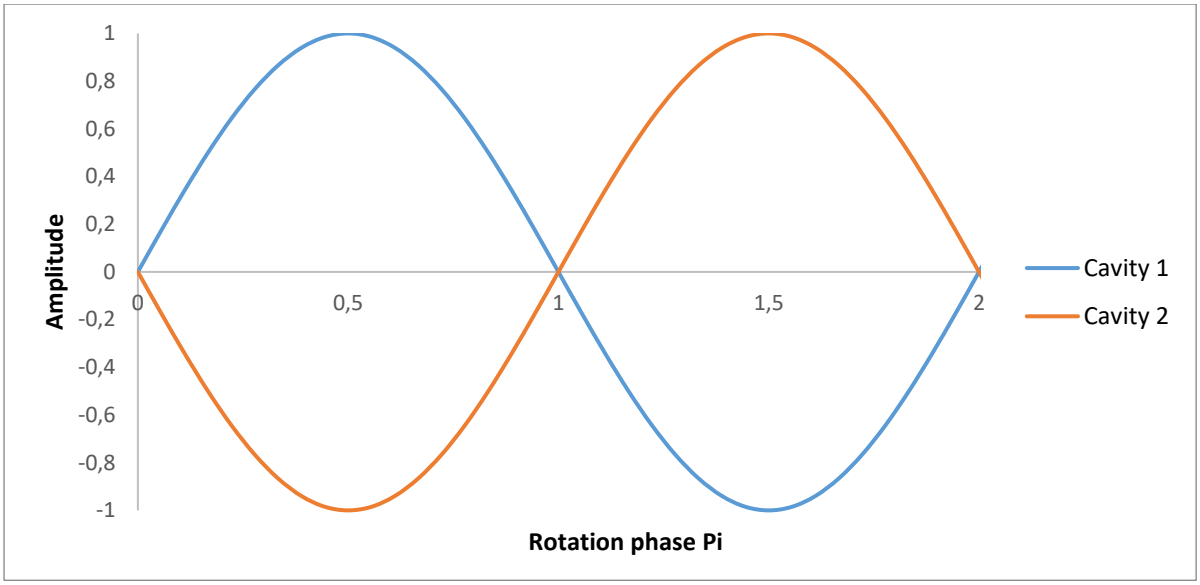

Figure 27:Rotation of a cam driving a double action pump. A positive amplitude shows that the cylinder is discharging, and a negative amplitude shows charging. (Generated via. Excel)

Figure 27 is the graph representation of Figure 26. This is the unrectified flow without check valves. The amplitude is proportional to the rate of horizontal motion in the cylinder. It should be noted that when one side is discharging at its maximum rate the other side is charging at its maximum rate. The arrangement of the one-way valves would afford the regulated flow. It should be noted that 4 one-way valves are used for one double one-way pump which makes them more expensive. This also doubles the risk of one-way valve failure.

At the π and 2π phase the flow stops are instantaneous. This flow profile creates pulsations which can cause inefficient mixing in micro channels as well as stress on the system. This problem can be partially overcome by using a pulsation dampener. A pulsation dampener consists of a vessel with a flexible septum that separates two spaces. The one space is filled with air and the other area with the fluid being pumped through. This technology is widely used with larger pumps as well as HPLC pumps that protect the overall system form pressure spikes. A graphical representation can be seen inFigure 28.

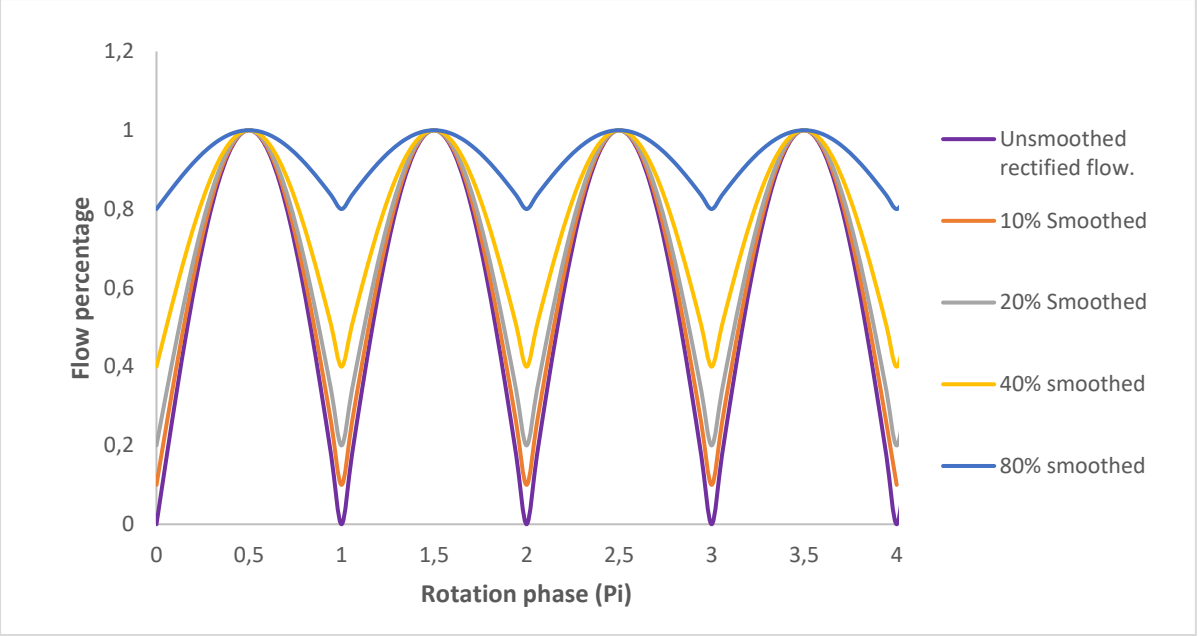

Figure 28: Effect of pulse dampers on the regulated flow of a double action pump. (Generated via. Excel)

Figure 28 shows the smoothing effect of pulse dampers on the flow. Numerous factors play a role in the efficiency of dampening. For the dampening to be effective it needs to absorb the pressure spikes. This requires the pressure inside of the bladder to be in the same range as the liquids pressure. Additionally, the energy capacity of the gas needs to be enough to offset pressure drops at the π and 2π phase. Since pressure is the only factor that alternates the only way to increase the energy storage of the gas, at a specific range, is to increase the volume at a fixed pressure. The drawback of increasing the bladder's volume is that it will take more time to equilibrate and product collection downstream will take longer to start. Commercial dampeners are available especially geared towards HPLC which means that it will be relatively easy to implement into a microfluidic system due to universal fittings being used. Additionally, these dampers are adjustable for different pressures.

Another possible theoretical design approach could be where the cylinder's volume is reduced and frequency is increased to such an extent that the pulsations would become insignificant compared to the reactor volume. However, since microreactors' volumes are so low, designing such a system would be a challenging undertaking.

Apart from dampening the pulsations for plunger and piston pumps, two other solutions are used. The first solution would be to modify the cam system. The cam system is responsible for timing the strokes of the plungers. A circular cam would

give a sinusoidal function as depicted in Figure 27. However, this does not apply to a double action pump, It applies to a dual head pump, where the plunger or piston is not linked on the same shaft. Thus, the movement of each shaft can be isolated and have its own function.

One approach is to have a quick recharge cycle with a slower discharge cycle. This pump design does not split the stream up into two streams, but the stream is passed through both heads. The first head is a low-pressure head that charges slowly and when it is full it quickly discharges the volume into the high-pressure head. This quick transfer should only take up a fraction of the cycle to minimize overall pressure spikes. The plunger's volume is also kept as low as possible to even out the spike further. Another advantage of this technique is that it only requires three check valves, which is an advantage compared to above mentioned designs.

The most common design in the HPLC pump is to double the plunger stroke volume of the first head. The second head's plunger volume is half of the first head. As the first plunger discharges, the second head is filled by half of the first head's discharge value. The other half is pumped downstream. As the strokes reverse the second plunger pumps, the volume charged during the first plungers discharge. Therefore, a continuous flow is obtained, with a slight spike when directions change. This design also provides the advantage of using only two check valves. Thus in theory it is twice as reliable as double action pumps, with a much flatter pulsation profile which is good for microfluidic applications. The drawback of this system is the driver; It is a geared system which is relatively complicated, which makes it more expensive. However, most HPLC pumps adopt this design. (40) Most of these pumps are made out of stainless steel 316 which affords an excellent corrosion resistance, but it is susceptible to pitting corrosion. More expensive options such as Hastelloy 276 are available, but it is not feasible for this study due to cost and manufacturing complications.

1.7.5 Syringe Pump

Although reciprocal, especially HPLC, pumps are an excellent choice for microfluidics, but their price deters the use, especially in underfunded labs. Syringe pumps provide an affordable alternative to HPLC pumps. They are simple to use, have no check valves for non-continuous setups and have a pulsation free flow rate.

Current trends in the open-source community have made these pumps extremely affordable for underfunded labs. Workable models are available that are free to be modified, but quality still lacks behind in commercial models. However due to the nature of open-source technologies it may become a robust system if enough development and financial backing is received. (41)

Syringe pumps, as the name suggests, use a syringe to pump the fluid. The plunger is driven by a screw which is driven by a stepper motor or servo motor. Since the plunger is driven by a screw, which translates rotational motion into linear motion, the flowrate of the pump is proportional to the rotation. Therefore, precise control is required when rotating the screw to deliver accurate flowrates. The main drawback of a basic syringe pump is that the flow can only continue if the syringe is filled. When considering a syringe pump for a large-scale production it is therefore not practical to use simple syringe pumps.

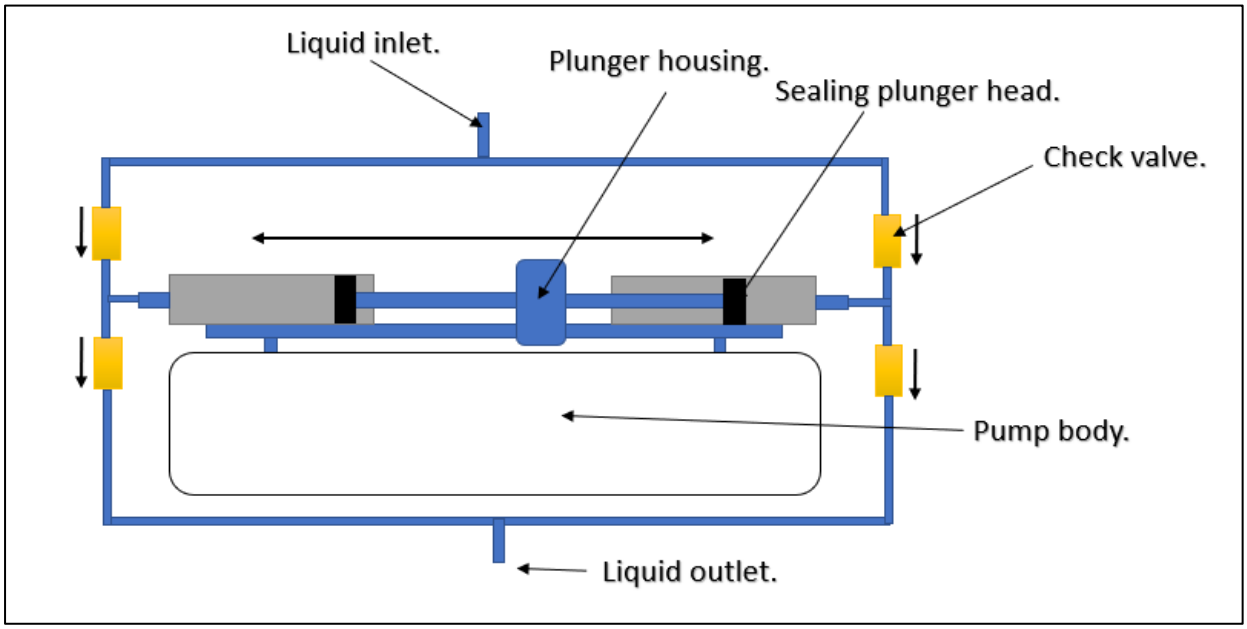

Figure 29: Simplified representation of an automatic refilling syringe pump. (Generated via. PowerPoint)

To get around the volume issue, syringe pumps have been developed that afford automatic refilling. It uses two pumps which pumps 180° out of phase. Some models drive both syringes on the same pump where thepiston is situated in reverse for the reverse phase stroke. As the one is charging the other is discharging, such as in the case of reciprocal pumps. Nevertheless, as with reciprocal pumps this setup also requires check valves. This layout requires up to 4 check valves which greatly increases the risk of the pump to fail.

Another issue with syringes is the seals. Due to the friction over time the seal material will wear out and the risk of leaking will increase. In contrast, plunger pump seals are spring-loaded. As the material lessens with friction, the spring keeps the tension around the plunger and consequently the seal's lifetime is extended until completely degraded. PTFE is a commonly used material for plungers due to its low friction coefficient and excellent chemical resistance. The drawback of this material is that it is susceptible to cold flow creep. (31) This problem can be partially overcome by filling the material, which strengthens the matrix against mechanical forces.

The syringes are usually glass for low pressure applications. Steel syringes are available for high pressure applications, but the prices are high compared to those of glass. Another issue is chemical corrosion of steel syringes. Therefore, glass is usually the default choice. The main drawback of glass is cracking due to a high Young’s Modulus.

1.8 Electronics and Electro Mechanicals.

1.8.1 Microcontroller

As a body requires a brain, so a mechanical object requires a controller. A controller is responsible for doing the calculations and timing which completes the system. Since manual control has too much variability, digital control is preferred for reproducibility of data from one experiment to the next. Microcontrollers are programmable application specific stand alone processors. They have an extremely small footprint and can hence be used in extremely compact systems. One might suspect that this versatility is expensive, however due to developments in the semiconductor industry and large scale commercialization these units are extremely affordable, versatile and energy efficient. (42) The drawback of these chips is the steep learning curve that goes with assembly language. Assembly language is also chip specific which compounds the learning curve even more. To circumnavigate this issue higher level coding languages have been developed. One such example is the renowned C language from which most modern languages are derived in some sense. C has evolved into C++ which affords even more user friendliness. Modern-day trends in the open source community have developed a compiler which uses C++ in conjunction with a library known as the Arduino library.

Figure 30:Clone of an Arduino Mega Developement board (Dragan Simic CC4.0)

In combination with the software, open source development boards have been created. These boards, see Figure 30, allow for easy connections and prototyping

which can be programmed rapidly through a USB port. Another useful feature of these boards is that they are stackable. Printed circuit boards (PCB's) can be designed where the electronic components are embedded in the PCB's. Male header pins can then be soldered into the PCB's that fit the female headers of the Arduino. This provides a wireless system that organises the project significantly.

This system has provided the opportunity for non- engineers/programmers to use it as a foothold into the mechatronics field. This, combined with the internet, has decentralized certain technologies such as CNC methods especially in the field of 3D printing. Since previous examples the equiptment became more affordable by orders of magnitude. This trend is also starting to pick up in sciences where quick development of instrumentation is possible that exceeds the capabilities of manual control of equipment.

1.8.2 Motor driver.

Although MCU's are excellent at providing logic control to a system their chips aren't suitable to handle high currents and voltage. The transistors that handle the logic are microscopic, hence external transistors are required to amplify smaller signals. In some applications, such as stepper motor control, post signal modification is required which converts a 5V digital pulse into a pole inversion in a motor coil. Drivers take control of this external signal modification. They also protect the sensitive MCU electronics from external voltage surges. In some drivers, MCU's may be present which take computational load of the main controller, such as the case of servo encoders. It should be mentioned that a circuit, which is present in most drivers is an H-Bridge. It consists of a minimum of 4 transistors which afford the forward flow and reverse flow of current within a system. Hence, in a DC motor it can rotate the motor forward or backward with relative ease.

1.8.3 Motors

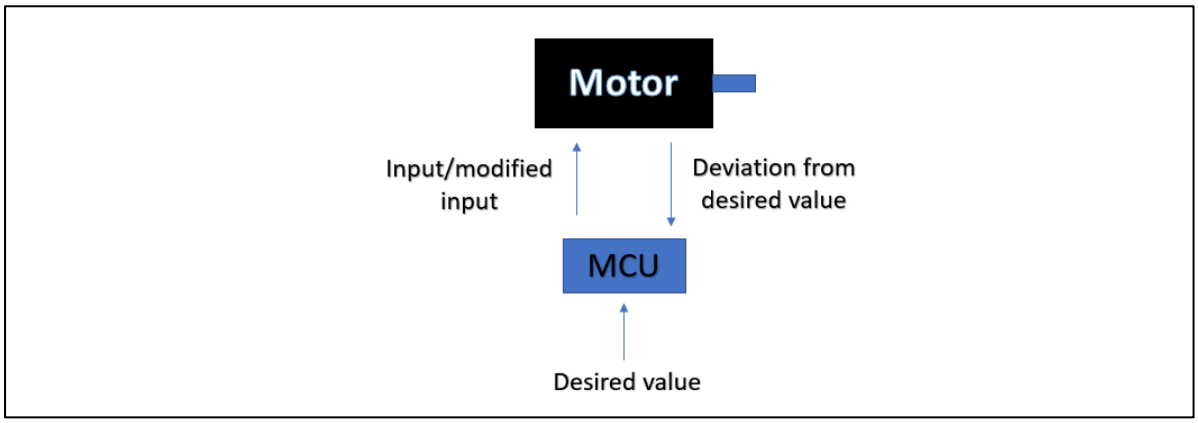

Figure 31: Simplified representation of a closed loop servo motor controller.

Motors convert electromagnetic energy into rotational energy. Based on the context of this study servo motors and stepper motors will be discussed. Servo motors rely on a system of continuous feedback. A system is required which measures the output, such as rotation or position. The output is processed through a control algorithm, such as Proportional Integral Derivative(PID) and then the input power output is updated. This system is known as a closed loop system where errors are corrected. These systems afford more power over a wider output range when it is compared to stepper motors. The drawbacks are that it requires tuning for every application and that it is significantly expensive when compared to stepper motors. Therefore, for the scope of this project servo motors will be excluded as a driver.

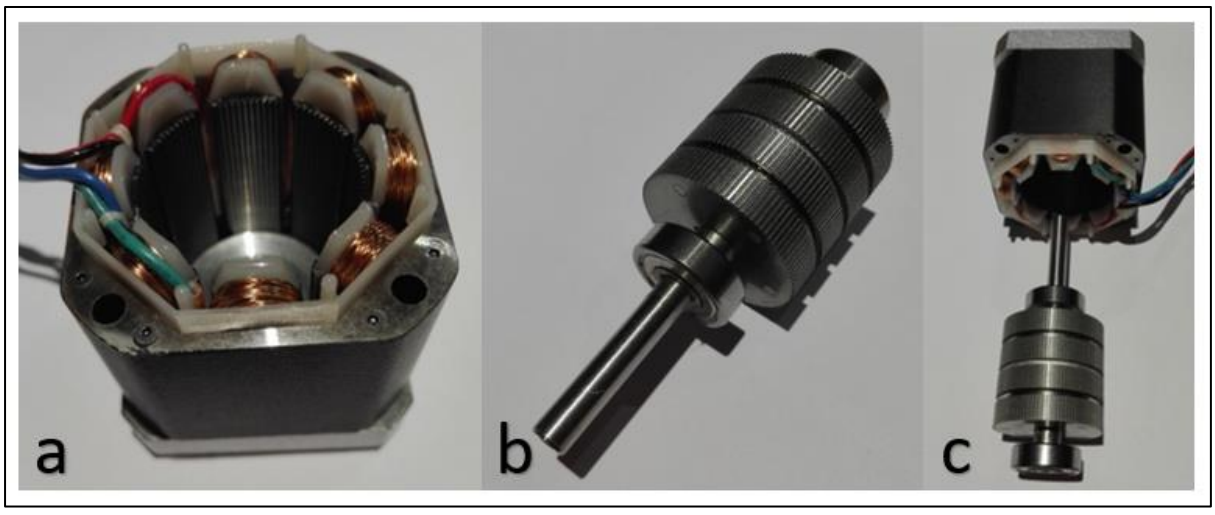

Figure 32: Disassembled hybrid bipolar stepper motor. a:) Stator in which coils are packed with teeth which hold the rotor. b:) Magnetized rotor that fits into the stator. c:) Rotor and stator comparison.

Stepper motors are motors that rotate through digital pulses. Each pulse turns the motor a certain increment based on the magnetic poles. Since the pulse turns the

motor at fixed increment, the system can be open loop which simplifies the design significantly. Common hybrid bipolar stepper motors in which the rotor is magnetized, provide up to 200 pulses/rotation. The stator of a hybrid stepper motor is the coils which the driver energizes to hold the rotors teeth, as seen in Figure 32. The stator has fewer teeth on it which is paired up around different coils. Pulsing different coils creates movement which is the source of the rotation. And synchronizing the pulses in a sequence rotation is obtained. Most conventional stepper motors are limited to 200 steps/rev on full steps. Most modern drivers can micro step. This works by charging two coils at once, but at different currents. The strength of the magnetic field of the two coils will determine to which coil the rotor is aligned the most. Thus, by the careful manipulation of the coil currents the steps can be increased by creating small steps between the motor's stator and rotor teeth. This can be done up to 256 micro steps with current technology, which equals to 51200 steps per revolution. The drawbacks are that the torque between each sequential micro step varies, which can contribute to irregular motion where the power requirement is too much.

1.9 Research questions and aims

For this study a proof of concept pump and reactor will be designed and manufactured. The design will be a hybrid of the beneficial properties of each of the pumps and reactors. The pump will adopt a positive displacement type design. However, it will also use the simplicity of the syringe pump screw driver. The pump cylinder will have a primary and secondary cylinder which is aligned on the same plane. The primary cylinder will charge two volumes while the secondary cylinder is discharging one volume While the secondary cylinder is charging one volume from the primary cylinder, the primary cylinder will discharge two volumes where one volume keeps the flowrate constant. This design requires only two check valves instead of four. A stepper motor will be used instead of a servo motor which is more affordable.

A Hastelloy C276 reactor will be developed which will be clamped instead of bonded to seal its channels. This will allow for easier blockage removal. The channels on the reactor will be etched by laser ablation. To keep the cost down, open-source technology will be employed where possible.

Microfluidics is a useful technology for circumnavigating certain issues that are encountered at batch scale chemistry. But the main problem with this technology is that it is expensive, especially for poorer countries in Africa. Although third world nations could benefit from it the most, it is limited from third world laboratories due to high exchange rates. The questions regarding this research can be summarized as follows.

- Is it possible to design and manufacture a microreactor which is-
- Affordable compared to European counterparts?
- Similar performance to commercial units?
- Able to be manufactured in a non-specialised factory?
- Is it possible to design and manufacture a pump which is-
- Able to accurately dispense at different flowrates?
- Have continuous flow?
- Able to be manufactured in a generic factory?

A novel reactor and pump will be designed, using affordable materials where possible. Fischer Esterification will be used as a model reaction to test the reactor as there are several papers on this which may be benchmarked. Additionally the flowrate of the new pump will be investigated. (43-46)

2. Design and manufacture

The design and manufacturing of the equipment will be discussed separately. Any preliminary studies will be discussed first, followed by the actual construction.

2.1 Reactor

The reactor will be designed to be as “general purpose” as possible. Although microreactor’s internal volume is usually very low, in some cases this is disadvantageous, therefore the volume will be maximized to increase throughput. The reactor should also consist of an inert material to counter any corrosion that might risk the material. The volume of the reactor should also be known to accurately calculate the residence time.

2.1.1 Material selection

Glass is ideal due to its price and chemical corrosion resistance. However the drawback of using glass as reactor material is the requirement of HF and it also requires elevating temperature for bonding the layers. Milling glass requires a high-speed mill with expensive diamond tips. Since these facilities are limited in most labs, glass as a material is omitted.

Polymers may be considered due to their machinability. The drawback is that chemical corrosion resistance is not as good as that of glass, and thermal conductivity is limited. Additionally, elevated temperature chemistry is limited by the polymers’ melting point. As discussed PEEK and PTFE are the two main options, PTFE is easy to machine, but susceptible to creep behavior. PEEK is easy to machine but it is expensive.

Metals have excellent thermal conductive properties. The alloys vary in chemical corrosion resistance, therefore a corrosion resistant alloy needs to be selected. Stainless steel 316 affords excellent machinability as well as reasonable chemical resistance. However chloride pitting corrosion does take place. Hastelloy C276 has superb chemical corrosion resistance, but is very difficult to turn and mill.

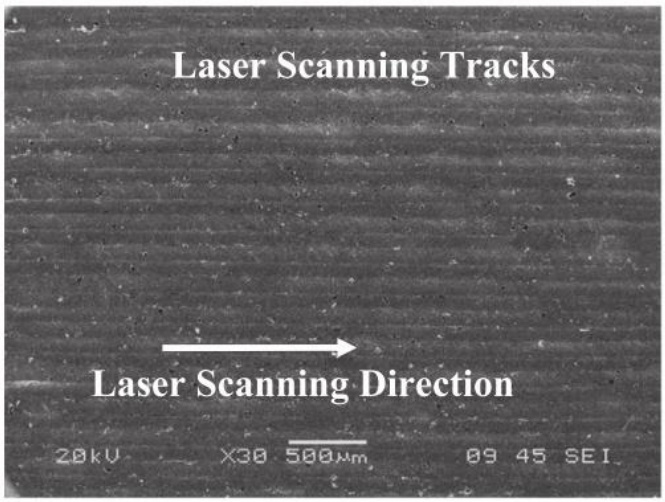

Figure 33: Laser Micro-Textured Hastelloy C276 plate which shows superior hydrophobicity. (34)

One study of Hastelloy C276 has shown that laser micro-texturing, with a CO_2 laser under N_2, has shown to increase the hydrophobicity. (34) The advantage of an increased hydrophobicity reduces the penetration of liquid into the metal and consequently reduces corrosion potential from the liquid. Since Hastelloy C276 is difficult to mill, another approach could be laser ablation. Laser ablation is a non-contact method of machining which would considerably reduce tool wearing for the metal.

2.1.2 Hastelloy C276 etching preliminary study.

Laser ablation facilities weren't available locally, and since the purpose of the project was to make it affordable an alternative route was obtained. A fiber laser engraver was screened for its ablation rate onto hard metals. Hastelloy C276 was not available at that time hence stainless steel was used to ascertain the laser's ablation rate on hard metals. Lines were engraved horizontally across a plate at different amounts of passes to get an estimated range to create a standard curve. These plates were investigated via SEM to establish the feasibility of this technique.

2.1.2.1 Equipment.

- Raycus 20W Fiber Laser with Galvanometer.
- FEI HELIOS NANOLAB 650 (SEM + FIB)

2.1.2.2 Settings.

Table 5: Laser engraver settings.

Scanning speed(meter/min)	**Average power (W.)**	**Frequency (kHz.)**	**Q-Pulse (ns.)**
1,500	19.2	120	30

2.1.2.3 Materials

- 20mm x 60mm x 1,2mm Stainless-steel acid etched plate.

2.1.2.4 Methods

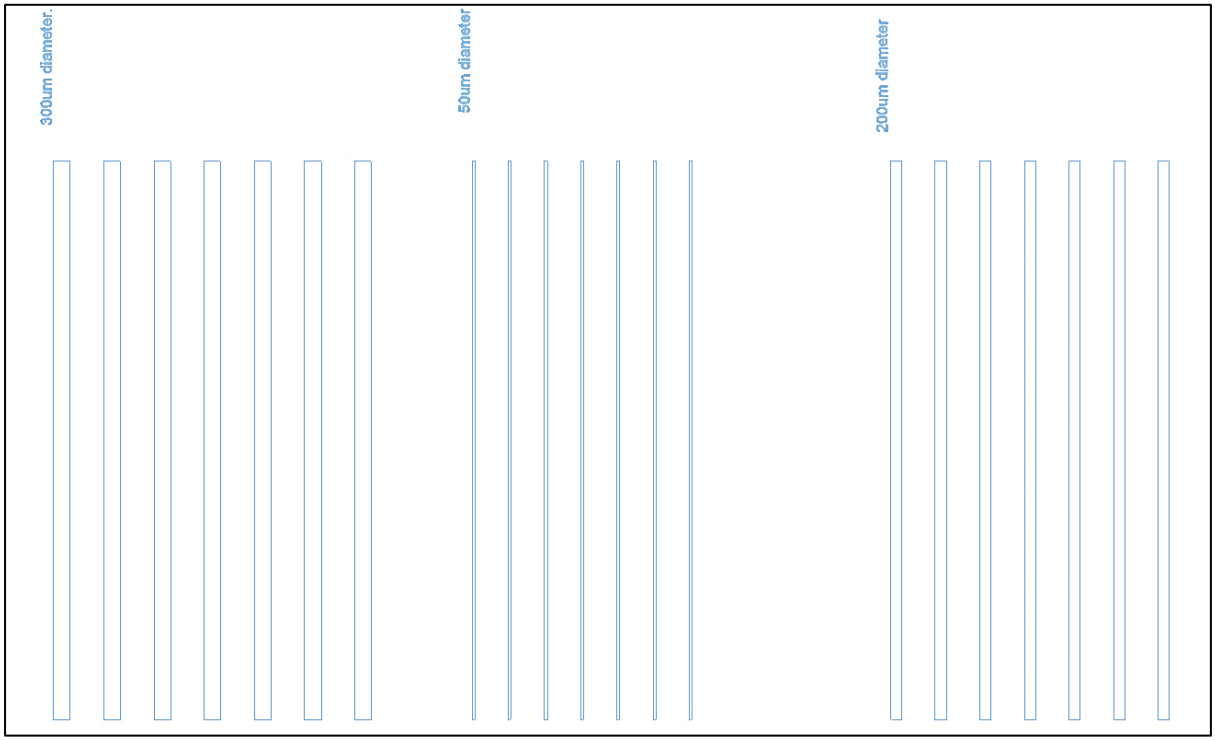

Figure 34: CAD drawing of standard curve grooves. (AutoCad2017)

The CAD drawings of this entire project have been personally done, using Autodesk AutoCAD 2017, by way of an academic license. The engraving was done for different channel diameters within the micrometer range. These channels were engraved multiple times too see how increasing the number of engravings would affect the depth of the channel. Preliminary engravings have been done for 3, 5 and 10 passes(X) to get an estimation of the depth achieved by the number of passes. Each line had a length of 10.00mm with 1.65mm between repeating areas on the adjacent line.

Acid etched stainless steel 316 plates were obtained from the engraving service. These plates' dimensions were 20mm x 60mm x 1,2mm with a slight opaque discolor due to the etchant. Visually the edges of the grooves were not affected significantly by the heat.

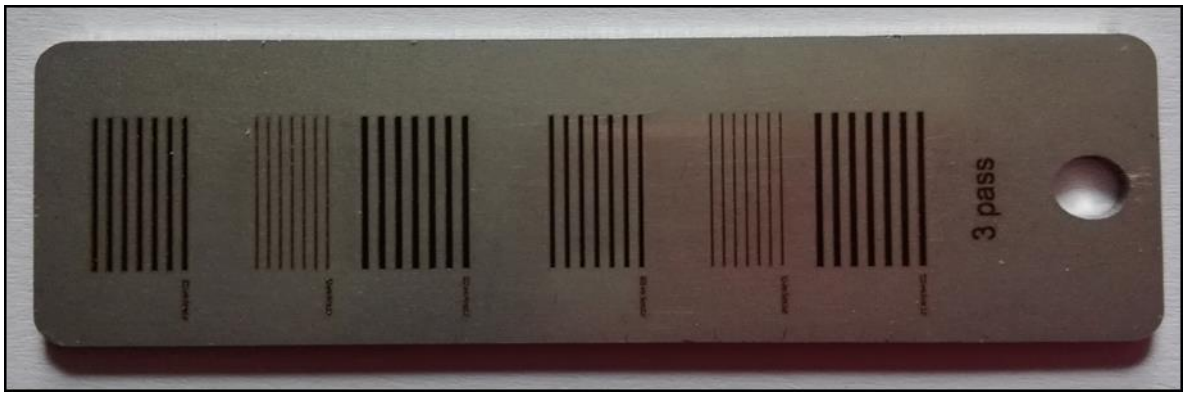

Figure 35:3 X laser engraved stainless steel 316 plate.

These plates, Figure 37, were washed in acetone to remove any contaminants on the surface. The purpose was to reduce electron accumulation on the surface which is caused by non conductive contaminants. Perpendicular and 30° electron micrographs were taken and compiled for comparative purposes. Assistance was provided by the Centre of High Resolution Transmission Electron Microscopy on Nelson Mandela University's South Campus.

2.1.2.5 Results

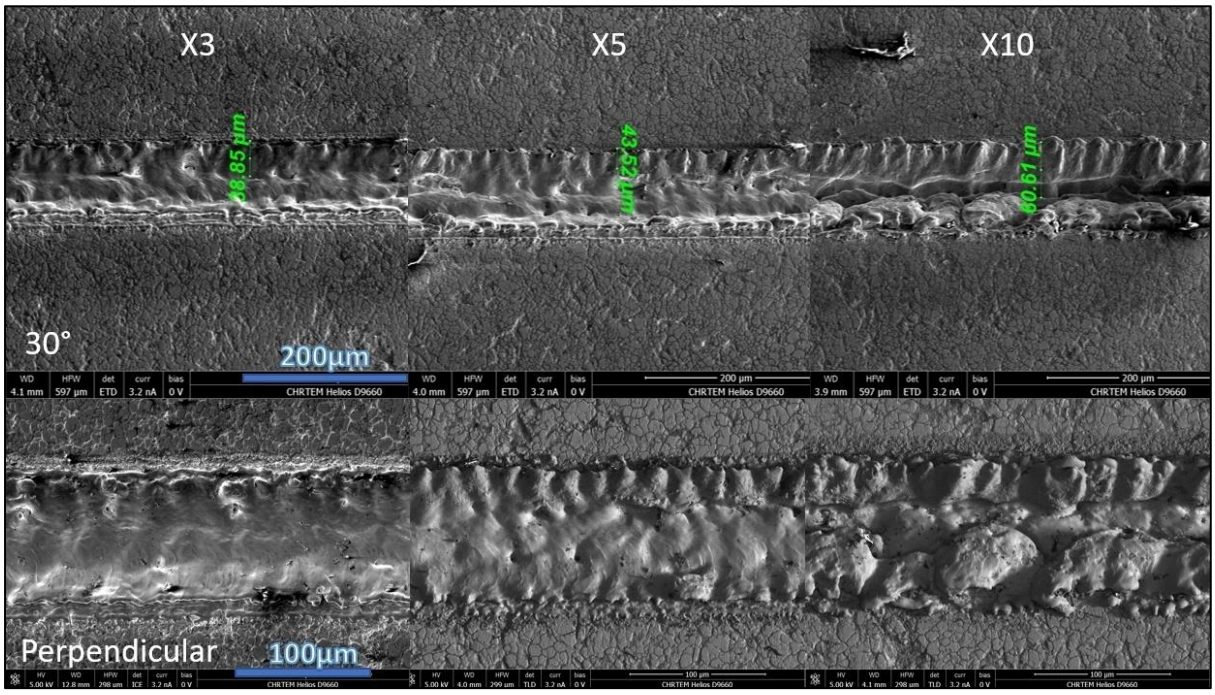

Figure 36: 50µm channel width of 3x, 5x and 10x. Top Shows the 30° views from the perpendicular angle and bottom from the perpendicular view.

For the 50µm channel, see Figure 36. The engraving had a notable effect on the metal. The width of the channel was not 50 µm, however when considering the inner channel, the width was much closer to 50µm. The average outer width was 90.6µm, thus a 45.3µm edge is present on each side, assuming the calibration was correct. However the calibration was done in Table 6.

This effect can be seen more clearly in the 200µm (Figure 37) and 300µm (Figure 39), where an inner ridge is clearly present with a flat surface on the inside. As the depth increased, by increasing the number of passes, the roughness increased significantly for stainless steel 316. It is suspected that the roughness is due to metal sputtering which becomes more pronounced as the steepness of the channel increases. However, a channel could be observed although its surface is very irregular. From these micrographs it was difficult to estimate the profile of the channels, therefore cross-sectional shots were prepared for the following experiment.

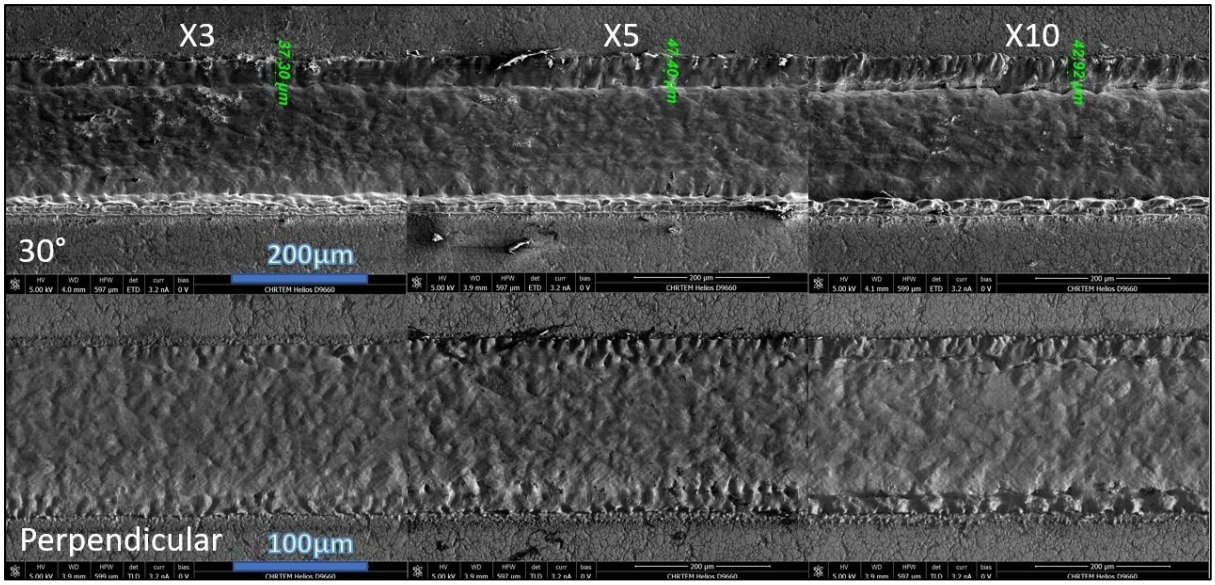

Figure 37: 200µm channel width of 3x, 5x and 10x. Top Shows the 30° views from the perpendicular angle and bottom from the perpendicular view.

As seen in Figure 37, the 200µm channel shape was much more uniform. The shape was trapezoid instead of square in the middle of the channel and slightly raised. At the 10X etched there appears to be a ridge that was not present on the X3 and X5 plates. At the planar regions the surface appears crystalline. This could be due to the scanning pattern; however, the scanning pattern was in a zigzag pattern which does not fit the pattern observed above. Therefore, this was most likely due to selective ablation that can be attributed to the crystal structure of the metal.

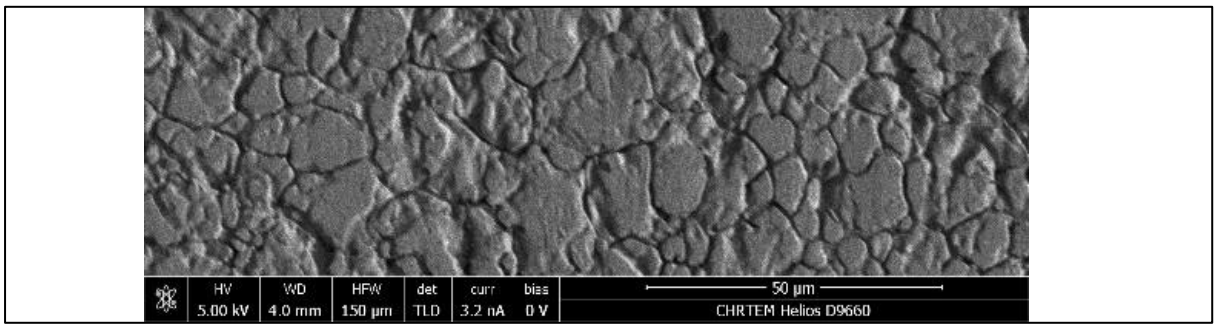

Figure 38:SEM of non-engraved acid etched surface.

Evidence for the crystal structure can be seen in Figure 38, where the regions between the crystals has selectively been etched. If the structure was amorphous, etching would have been uniformed in all directions.

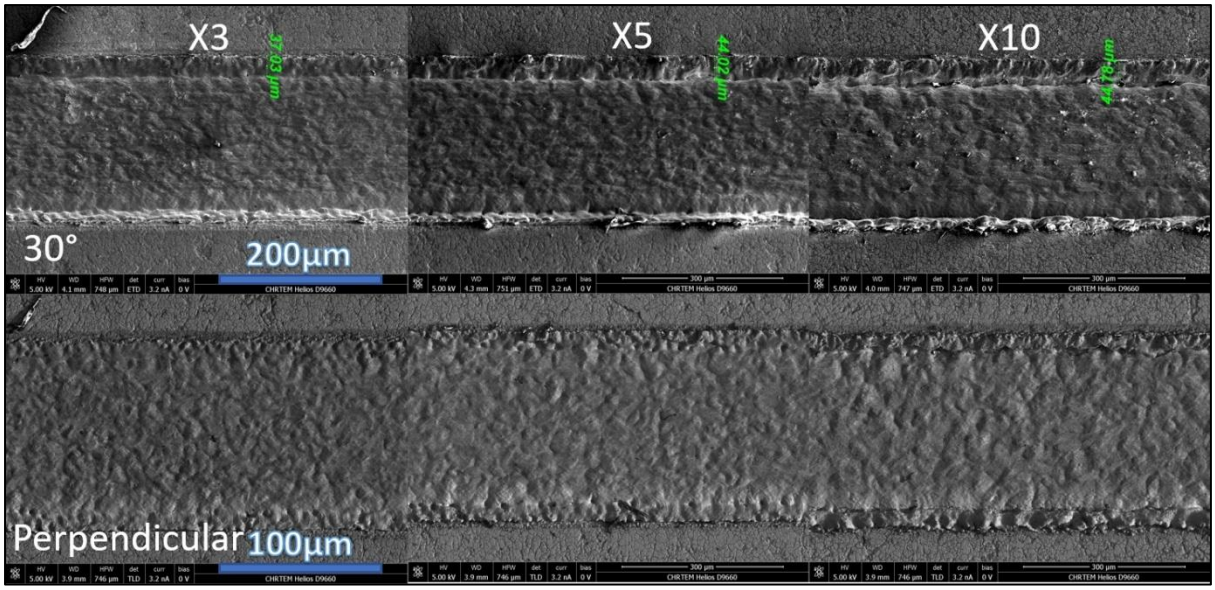

Figure 39: 300µm channel width of 3x, 5x and 10x. Top Shows the 30° views from the perpendicular angle and bottom from the perpendicular view.

Figure 39 has a similar structure to Figure 37. However, due to Figure 37 being 200µm, it has a deeper aspect ratio. The accuracy of the lasers ablation dimensions could be determined from these micrographs.

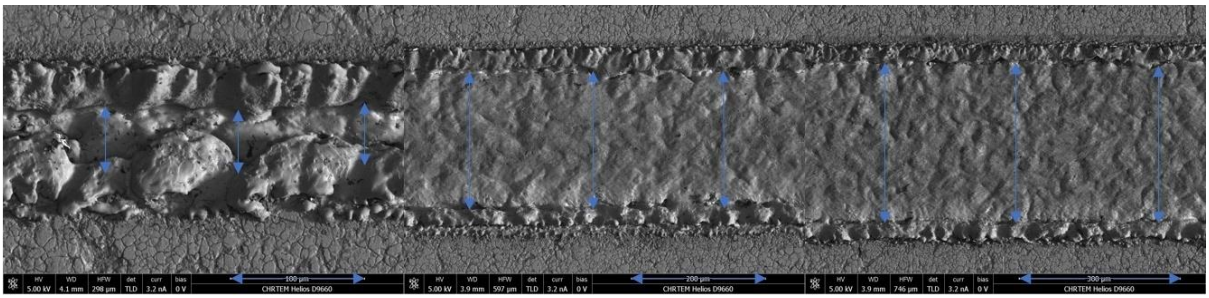

Figure 40:Measurement of 10X channels.

The width of the channels was determined to show the calibration status of the laser. Since the engraving service was a non-scientific service and primarily geared towards aesthetics the calibration had to be done.

2.1.2.6 Summary

Table 6: Laser calibration from stainless steel plates.

Channel (µm)	Observed avg. (µm).	SD (triplicate)(µm).
50	48,5	1,38
200	204	0,379
300	297	1,92

Table 6 shows that the width of the channels is within reasonable limits when compared to the ideal dimensions. Therefore, this system was used to mill the channels on stainless steel 316 as well as Hastelloy C276. However, depth determination was still an issue.

2.1.3 Standard Curve Preparation

2.1.3.1 Equipment

- Leica DM500 microscope.
- Raycus 20W Fiber Laser with Galvanometer. (Same settings as Table 5)
- Dremel 4000 with EZ grinding clip.
- MULTIPOL 10 Polishing Machine.

2.1.3.2 Materials

- 3 Hastelloy C276 20mm x 60mm x 3.2 plates (Hydrocut)
- Sanding paper grid (320, 400, 600, 800, 1200, 1800, 2500, 3000)
- Conductive Polymer

2.1.3.3 Methods

Since the channels appeared shallow, the following plates were engraved at a higher number; namely 100X, 200X, 300X and 400X. Since the melting point of Hastelloy C276 is higher the explosion temperature would also most likely be higher, therefore more passes would be required to attain the same depth.

Another requirement was to determine the depth of the channel; thus, a cross-sectional cut of the material was prepared. The plates were engraved in the same

manner as Figure 34, except that 3 channels were engraved instead of 7. This was to save time on the laser.

The plates were first polished manually from a 320-grit disc in sequential jumps to 3000-grit disc. The plates were then engraved at 100X, 200X, 300X and 400X

The cross-sections of the laser engraved plates were cut using a Dremel. It was observed that the Hastelloy C276 did not have any sparks, which suggests its resistance towards oxidation. Since the cutting damages the cross-sectional profile, further processing was required. CHRTEM assisted in inlaying the plates within a conductive polymer. The top was further polished with a diamond coated plate until the cross sections were free from artifacts from the original cut. The product of this can be seen in Figure 41.

Figure 41: Cross-sectional cuts of Hastelloy plates that is polished in a conductive resin inlay.

As it can be seen in Figure 41, the finish on the plates, the cross-section was mirror-like. Careful observation on the edges the channels could be observed with relative ease. The dark polymer also increased the contrast making visual inspection significantly easier and hence the need for SEM was omitted.

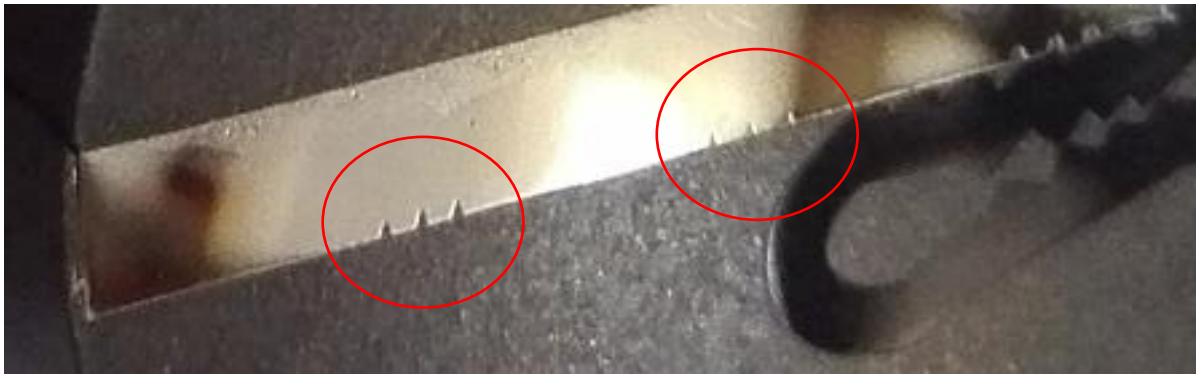

Figure 42:Zoomed in section of figure 42 showing penetration depth of the ablation.

Figure 42 shows the top right unit's zoomed in section. As can be observed, a significant depth has been achieved using this method. Further investigation was done using light microscopy.

A Leica DM500 microscope with built in camera was used to take the images. Both the 10X and 40X objective were used. The dimensions were irregular therefore the surface of the cross-sectional area was utilized, using Image J, which is an open-source scientific image processing system.

Figure 43:Example of processing using image J. 300µmX 200µm image selected.

Figure 43 was obtained through optical microscopy. Image J was used to further process the image. The image's scale was first calibrated at the scale bar below. After the calibration, the area of each of the plates were determined. An example can be seen in Figure 44.The top edge was estimated and the protrusion from the top of plate was ignored as an contributor to volume.

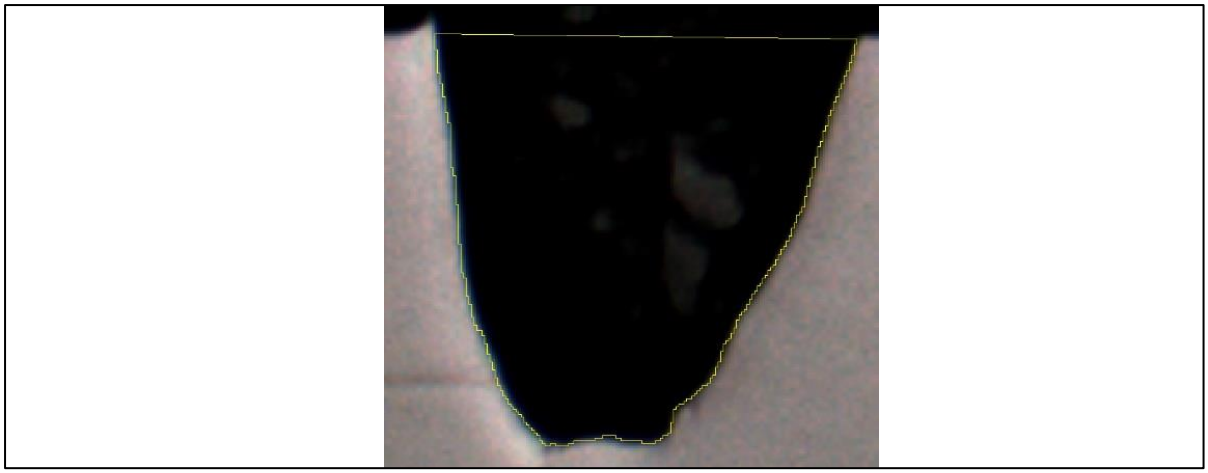

Figure 44:Example of area determination using image J.

All the following areas, example in Figure 44, were processed in triplicate for reproducibility. The average value and the standard deviation was obtained from the triplicate values.

2.1.3.4 Results.

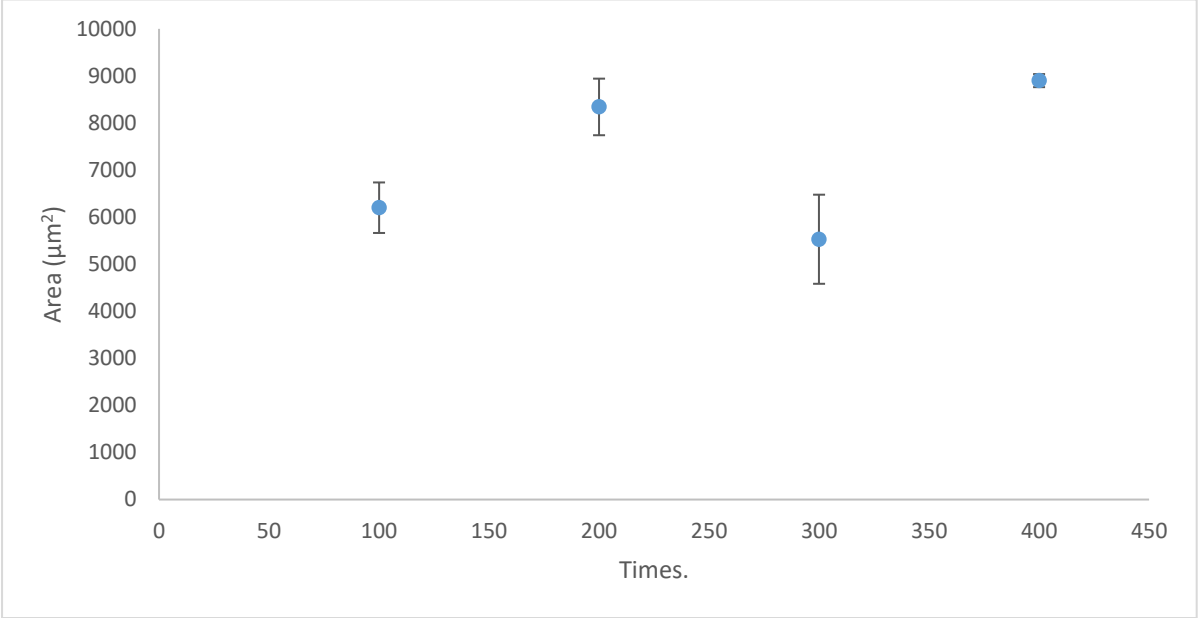

Figure 45: 50µm Channel cross-sectional area vs engraving number.

Figure 45 shows the curve obtained for the 50µm average cross-sectional area vs. the time of engravings. A logarithmic function was expected for the regression model. The reason for this being that as the depth of the channel increases the surface of the material becomes more distorted. This creates less perpendicular absorption of light which is not as efficient for laser ablation. Additionally, the V-taper

of the walls reflects more and more light. Therefore, the mechanism of ablation is more complex.

A third order polynomial was suggested for Figure 45. The Residual is a measure of deviation from the model's perfect value. A value of 1 indicates 100% of the information which can be explained through the model.The residual squared suggest the model could only be explained 73.4% therefore the data is not as reliable as the 200µm and 300µm graphs (see Table 7). Additionally the 200X value was far higher then expected for the model, thus the model was excluded .It is most likely that most of the light is reflected and the intensity of the beam is reduced. Further investigation is required to accurately model the above mentioned graph.

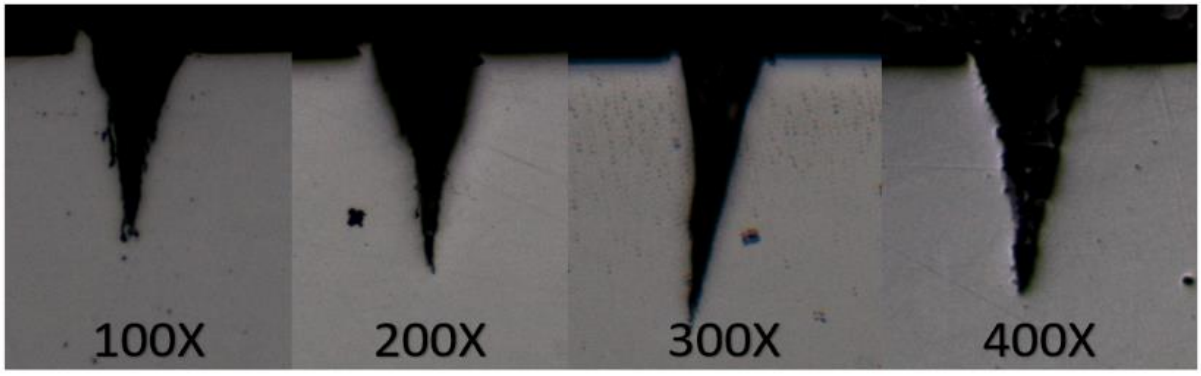

Figure 46: Closeup view of cross-sections of the 50µm plates at different engraving numbers.

The standard deviation vs. area in Figure 46 was also large when compared to Figure 47 and Figure 49. For the 50µm graph the efficacy of the ablation rate declines significantly as times of ablation increase. Since a perpendicular incidence affords the most absorption of energy, the initial ablation rate would be higher. Another factor which can contribute to this is that of the absorbance of heat by adjacent material mass. As the depth increases, the absorbance of heat will intensify due to increased material mass around the ablation zone. This will reduce the intensity of energy delivered at the region being vaporized .Microscopy revealed that the cross-sections had similar morphological features. It should be noted that there is no planar bottom, which is unique to the 50 µm plates. There is also variability in the wall of the channels which is most probably due to the metal's crystal structure or sputtering. However further topographical microscopy is required to confirm this.

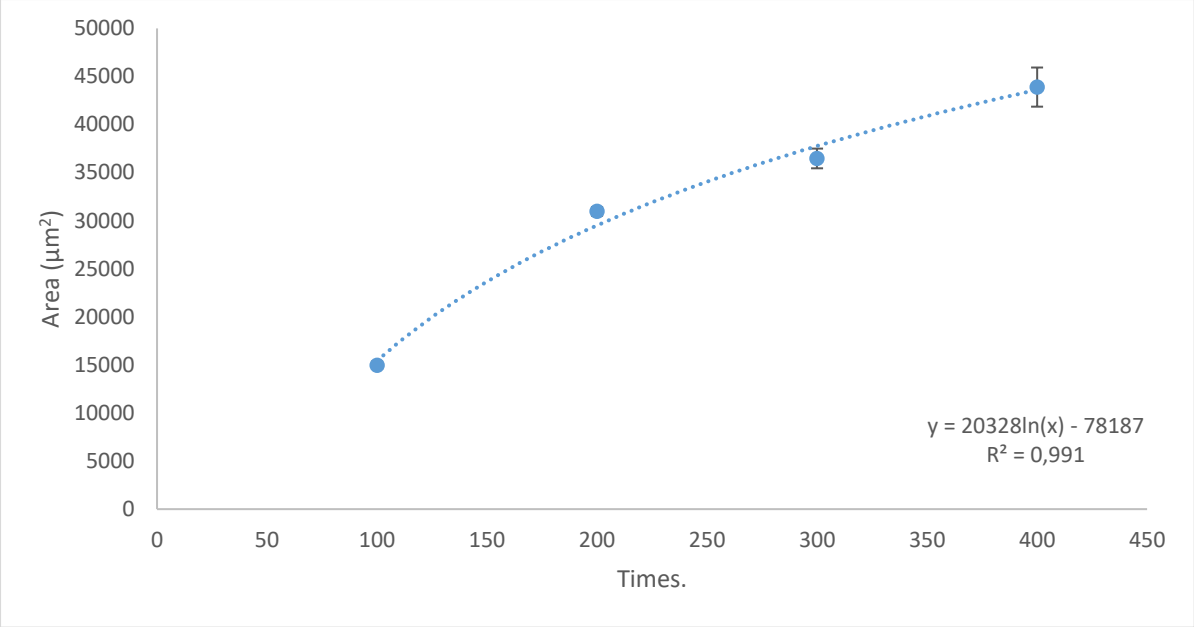

Figure 47: 200µm Channel cross-sectional area vs engraving number.

Comparing Figure 47 to Figure 45 shows that Figure 47's slope is steeper, which suggest the ablation efficacy is more efficient. A natural logarithmic graph has been obtained which suggests that efficiency decreases as the depth increases. The correlation of this model also fits the data better when compared to the 50µm values. The magnitude of area vs standard deviation is also lower which suggests the data is more reliable than Figure 45's data. As the engraving number increases the size of the channel clearly increases, which was not as obvious with the 50µm channels.

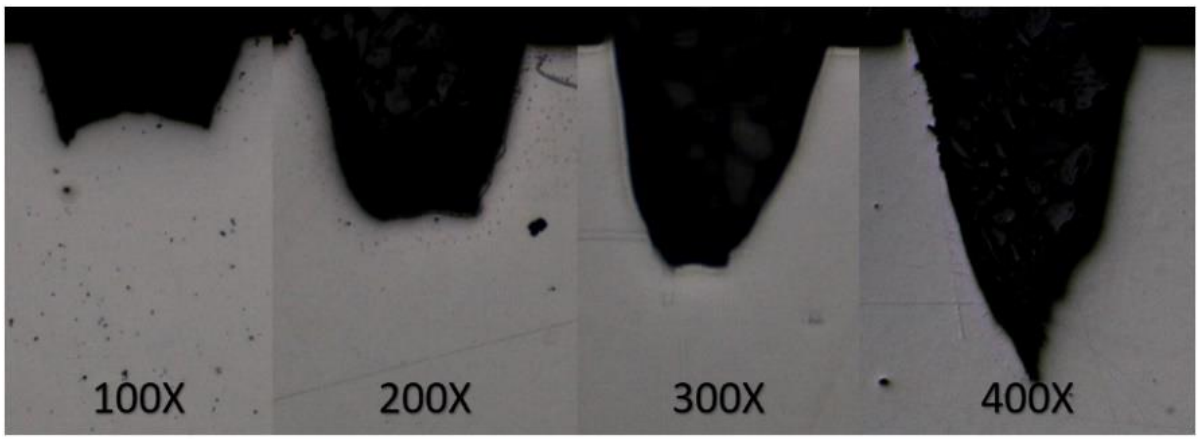

Figure 48:Closeup view of cross-sections of the 200µm plates at different engraving numbers.

For lower engraving numbers the channel had a trapezoid shape to it and as the number increases a triangular shape is obtained. It is clear from Figure 48 that the slope propagates itself at the same angle as the depth increases. Two possibilities

may account for this. The first being that the angle of the slope favours the reflectance of the photon more than the absorbance. The reflected photons would focus close to the base depending on the slope angle. This will increase the ablation rate at the base, which seems to happen in Figure 48.Another possibility could be that at the bottom edges heat becomes absorbed in the vertical and horizontal plane, therefore the etching direction of the channel will favour the side with less mass which is more easily vaporised. This was not further investigated due to the scope of the project. However, this effect is represented by the model obtained in Figure 47, where the increase in depth reduces ablation rate.

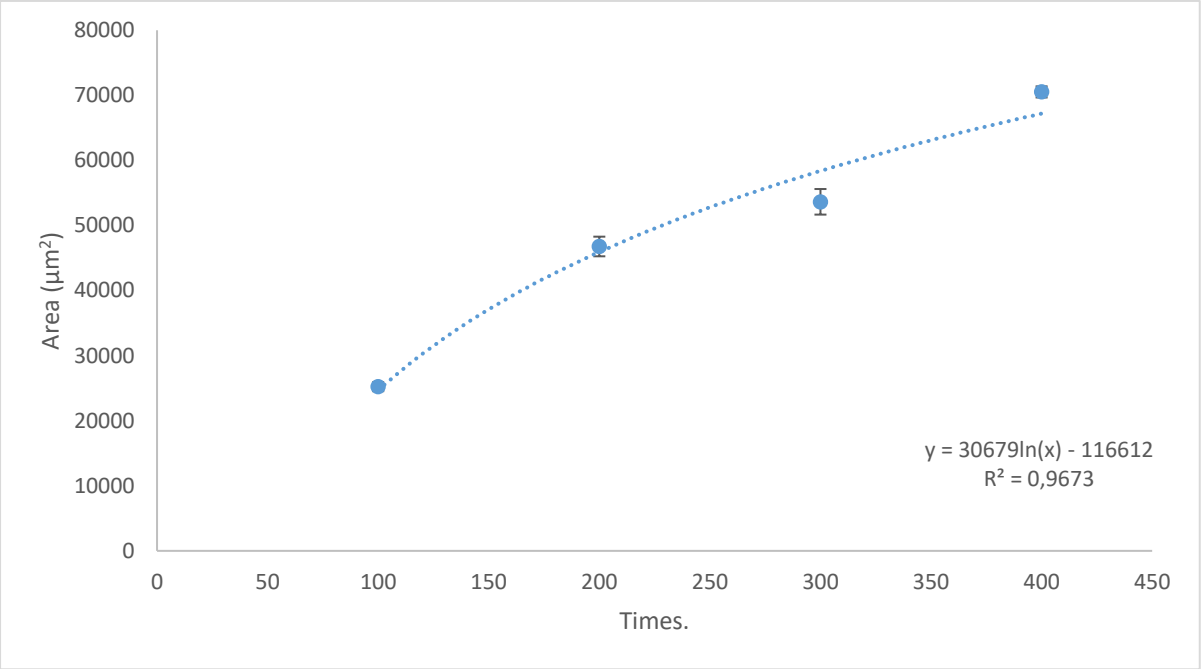

Figure 49: 300µm channel cross-sectional area vs engraving number.

In Figure 49 the cubic function's contribution is more (compare to Figure 47). The linear contribution is steeper than both previous graphs, which is expected with a larger channel width. From the regression all 3 channel diameters are engraved through the same mechanism.

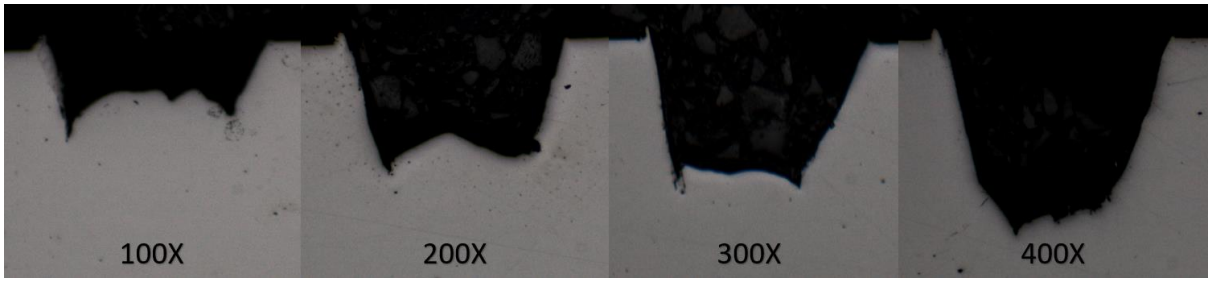

Figure 50: Closeup view of cross-sections of the 300µm plates at different engraving numbers.

In Figure 50 the same pattern was observed as in Figure 48, where the bottom width reduces as the depth increases. It should be noted that the irregularity on the bottom of the channels is much more asymmetric when compared to Figure 48. Since laser ablation is a slow procedure, speeding up the process is essential for economic viability. While comparing all three channels, there appears to be numerous factors at work which are influenced by channel width. Comparing these to each other needs to be done in a numerical method in order to draw a clearer conclusion. The width of the channel is constant in each graph, therefore the whole model needs to be considered for its efficacy.The area underneath each graph will be calculated between 100X and 400X through integration, and normalised according to its width. Normalisation will afford easier comparison to see which width removes the most material for its fluence.

Table 7:Standard curve's regression model's integration.

Graph	Function	$\mathbf{R^2}$
50µm f(x)	$y = 0{,}000839x^3 - 0{,}576596x^2 + 118{,}243068x$	0.737
200µm f(x)	$y = 20328\ln(x) - 78187$	0.991
300µm f(x)	$y = 30679\ln(x) - 116612$	0.967
50µm ∫f(x)·dx	$y = 59.1215\ x^2 - 0.192199\ x^3 + 0.00020975\ x^4 + C$	
200µm ∫f(x) ·dx	$y = 20328x\ln(x) – x – 78187x + C$	
300µm ∫f(x) ·dx	$y = 30679x\ln(x) - x - 116612\ x + C$	

Table 7shows the models and integrated models obtained from Figure 45, Figure 47 and Figure 49. Using the fundamental law of calculus, the area under the model's curve will be calculated for each function between the 100X and 400X range. The fundamental law of calculus for this range gives the total area under the model between the 100X and 400X region. This area represents the total efficiency for this process at that width. Further, the area will be divided by the width to normalise the

data for comparative reasons. A unitless value was obtained for each function. This value is a measure of how efficiently the ablation takes place at a certain width.

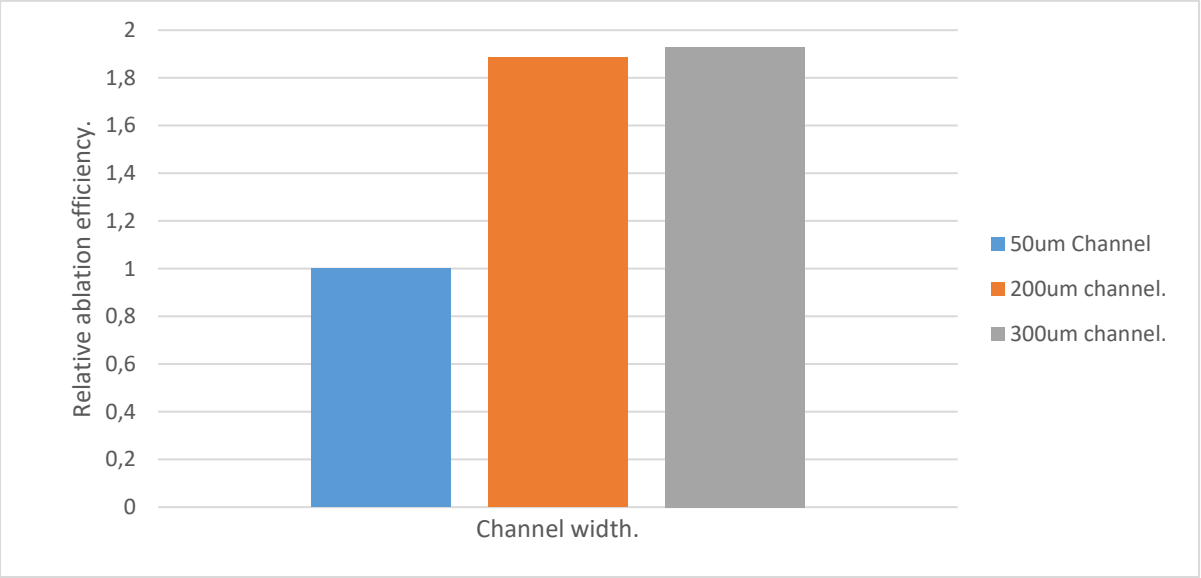

Figure 51: Ablation efficiency vs. channel width between 100X and 400X.

In Figure 51 there is a clear progression of ablation efficiency as the channel width increases. However, the greatest increase of efficiency takes place between the 50µm and 200µm. After 200 µm the increase in efficiency becomes depreciated. For the reactor to have maximum surface to volume ratio one needs to decrease the channel width as much as possible, without reducing the efficiency for affordability. Additionally, by increasing the width by 50% increases the etching time by 50%, therefore the additional time will not be worth the extra efficiency gained.

2.1.3.5 Discussion

Further investigation between 200µm and 50µm would be beneficial to narrow the channels even further. But for the scope of this project the 200µm channel width will be selected for the reactors channel width, and the mixing structure would contain parts of all three widths. It should be stressed that Figure 51 is for comparative purposes only and not to quantify individually.

The etching above was done with a 20W laser. Stronger lasers are commercially available which will further reduce the etching time. However, the results above are only limited to the laser used. Generally ablation lasers have a stronger laser compared to what was used therefore comparing data was not possible, especially

with a rarer metal like Hastelloy C276. However, a 20W laser was sufficient for this process although most likely not ideal.

2.1.3.6 Summary

Both Stainless steel as well as Hastelloy C276 were shown to be suitable for ablation, however Hastelloy was chosen as the preferred material due to its preferred chemical resistance. All the dimensions from 50µm to 300µm will be used, however only up to 400X engraving numbers. due to increased inefficiencies as the depth increases .

2.1.4 Reactor layout

The main idea behind the reactors layout is the versatility. For the reactor to be useful it needs to be as general as possible. Most reactions require two reagents which are mixed together, reacted and often quenching. Therefore 2 inlets are required, a mixing structure where two inlets are mixed a reaction zone, quench inlet followed by a mixer which leads to the outlet. A multi-level split and recombine mixer reactor was attempted with a laser cutter, however due to sputtering the microstructures got blocked and therefore another method was explored.

As discussed in the mixer section of the introduction, a three-split mixer provides a simple yet effective design for a mixing structure and therefore this was chosen to be the mixing structure. (19) This structure provided the user the ability to stack the units in series, where after each pass it gets, mixing is increased. The two-split had a slightly smaller mixing index compared to the three-split according to literature.

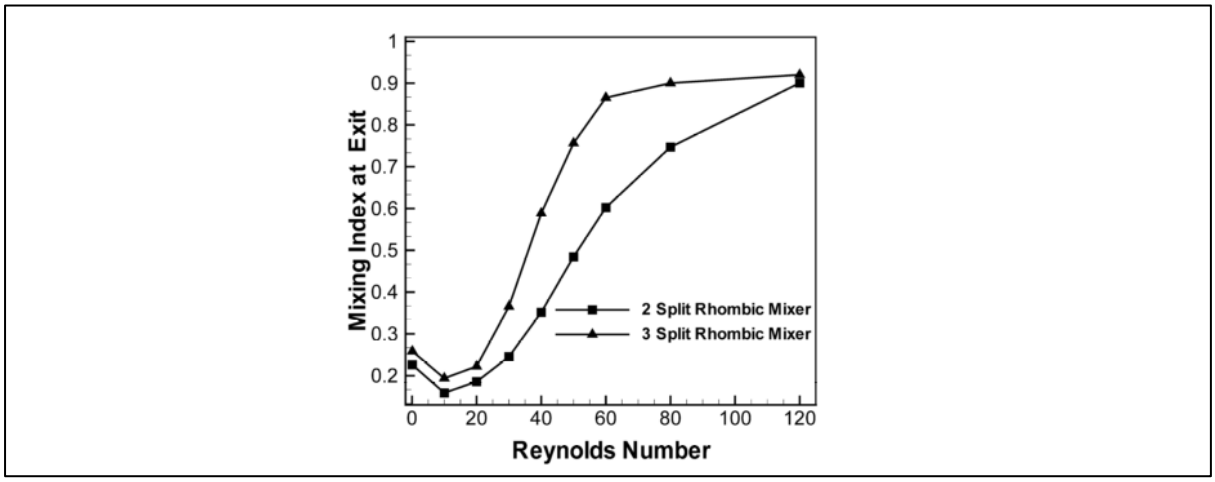

Figure 52:Mixing index of 3 split rhombic and 2 split rhombic mixers at different Reynold's numbers. 4 repeating rhombic units were used in this study. (19)

The rhombic structure is repeated 12 times. The structure also is easy to manufacture with 2D laser etching, which will be used for this study.Contrariwise, a T-mixer would only allow the presence of one intersection. This was placed at the inlet as well as the outlet where the reaction becomes quenched in specific reactions.

2.1.5 Reactor dimensions

As discussed in the standard curve's study, the reactor's width will be 200µm. The engraving will be at 400X which delivers an average depth of 441µm with a 22µm standard deviation. In Figure 48 the shape is triangular. For slower reactions the distance of the channel needs to be maximized to afford maximum residence time. This greatly improves chemical throughput for slower reactions. The drawbacks of this is the increased backpressure, increased engraving time as well as higher possibility of blockages. If the blockages can be reduced the higher throughput would outweigh the increased back pressure, since the dimensions are slightly larger compared to other similar commercial units. The following Drawing illustrates the intended design.

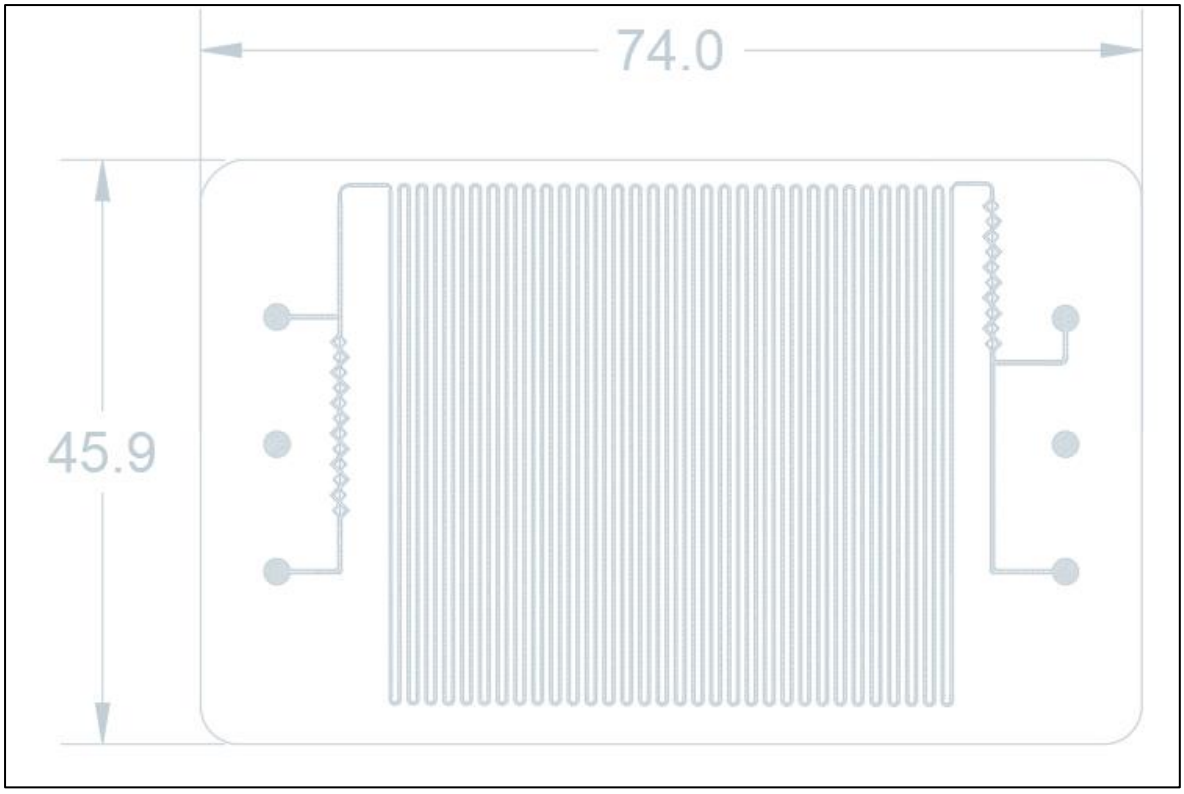

Figure 53: Reactor design CAD file.

Figure 53shows the CAD design of the reactor.The reaction parts channels length is 40mm long with a circular connecting path between each with radial distance of 0.25mm. Therefore, the distance between each adjacent channel is 0.5mm. There are 64 bends in the reactor zone.Therefore, the distance of channel is approximately 2.56m.The volume of the reaction zone is estimated to be 194,29µL based on the average dimensions obtained from the distance and cross-sectional studies.

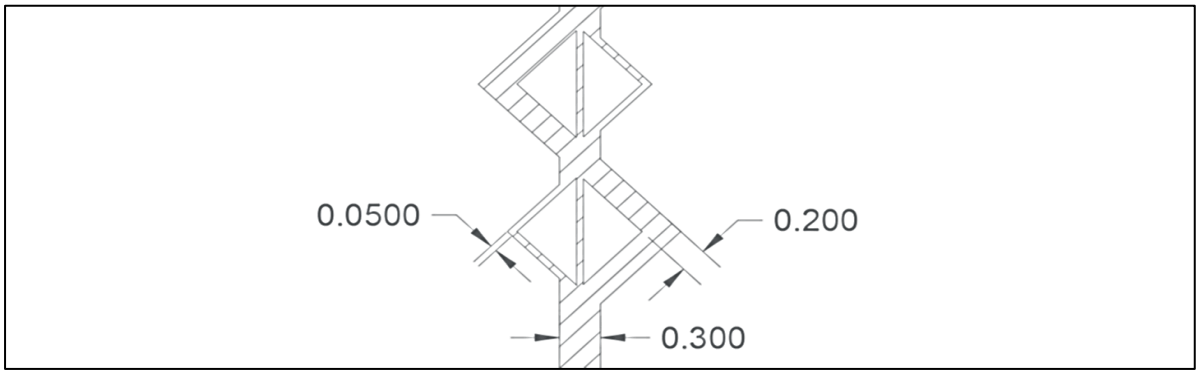

Figure 54:Zoomed in region of three-split mixer on reactor surface.

The mixing structure design can be seen in Figure 54. Dimensions of the mixing structures were obtained from literature. Figure 52's simulations have been done on the same dimensions. The smaller dimensions are 50µm while the larger are

200µm. The smaller channels disrupt the flow through the orthogonal shape. This structure repeats twelve times, three times more than the litrerature's, to insure proper mixing.

2.1.6 Reactor disc manufacturing.

2.1.6.1 Equipment

- Raycus 20W Fiber Laser with Galvanometer. (Same settings at Table 5)
- Leica DM500 microscope.

2.1.6.2 Materials

- Hastelloy C276 40mm x 60mm x 3.2 plates (Hydrocutted)
- Sanding paper grid (320, 400, 600, 800, 1200, 1800, 2500, 3000)

2.1.6.3 Methods

Since Hastelloy C276 is a wrought metal, the surface had to be treated to smooth it. The surface of the plates had a rough appearance. The dimensions, 40mm x 60mm, did not fit in the polishing machine used. The plate also did not fit on a surface grinder due to its ferromagnetic properties, therefore the polishing was done manually. It was polished on a planar metallic surface to minimize rounding on the corners. The polishing started at 180 grid paper, and progressed up to 3000 grid sanding disc. The sequences of sanding were 180, 320, 400, 600, 800, 1000, 1200, 1500, 1900, 2500, 3000. The jump in coarseness was reduced due to the metal's hardness. Too large of a jump drastically increased the polishing time. The plate had a mirrorlike finish after the polishing process.

The polished plate was submitted to the engraver at the same settings as in Table 5. The CAD file in Figure 53 was engraved on it at 400X.

2.1.6.4 Reactor etch results.

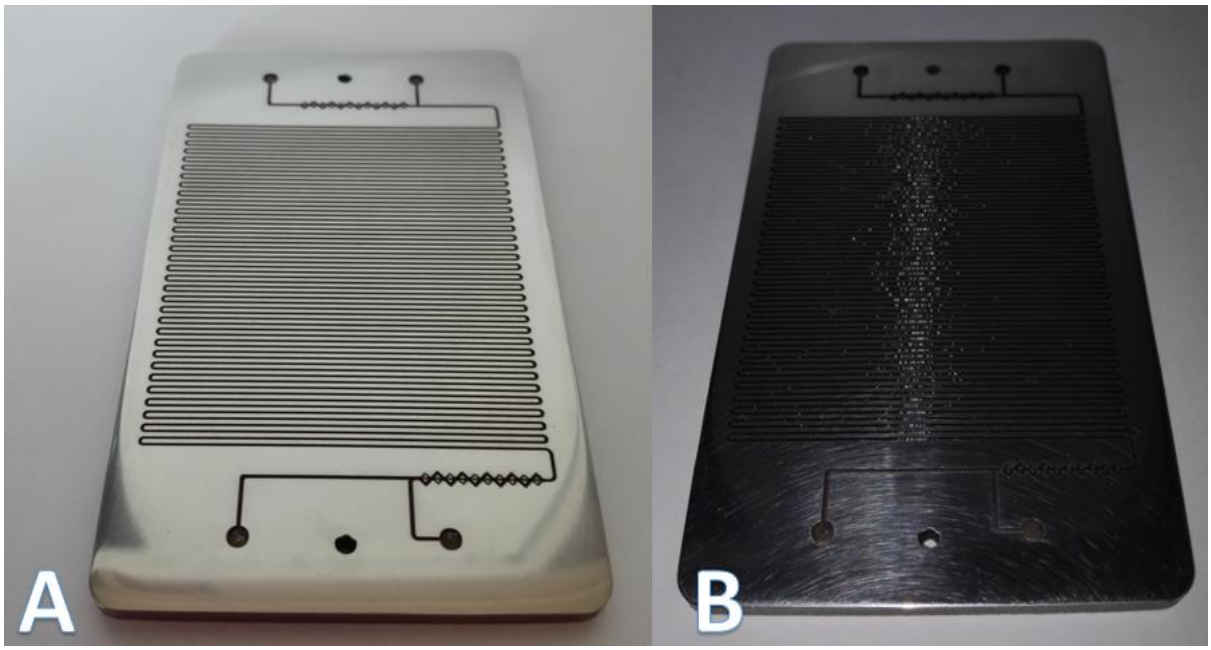

Figure 55: Photo of reactor at different angles of light. A:) Light from behind on a diffused surface. B:) Light from camera.

Figure 55 shows the photographs obtained from the etched reactor. Two angles of lighting were selected to highlight distinctive features. Part A highlights the flatness of the surface. Although steps were taken to minimize rounding at the corners, it still happened. Other methods of polishing need to be investigated to keep the surface flat. However, the slightly raised area at the reactor zone might improve the sealing ability. Part B highlights the surface finish of the reactor. As can be seen, slight rotations are present on the surface. This is most likely due to insufficient polishing. It should be mentioned that the process took hours, therefore a mechanised system would be superior for polishing. An interesting feature was the reflection of the channel walls from the camera's light. Since the laser engraving took place at elevated temperatures it was expected that some oxidation would be present, however the reflective surface within the channels highlights Hastelloy C276's superior oxidation resistance compared to other more common alloys.

The work-piece was too large for Scanning Electron Microscopy (SEM). Therefore, its surface analysis had to be done with light microscopy. Atomic force microscopy was considered. However the cantilevers used are not suited to analyse steep overhangs such as the channel, and the scanning area orders of magnitude is smaller than the reactor's surface. Therefore, light microscopy was used to

investigate the integrity of the structures. Further processing combined with focal distance manipulation afforded a pseudo 3D structure. The depth was calibrated with the 200µm 400X cross-sectional piece in Figure 48.

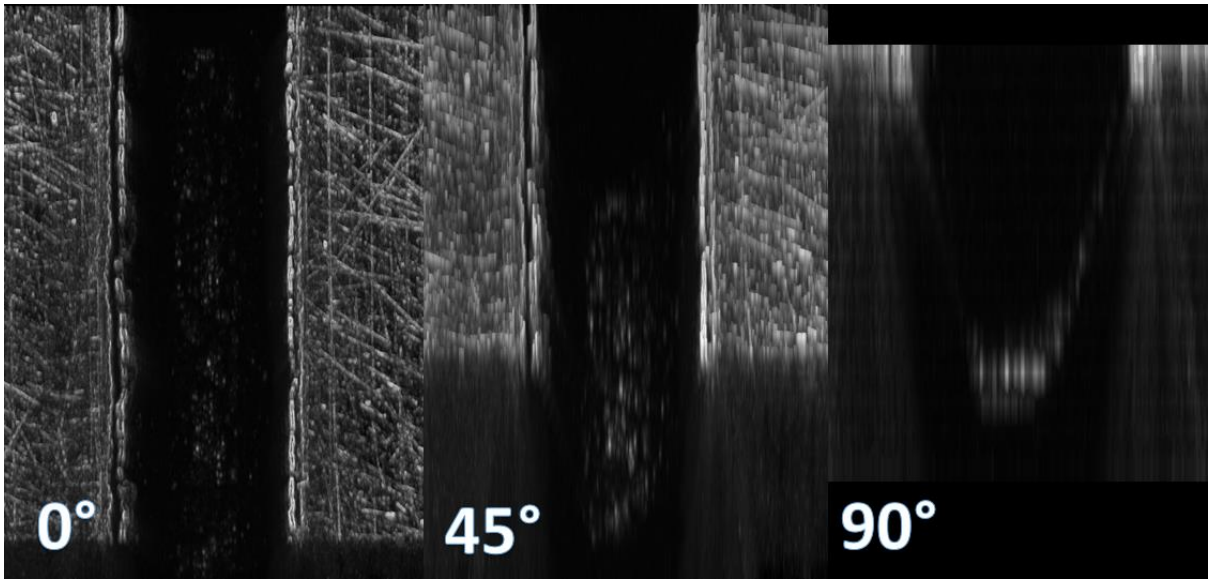

Figure 56: 200µm channel in middle of reactor at 0°, 45° and 90°.

Figure 56 was compiled as stated above. The rotation was done in the X-axis to show the bottom of the reactor. At the 90° angle the channel has a symmetrical shape. However at the bottom of the channel it appears that the structure is rougher than the sides. It is expected that as it goes deeper and approaches the V shape the roughness will reduce. The top surface has shown that the polishing was incomplete and further polishing is required to obtain a smooth surface. Another 3D image was generated where it tilted in the Y-axis and a uniform bottom depth was observed throughout the channel.

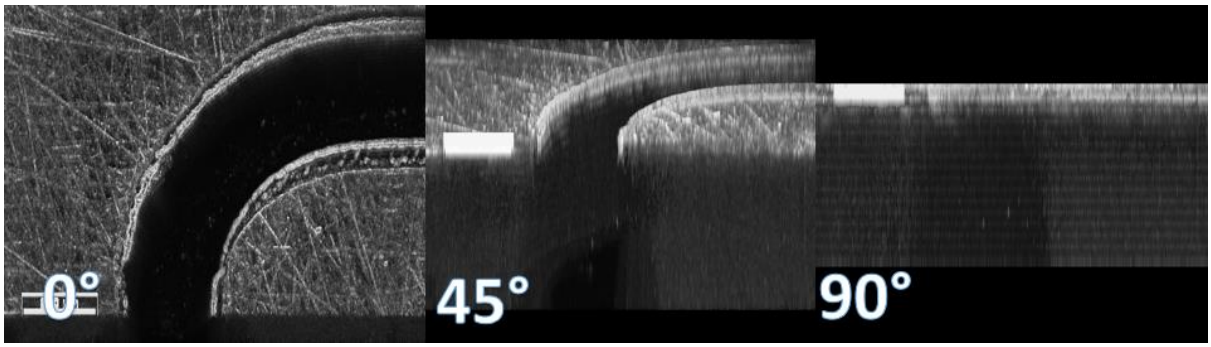

Figure 57: Entrance from mixer, 300µm, into reactor zone 200µm at 0°, 45° and 90°.

Figure 57 shows the entrance from the mixing structure into the reactor. The bottom of the channel developed an asymmetrical depth, but the effect is only slight. However, this is not visible in Figure 57.

Figure 58: Entrance of mixing structure at 0, 45 and 90.

Figure 58 shows the entrance of the mixing structure. The depth has a lot of variation when compared to the other micrographs. Comparing the 0° with the 90° the depth in the top right channel appears to be deeper compared to the other channels. When observing the 90° 3D stacked image, the reflected regions in the bottom, pointed by the arrows, show the depth from the side. The 200µm channel in the mixing structure achieved the deepest engraving while the 50µm channel experienced the least. Possible reasons may be the scanning pattern, Vertical movement could concentrate the beam for longer in the 200µm channel due to up and down movements. The build-up of heat would increase the ablation rate within this area. The 300µm had an intermediate depth. Since the modelling of the mixing structure was done at an equal depth, it is expected that the mixing ability of this mixing structure will differ slightly. Since the volume of the 200µm is larger than the modelled one it is expected that more of the flow will ocur in this direction. There was a slight difference in the depth of the two 50µm channels. The 50µm channel on the side had a higher ablation rate.

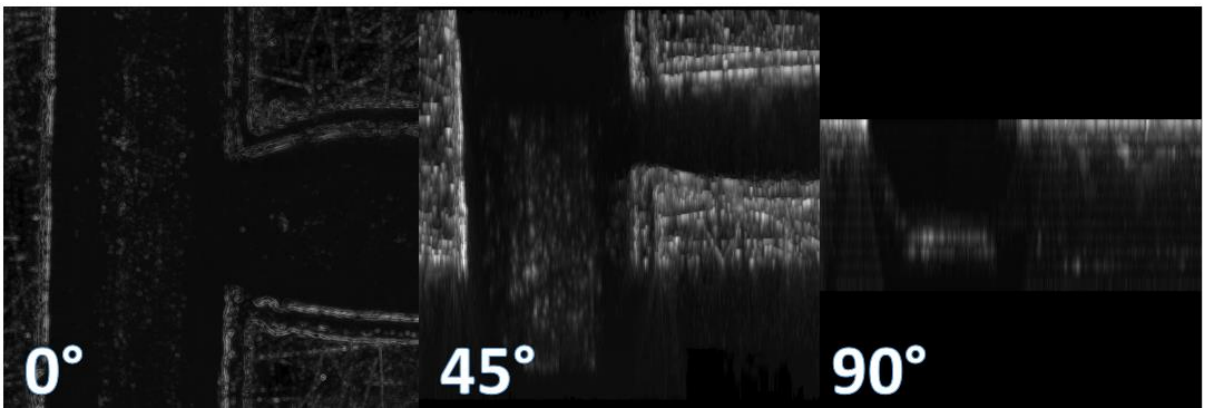

Figure 59:Reagent stream entrance at 0°, 45° and 90°.

Figure 59 shows the entrance into the mixing structure from the pump's inlet into the reactor. The entrance is at the funnel shape. The depth of the mixing inlet is shallower than the depth on the pump inlets side. It is expected that this is due to the linear scanning pattern of the laser which concentrates heat at certain spots more than at others. The scanning pattern had a vertical zigzag pattern. Since the left-hand channel is longer vertical the laser does not remain in a small, concentrated region for long. On the contrary the zigzag pattern on the horizontal channel would have concentrated the beam more over time, heat would have built up and hence the ablation rate would be more. A similar trend was observed in Figure 55 where the horizontal plane had a greater rate of ablation. Therefore, to assure a higher rate of ablation in the reactor's X and Y plane should be switched, because the reaction zone channels run in the X-plane.

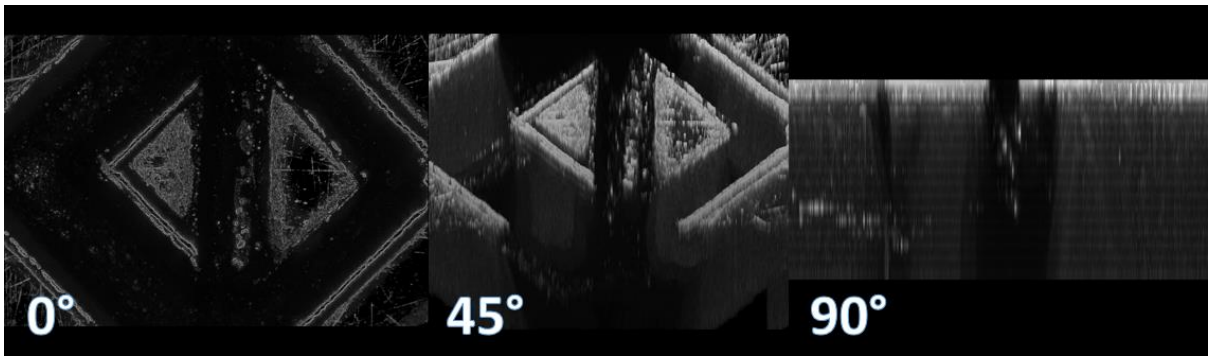

Figure 60: 3D plot of mixing structure at 0°, 45° and 90°.

Figure 60shows the mixing structure of the reactor. As seen in figure 62, the 200µm channel had the deepest engraving. With the middle 50µm having the least. The toolpath for this was also in a vertical zigzag pattern. Hence, the least exposure over

time was in the middle. At the 90 angle the light points indicate the depth and show that the 50μm channels have a reduced depth.

Overall, the quality of the etching was relatively uniform except for the mixers. Experimentation in different tool paths would most likely give different ablation rate at certain parts in the reactor. However, for the scope of this project, which is a proof of concept, the channel quality is sufficient. Nevertheless, better aspect ratios are observed when compared to anisotropic etching.

2.1.7 Etching summary

Table 8: Surface diameters of the channels of the fully etched reactor.

Dimension	Measured (μm)	Std. Dev (μm)	Measurements
200 (In reactor)	261.3	3.5	4
200(In mixer)	286.5	10.5	4
50(Mid mixer)	91.5	4.7	4
50(Side Mixer)	137.8	4.5	4
300(Inlet)	326.5	7.8	4

To summarise the laser etching's results the plane of engraving slightly affected the diameters of the channels. The measurements suggest that the increase localisation of time increases the ablation rate. Two methods of corrections are possible. The first is to alter the dimensions to account for the excess ablation on the edges. A more correct method, which will be easier to transfer, is to alter the Computer Aided Manufacturing (CAM) software which is responsible for the laser's movement. A localised scanning pattern, where the laser will engrave regions closest to the current point, would most likely be more efficient.

2.1.8 Reactor Clamp Design

Microreactors need to be fluidically sealed. Raised pressures further complicate the sealing process. Hastelloy C276 is a high melting point temperature metal thus thermal bonding will be extremely difficult, especially where the integrity of the microstructures needs to be preserved. Additionally, a blockage of a thermally sealed reactor will render the reactor useless and therefore reactor lifetime will be reduced. Another approach that will be taken is to create a disk that is clamped.

Between the clamp and the reactor, a sealing device will be required which seals the channels from leaking. Figure 61 shows the clamp that was designed for the reactor.

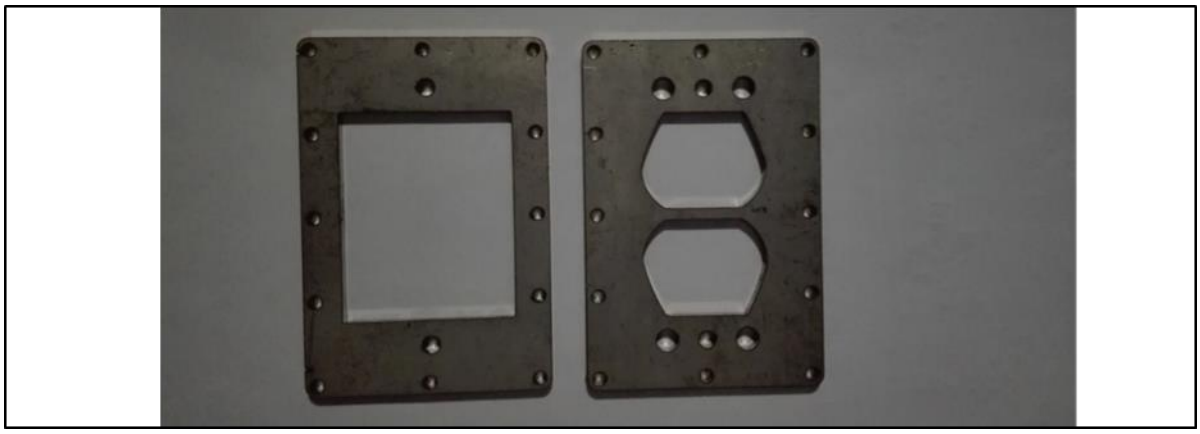

Figure 61:Top and bottom reactor clamp design. Tighten by M3 Bolts.

The clamp will be held in place by M3 bolts on the outside. The reactor will sandwich in the middle, where it will be sealed. A window region in the middle was cut to allow for photochemical reactions. Three holes adjacent to the windows are the through holes where the connectors are connected through. The inlet and outlet holes of the reactor need to line up with the holes on the side of the windows. The bottom of the clamp mirrors the top with the external holes lining up. Additionally, a square has been placed where the heat source will be coupled. The bottom of the clamp has a cubic hole for the heating block to fit through.

A clear sealing device is required between the top of the reactor and the clamp. A glass disc was chosen which had the same width and height as the reactor. The thickness of the glass was 5mm. A 60µm Teflon gasket was placed between the glass disc and the reactor. The purpose of the gasket was to squeeze slightly into the channels to seal it. Various attempts were made to ensure that the sealing was uniform in the reactor. Higher tensions in the clamps afforded the sealing of the reactorl. However, higher tension in the M3 bolts caused the glass disc to crack. Various attempts were undertaken to minimize the crack and the following design did not crack under pressure and heat.

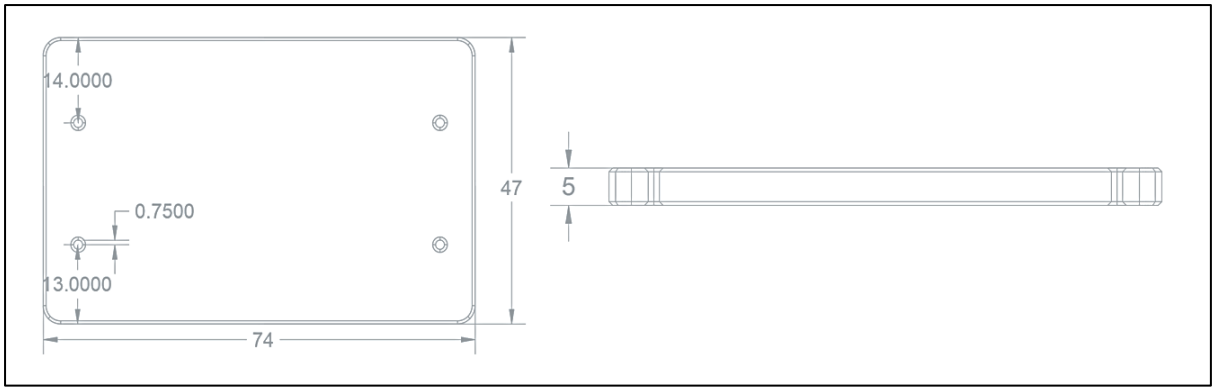

Figure 62:Design of glass disc. (units in mm.)

Figure 62 shows the design of the glass disc. It's width and height are the same as the reactor. A 5mm disc was used and was cut out with a diamond cutter. However, the most important steps are the post processing steps of the slide. The holes were originally drilled from one side with a 1.5mm tungsten carbide bit. The drilling was done with a coolant to reduce chances of fracturing. Drilling it from only one side caused small cracks around the exit hole. These cracks propagated and broke the glass as soon as any pressure as well as heat was added. Additional small cracks occurred on the edges where the glass was cut. Therefore, to circumvent this problem the holes were drilled from both sides with the two holes meeting in the middle. No cracking was observed inside. Additionally, the entrance of the holes was chamfered until a smooth finish was attained. All the edges around the glass ware also uniformly chamfered. This post process significantly strengthened the glass, enabling it to handle more force, hence improved sealing. The 1,5mm (1/17 inch) bit allowed the 1/16 inch PTFE to fit in tightly without affecting the flow. As an extra precaution, thermal silicon caulk has been applied to the inside of the clamp to equalise the pressure. The bolts of the clamp were also roughly torqued to equilibrate pressure deviations.

The tubes had to be fixed in place by some means. To keep the system as affordable and versatile as possible, easily acquired components were used. 1/4" UNF 28 Gang HPLC bits were used. Little Things Factory reactors uses the same bit as well as various High Performance Liquid Chromatography (HPLC) systems. ¼ inch tubing was used to act as a sleeve for the 1/16 inch tubing.

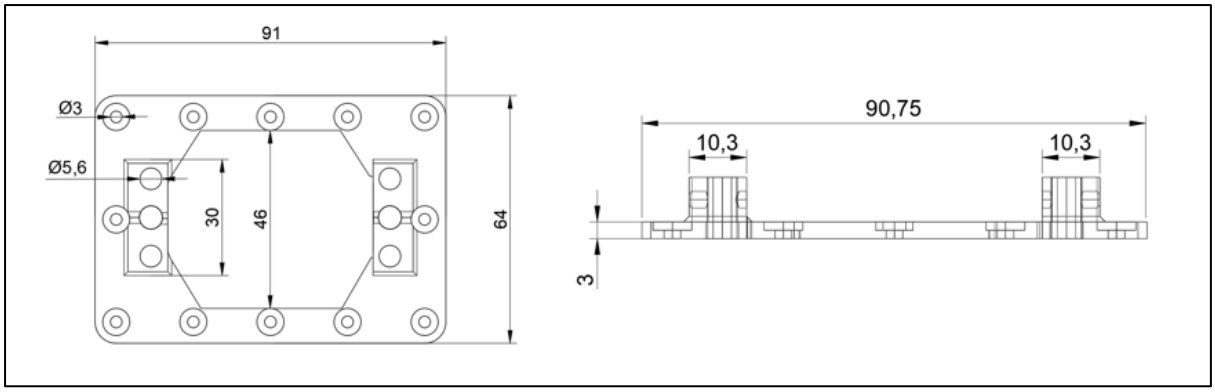

Figure 63:Clamp-cap design. (units in mm.)

A cap, as seen in Figure 63, was designed to hold the fittings in place through a threaded hole. The cap was bolted onto the clamping system. The cap also acted as a thermal insulator as well as a buffer system to apply more uniform pressure. This contributed further to sealing. Since the correct tapper, thread maker, was not available at the time, the fitting was used to cut a thread. Initially CNC machining was not available, therefore a proof of concept cap was 3D printed using ABS plastic. Since ABS plastic does not have a cold flow property such as PTFE the holes were wetted with acetone to soften the plastic. The fittings were then screwed in while the plastic was malleable and the piece was continually turned to assure that the fitting does not get stuck. Although ABS is not stable against most corrosive chemicals the fittings remained sealed and corrosive substances could be handled. A more useful method would have been to machine the piece out of PEEK or PTFE and cut the thread with the proper tapping tool. A better fit, as well as improved sealing, will be expected.

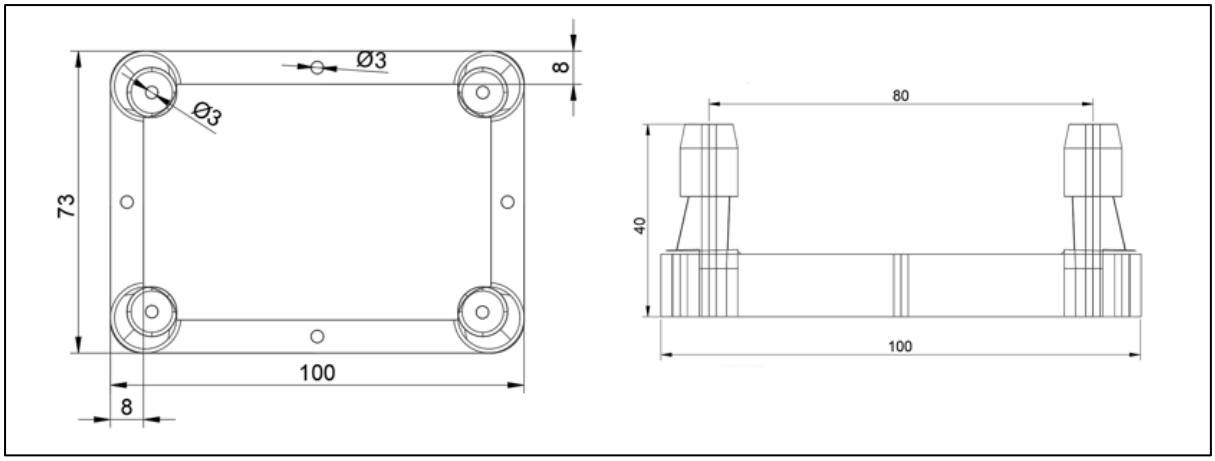

Figure 64:Reactor scaffold mount.

Figure 64 shows the scaffold which suspends the reactor to isolate the heater under the reactor. At the ends of the reactor, the M3 bolts were longer, which mounts the reactor in the scaffold. The part was 3D printed in ABS plastic. ABS was not the ideal polymer for this. A more useful one would be High-density polyethylene (HDPE). However it could not be acquired at the time. The scaffold was screwed to a base that contained all the electronics.

2.1.9 Heating system design

To maintain the temperature of the reaction an external heating source is required to operate at elevated temperatures. For this to work, a closed system is required where feedback controls the output in which the entire system strives to a set value. The output will respond in accordance with the feedback that is received by some sensor. The most common temperature sensors are thermistors and thermocouples. Thermistor operates by a change in resistance with a function of temperature. As the temperature increases, the thermistors resistance falls. These sensors are relatively affordable; however, their main drawback is that their resistance vs temperature function is not linear. As the temperature decreases the resistance goes up exponentially. Therefore, small defects in the thermistor design would drastically alter the readings outside of the thermistors temperature range.

A more superior, although complex probe is a thermocouple. Temperature creates a voltage difference which induces a current. The current is measured and is linearly proportional to temperature. Therefore, thermocouples offer a wider range of operation compared to thermistors. The drawback is that current is harder to measure compared to voltage, and requires specialised components. Therefore, to

circumnavigate the complex electronics. a Programmable Logic Controller (PLC) transmitter was used as part of an integrated system. The PLC also had a programmable interface where the temperature could be entered and programmed automatically. The following materials were used in the construction of the heating system.

2.1.9.1 Materials

- PR electronics 4501 programmable interface.
- PR electronics 4116 universal transmitter.
- PT100 4 wire thermocouple (RS-components).
- 2 x (50mm x 50mm x 10mm aluminium block).
- 2 x 50W 200Ω aluminium housed power resistor.
- Arduino Uno R3.
- FOTEK 25AMP Solid State Relay 220V AC compatible.
- 2200uF 15V electrolytic capacitor.
- Green 565nm. General purpose LED.
- 0.25W 100 Ω Resistor.
- 16 AWG gauge wire for signal and low power parts.
- 12 AWG gauge wire for power.
- 3D printed parts for aesthetics.

Complete systems were available, but, the downside was that the systems are considerably more expensive. However Asian markets might have given better options.

2.1.9.2 Circuit.

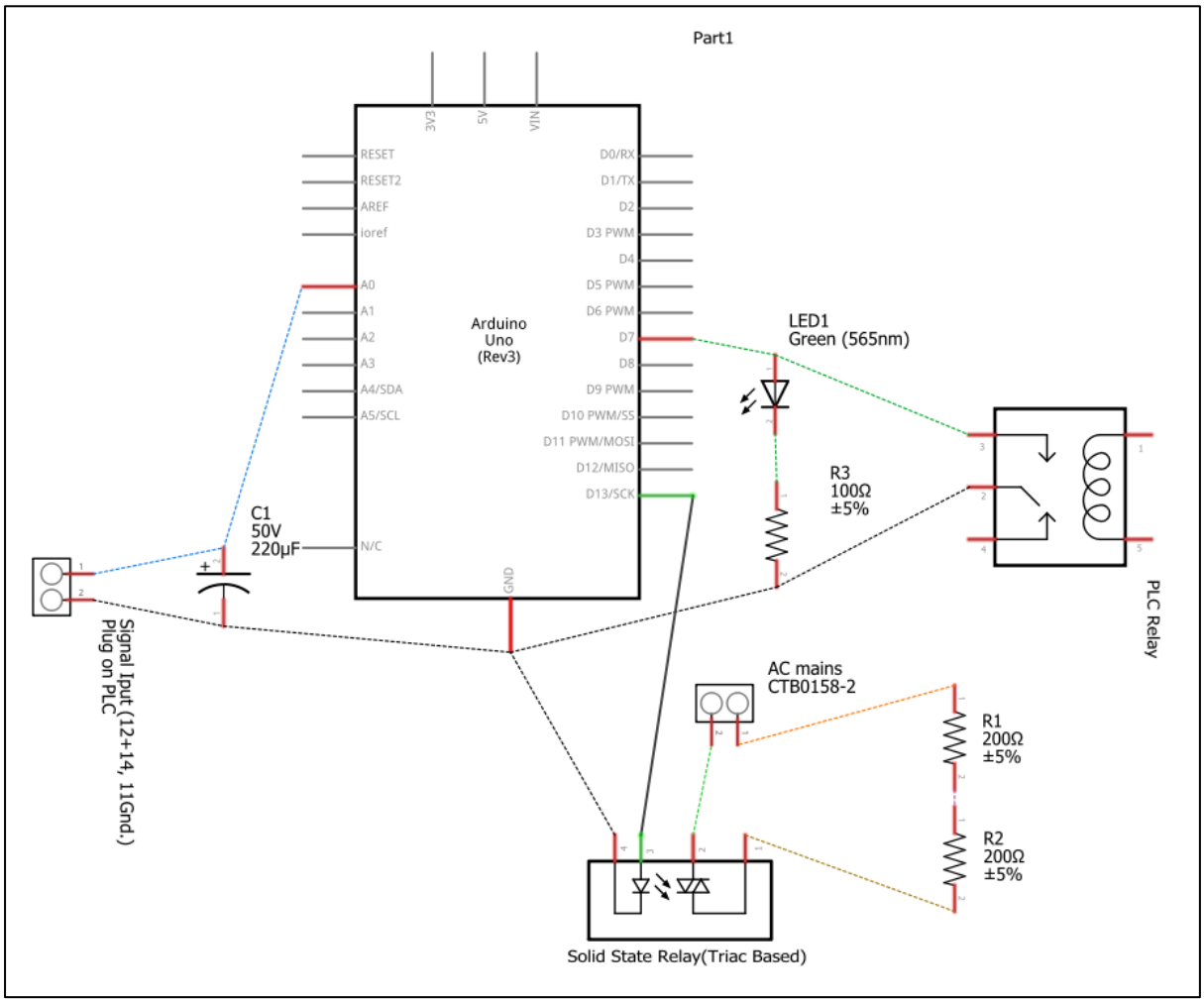

Figure 65: The wiring schematic of the reactors heating system. (Generated via. Fritzing)

Figure 65 shows the schematic of the reactors heating unit. The microcontroller, Arduino UNO, works in a synergistic way with the PLC. The PLC is responsible for taking the temperature and processing the signal. The microcontroller controls the PID algorithm which is tuned to the system. The processed thermocouple signal is expressed by the PLC as a voltage, 0V- 5V. This voltage is read by the microcontroller to alter the PID's algorithm's input values.

The user sets the temperature on the PLC and the mechanical relay at pin 23 and 24 opens once the temperature is reached. This signals the microcontroller to set the temperature to regulate the heat output. The code of the system will be discussed after the mechanics and electronics. The solid-state relay (SSR) allows for the microcontroller to handle high currents and voltages which are required to heat the reactor sufficiently. A green LED has been installed which lights up when the SSR is

open. The aluminum power resistors are put in series to reduce the current passed, since 220V AC is used as a power source. The solid-state relays' switching created a slight voltage spike which the microcontroller's Analog to Digital Converter(ADC) picked up. Since the algorithm used by the microcontroller requires this voltage as an input, the voltage spike caused incorrect data to be recorded in the algorithm. To reduce noise in the signal, a bypass capacitor was added which reduces the interference contribution to the signal. The bypass capacitor reduced the noise by approximately 4-fold.

The advantage of using AC mains power is that no bulky external power supply is required and thus the system is more affordable. The drawback of using an AC source is that a cooling device, such as Peltier thermoelectric coolers, are not feasible. Additionally, a cooling device would require an H-bridge circuit that needs to be cooled itself.

2.1.9.3 PID Arduino Code.

The coding uploaded to the microreactor can be found in the Index. It can be found on page 142 at title 4.2. Comments (//) is placed next to the code to explain the function.

2.1.9.4 Thermostat construction and casing.

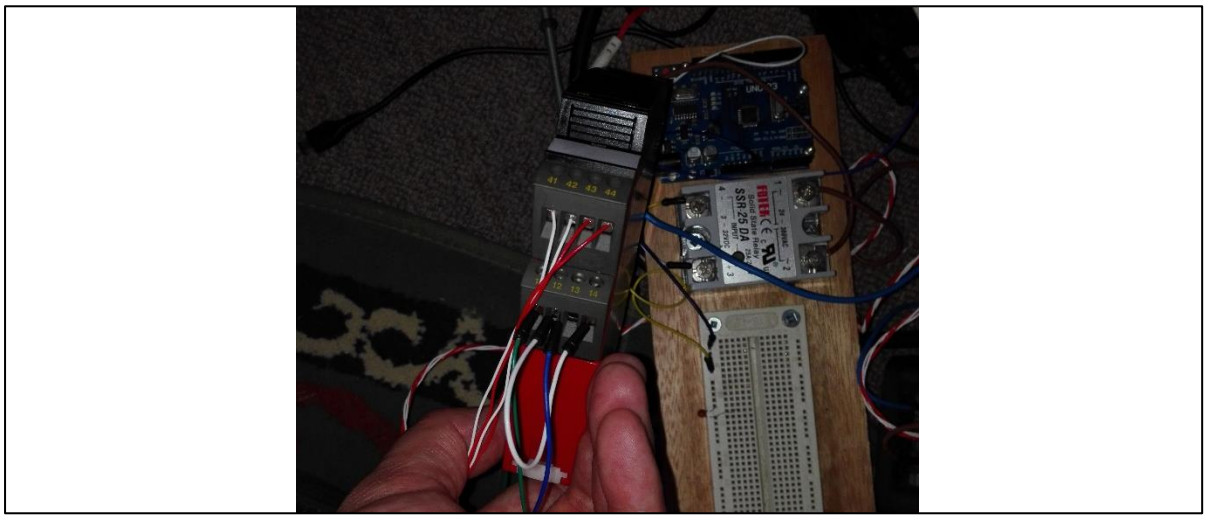

Figure 66:Prototype stage of reactor heating system.

The system was first prototyped via a breadboard, as seen in Figure 66, to test for any errors that might occurred. When the design of the electronics was sufficient the electronics were transferred into a wooden box constructed for the project. It should be mentioned that the purpose of the electronics box is not aesthetics, but simply to protect and organise the electronics as well as house the reactor holder on top. The system also had a large amount of wires which might cause issues with incorrect handling. A more sufficient design would be a polymer/metal hybrid casing. However due to time constraints and availability of materials, wood was selected. Another reason for the casing is for user safety. Dangerous voltage levels were used to heat the reactor, therefore adequate protection was required. Some inserts were designed to protect the edges of wood as well as the external components.

The power resistors were bolted on a piece of aluminium instead of onto the reactor directly. This allows various micro-reactor discs to be used on the same heat source. Just above the power resistor the PT100 platinum probe was inserted. A 3mm hole has been drilled in the aluminium. Aluminium has superior heat transfer when compared to Hastelloy C276, therefore the heat would be more uniform and diffused which also was a deciding factor.

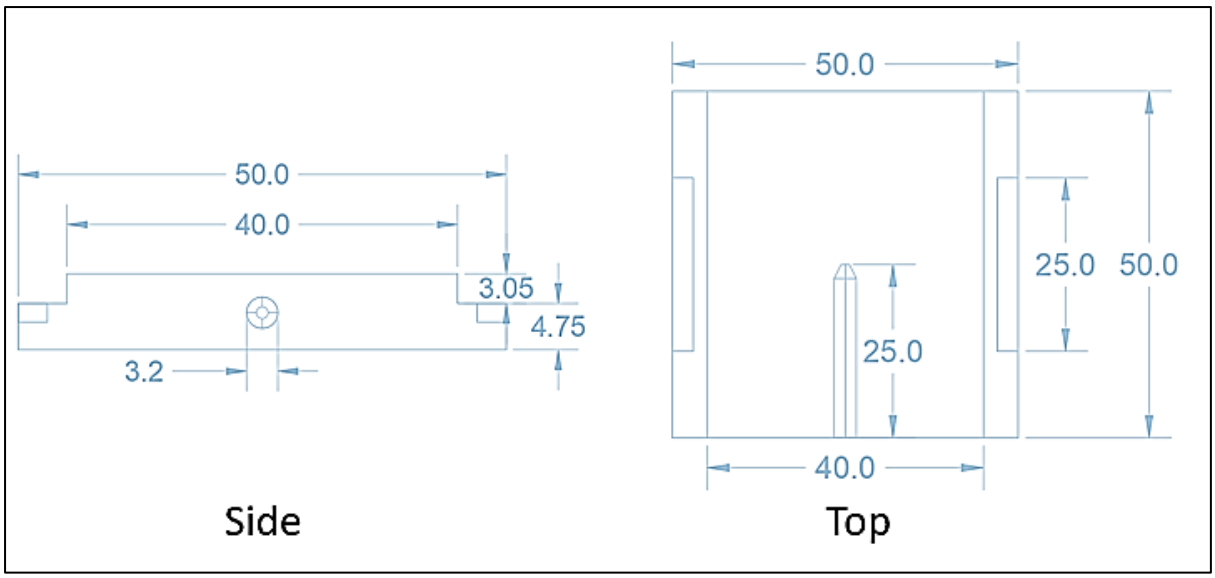

Figure 67:PT100 Thermocouple plate. Probe fits into 3.2mm hole. (All units in mm.)

Figure 67 is the plate in which the thermocouple fits. It fits between the reactor and the power resistors. It has a complimentary plate which in the future possibly will be interchangeable with a Peltier type thermoelectric cooler/heater.

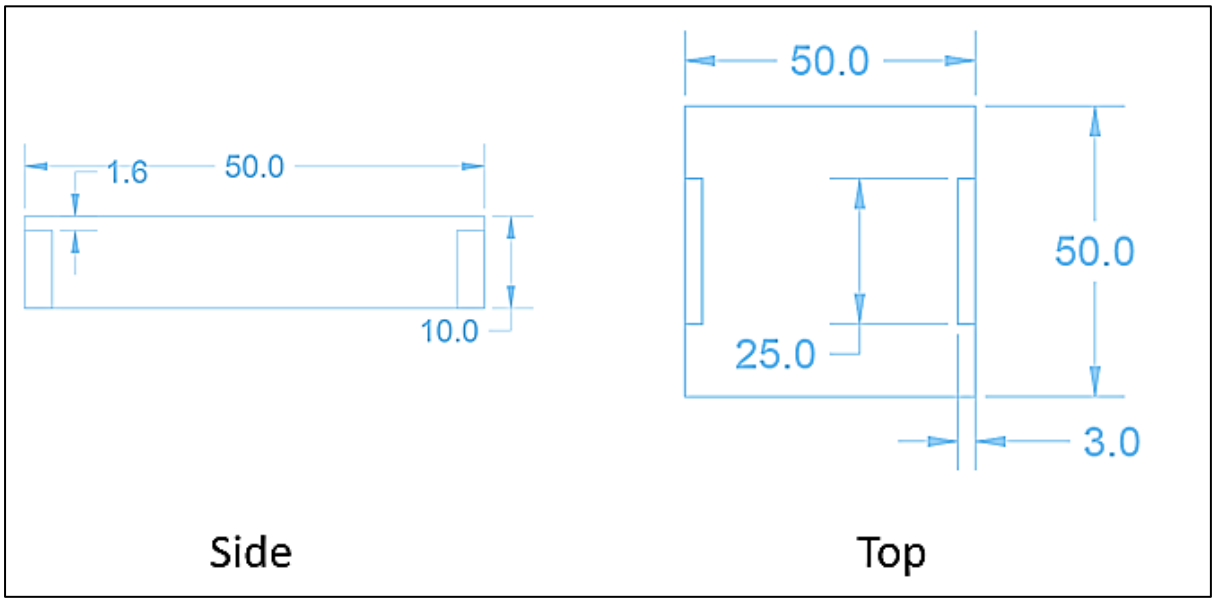

Figure 68:Power resistor aluminium plate. (All units in mm.)

The plate in Figure 68 clamps the plate in Figure 67 against the reactor. The power resistors are attached to Figure 68 where the heat diffuses through the plate in figure 71, which is where the temperature is measured. Originally it was designed so that a clipboard clip could keep it together, however a more secured system was required, and the plates were held in place through cable ties. This is by no means the final design, however it worked for proof of concept purposes. The temperature was kept

stable at +-~0.5C°. The thickness of the combined aluminium plates significantly contributed to the hysteresis of temperature. Probable future designs would reduce the thickness of the aluminium plates or employ a single plate design.

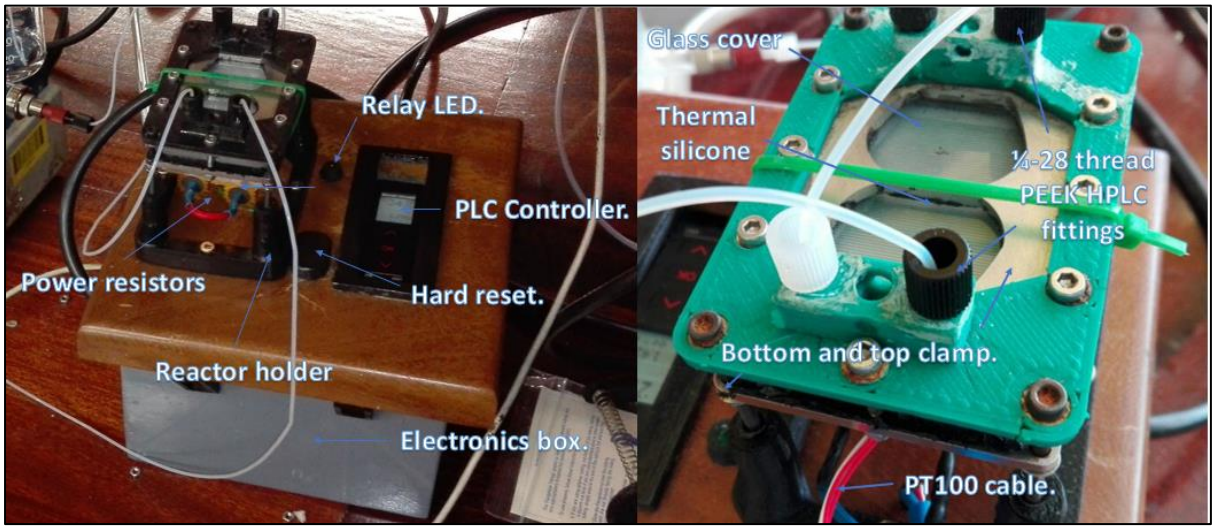

Figure 69:Final construction of the thermostat reactor holder and reactor.

The final product is shown in Figure 69. The design was compact compared to other systems, which is advantageous from small bench spaces. Acetic acid corroded the clamp cap as well as the reactor holder and these parts had to be reprinted. Therefore, it is of immense importance that a more corrosion resistant polymer be used. The non-stainless-steel bolts and washers also were sensitive against the compounds used in the testing section. Therefore, more careful consideration of components should be considered. The testing will be covered in the chemistry section.

2.2 Pump

2.2.1 Overview

The pump will use the same 2 stage volume transfer as a HPLC pump where the primary chamber charges with two volumes while the secondary is discharging one volume. When the secondary has completed its discharging cycle, it charges itself with one volume from the primary chamber and one volume of excess gets discharged. The two pistons will be screw driven from one Nema 17 stepper motor. All the parts except the cylinder, pistons, and M8 threaded rods and M8 bolts were 3D printed.

2.2.2 Materials

- ESun white ABS 1,75mm filament.
- Unfilled Teflon round bar 32mm diameter.
- 10mm Silver Steel round bar. (Optical axis preferred, but expensive)
- 4 x LM10UU linear bearing (29mm length)
- 2 x 013BS (Brittish Standard) PTFE O-rings.
- 2 x 16.62mm OD x 1,75mm CS PTFE O-rings.
- 4 x M8- Brass nuts.
- 1m M8 stainless steel rod.
- Standard 1/4-28 Inline Check Valve.
- Chemtrix one way valve as inlet.

2.2.3 Mechanical Design

The first cylinder should have double the surface area. The cylinders should be in each other's radial axis so that the same motion system can be used. As one side fills, the other side dispenses, due to the phase of the stroke.

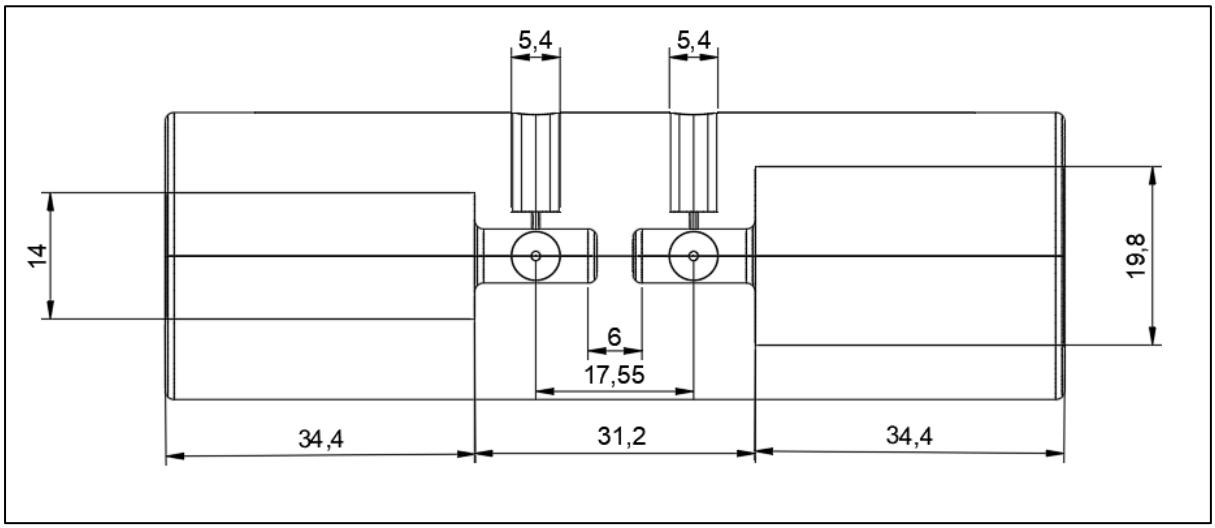

Figure 70: Hybrid syringe/HPLC pump cylinder.

Figure 70 shows the cylinder design that was used for the pump. The larger cylinder has a cross-sectional surface area of 308mm^2 and the smaller has one of 154mm^2. This system requires only 2 check-valves which makes it more affordable. The two pistons are driven by the same screw which simplifies the design and saves cost. The electronics and drivers will be based on recently developed technology in the open source 3D printing community. This will make the parts easier to acquire and it will be more affordable due to mass production. It should be stressed that this is only a proof of concept and still requires further development for commercialisation.

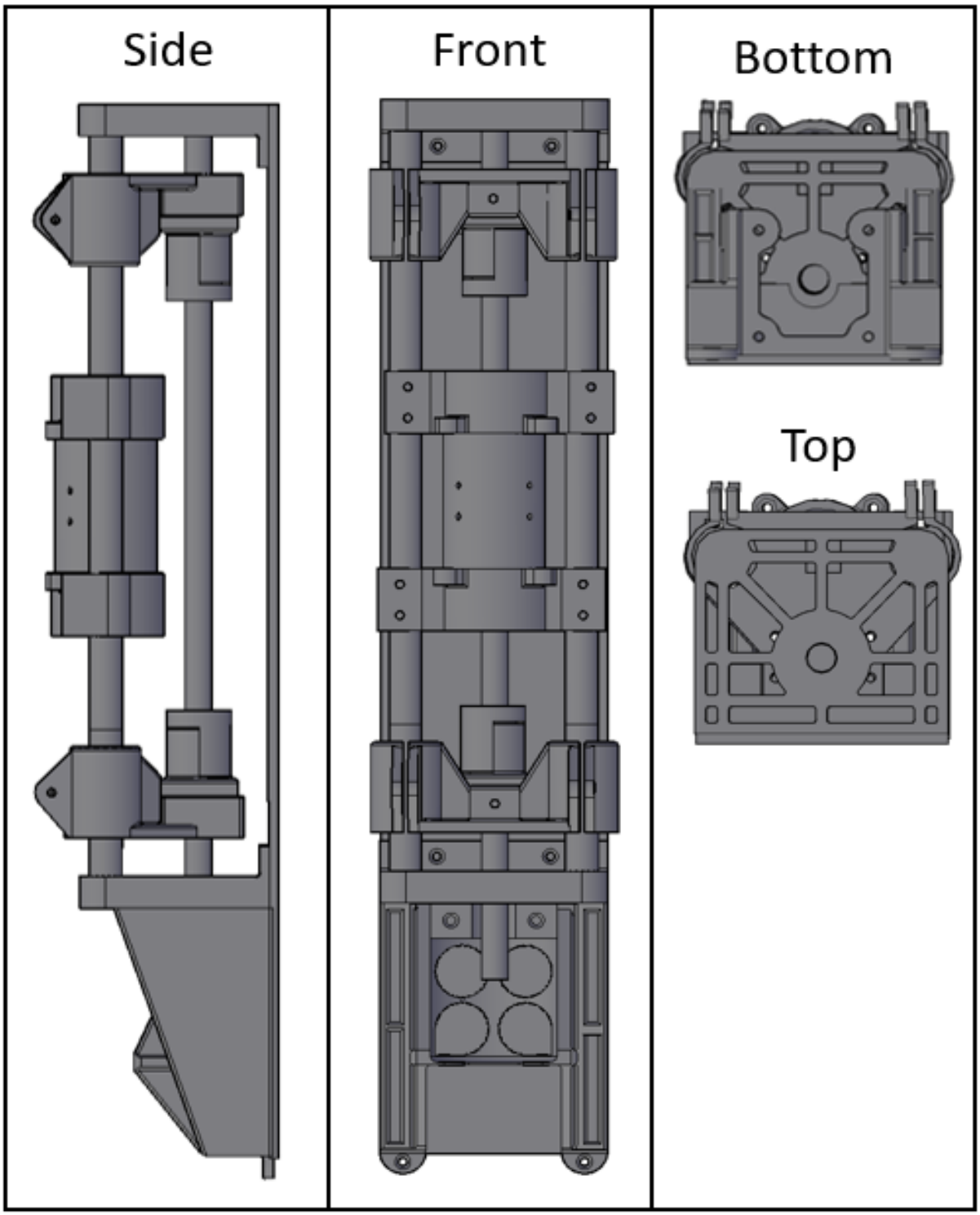

Figure 71: CAD design of the overall pump design.

The overall preliminary pump design can be seen in Figure 71. Originally the pump was placed flat. However it was realised that a vertical design will save considerable space especially where little bench space is available. The cylinder is mounted inside of two parallel shafts. Two units in which the piston is mounted are on both sides of the cylinder. These units are connected via an anti-backlash nut to a shared

screw behind the cylinder. The screw is attached to a stepper motor below the pump. At the top and bottom are end stop switches which change direction as the piston holding unit hits it. The speed is the same for both directions. Most of the parts were 3D printed with a home built one for this project. However, the cylinder was machined on a lathe where extreme precision was required.

The syringe manufacturing originally was attempted in Hastelloy C276. However, after various attempts it was decided that the material was not suited for affordable large-scale production due to its hardness and price. PTFE was proposed as a material which is much more affordable and gives the same corrosion resistance as Hastelloy C276. The drawback of PTFE is its cold flow. Cold flow is the tendency of polymers to creep over time. Fillers are available to improve its mechanical properties. Since this is a proof of concept study, different PTFE fillers were not investigated for the syringe. The internal structure of the syringe was also modified to accommodate the fittings, since PTFE is much softer, thus more area is required for the thread of the fitting. Figure 70 shows that the inner part of the cylinder has a smaller diameter to afford more stability for the fittings.

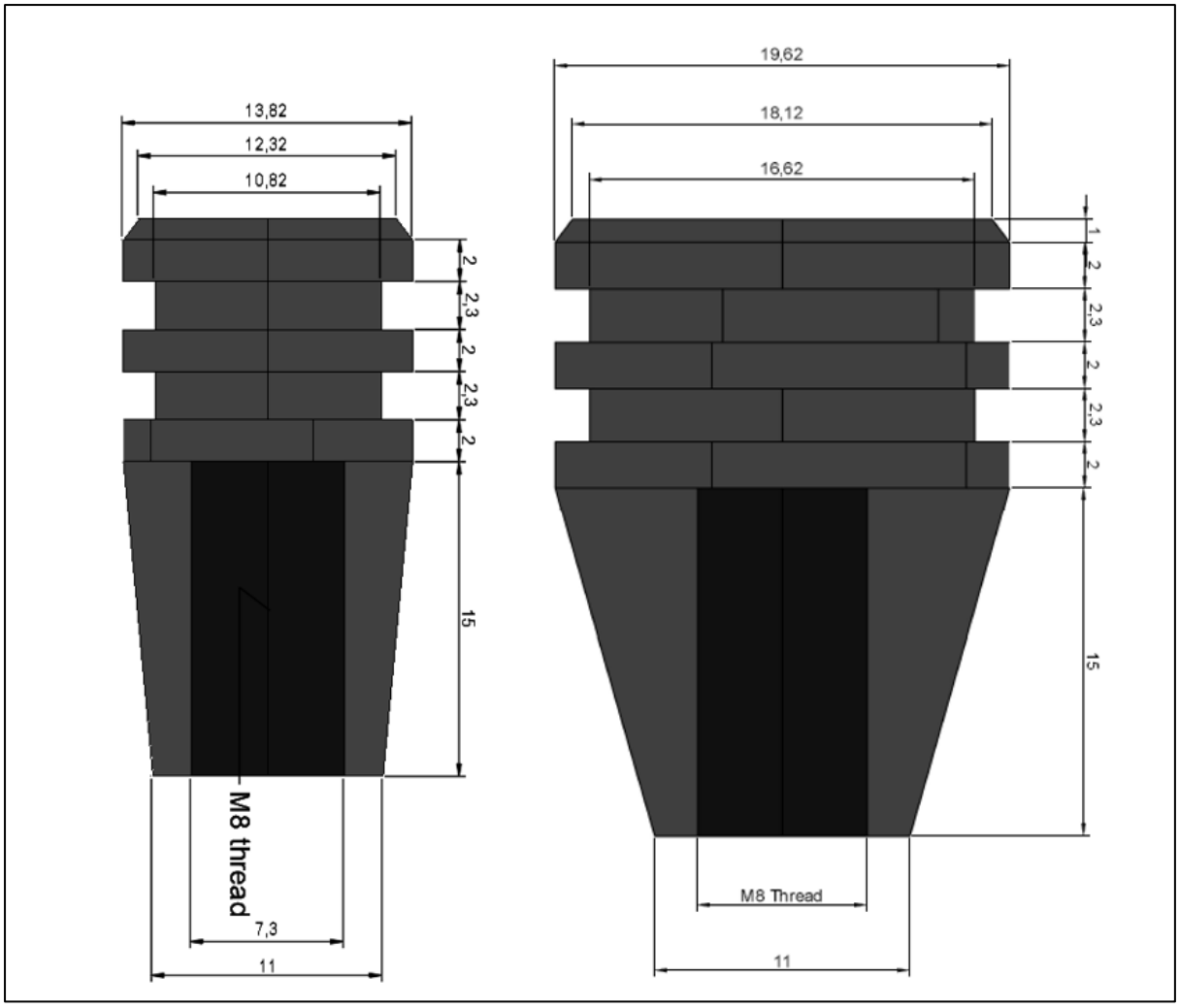

Figure 72: X-ray view of pistons for the pump's cylinder.

Figure 72 shows the design for the pistons. Two different pistons were turned on a lathe. The diameter of each plunger was slightly smaller than the wall of the syringe. Two O-rings were fitted into the grooves of each plunger. The diameter of both O rings was 1.78mm and its internal diameter for the smaller plunger was 1.82mm (013Brittish Standard O-ring size) and for the larger 16.62mm(Custom). Both rings were made from PTFE. Although some stretching of the O-rings was observed after the insertion into the groove, they returned to their original sizes after some operation time. The pistons were mounted on a M8 stainless steel threaded road. The top and bottom was tapered to aid with the insertion of the O-ring as well as mitigate some construction deviations which might cause strain. The piston’s shaft, which is threaded rod, was held secured in a piston guide device. Threaded rod also made the adjusting of the pistons depth possible.

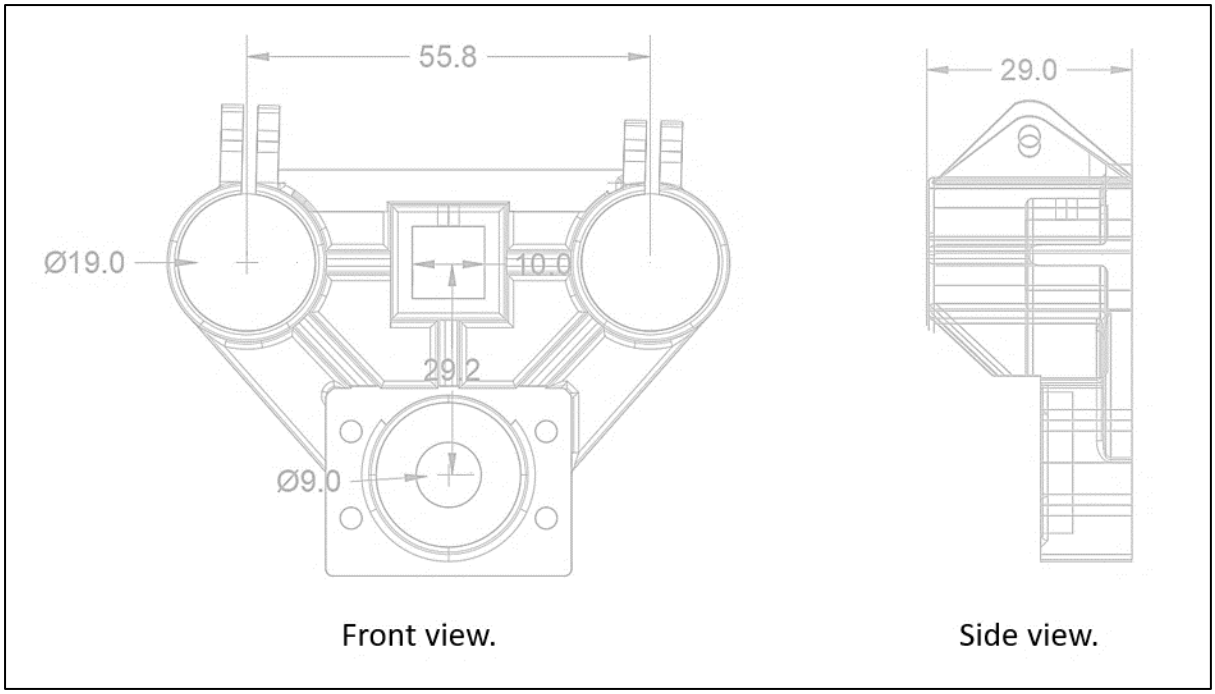

Figure 73: Piston holder device.

Figure 73 shows the piston holder which is responsible for keeping the piston in one axis as well as transfer the screw's movement to the piston. The sides of the holder have circular cavities in which LM10UU leaner bearings fit. These bearings are mass-produced for 3D printers, hence affordable. Cross bracing has been incorporated to reduce flexing in the part. The bearings are bolted in place on top of the device. A sleeve was printed that fits into the square 10mm cube into which the threaded rod is tapped. This provided adjustability for the piston's depth into the cylinder. The bottom section holds an anti-backlash nut system.

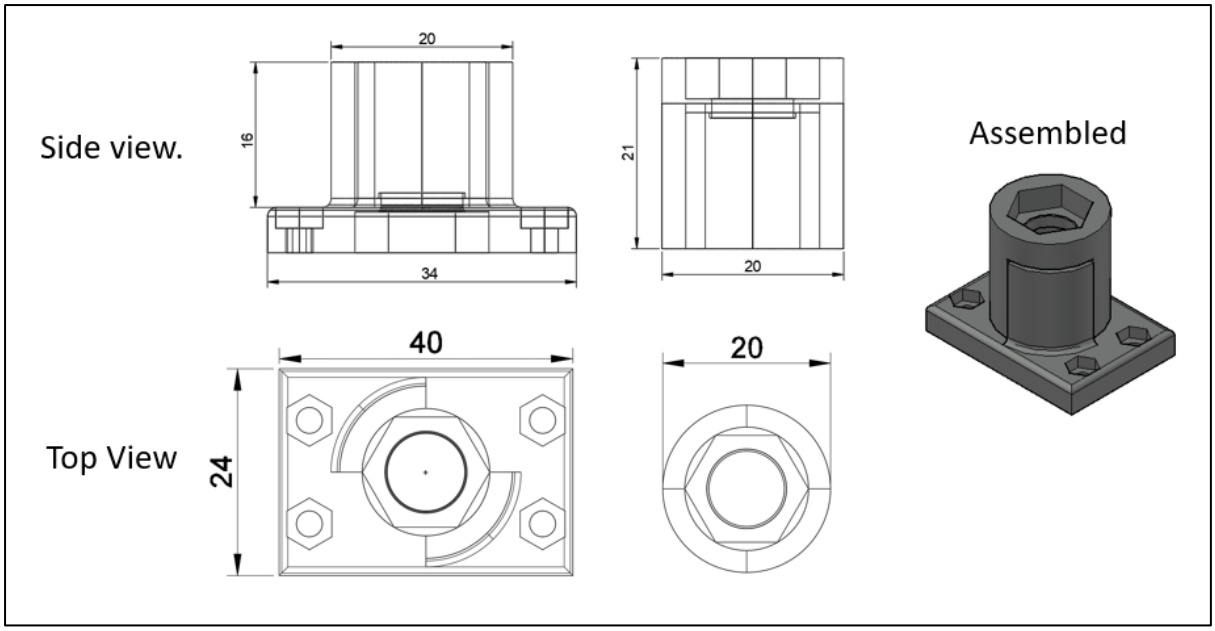

Figure 74: 8mm brass nut anti- backlash but design.

Figure 74 shows the anti-backlash nut that was designed for the system. The parts were 3D printed. For the movement to be efficient the friction should be minimized between the moving parts. Ideally a ball screw design would have been the best. A ball screw reduces friction by having circulating ball-bearings running between the thread of the rod and nut. However, these screws are much more expensive. Therefore, a leadscrew design was adopted. The friction was further mitigated by selecting a M8 brass nut with a stainless steel M8 rod, which has a static friction coefficient of 0.19. The brass nuts were pressed into the ABS blocks. The anti-backlash nut has an internal spring which is responsible for reducing interplay in the system. This is to ensure that at the change of direction the transition will be as quick as possible. A longer transition, where the piston stands still, will result in the arrest of the flowrate.

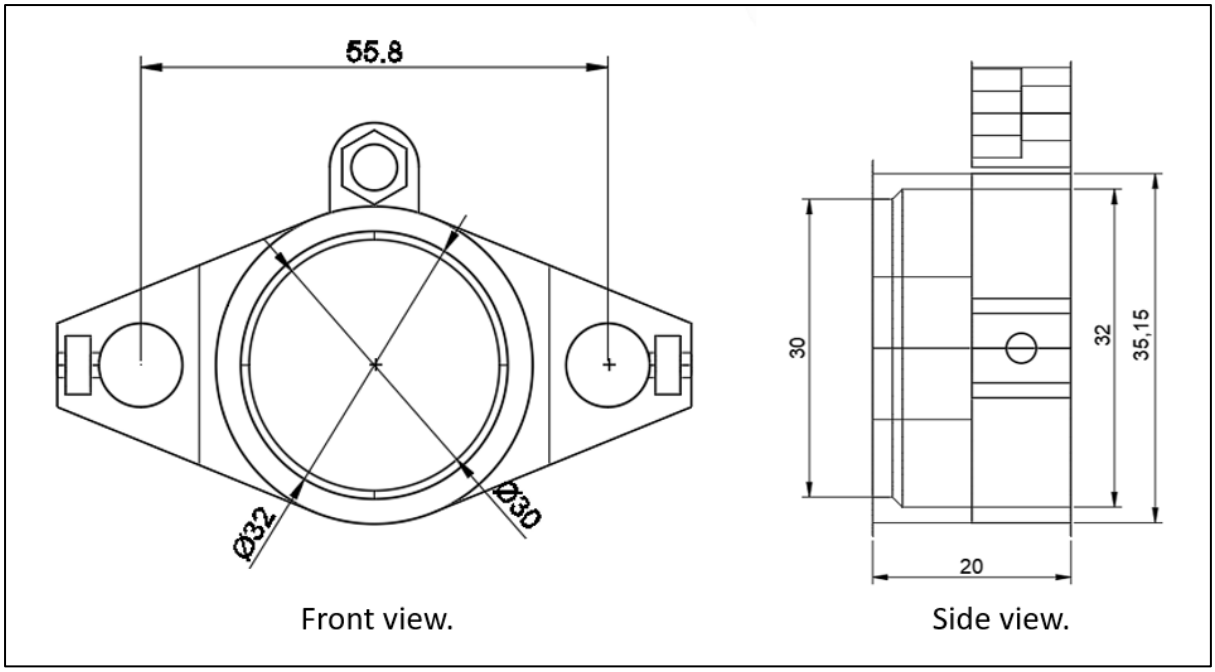

Figure 75: Syringe holder (all units in mm.).

Figure 75 shows the syringe holder. It is responsible for fixing the syringe between the two rails on which the piston. M3 nuts fit into the cavity on the sides, where bolts are used to fasten against the rail. On top of the holder an M5 is placed where the one holder is secured to the other with an M5 rod. The removes any interplay that the syringe might have in the holder. The syringe has a diameter of 32mm, which the holder accommodates. A 30mm diameter ring with a slight chamfer which acts to constrict the syringe in the housing.

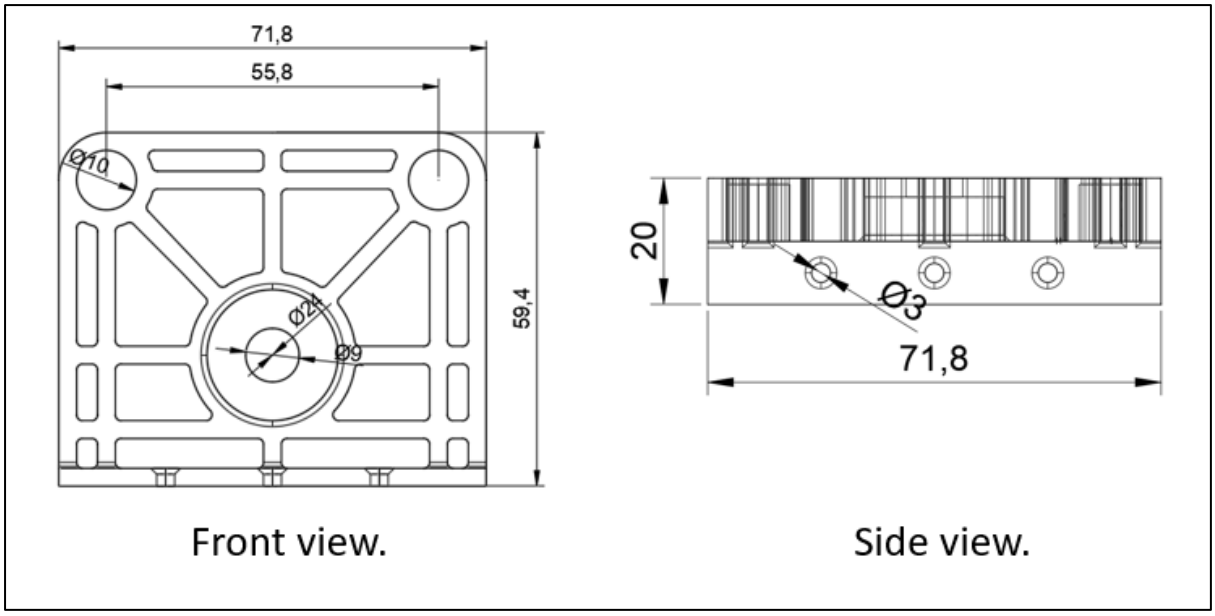

Figure 76: Axis holder (all units in mm.).

Figure 76 shows the axis holder. The function of this part is to anchor the axis in place as well as secure the driving screw. Two 10mm shafts are inserted into the holes above. In the middle of the front view a common 608ZZ radial bearing is pressed in. This secures as well as reduces friction for the driving screw. Since the screw drives the piston in an off-centre arrangement, some radial forces are expected. The part is identical for both top and below. The bottom piece is accompanied by the stepper holder.

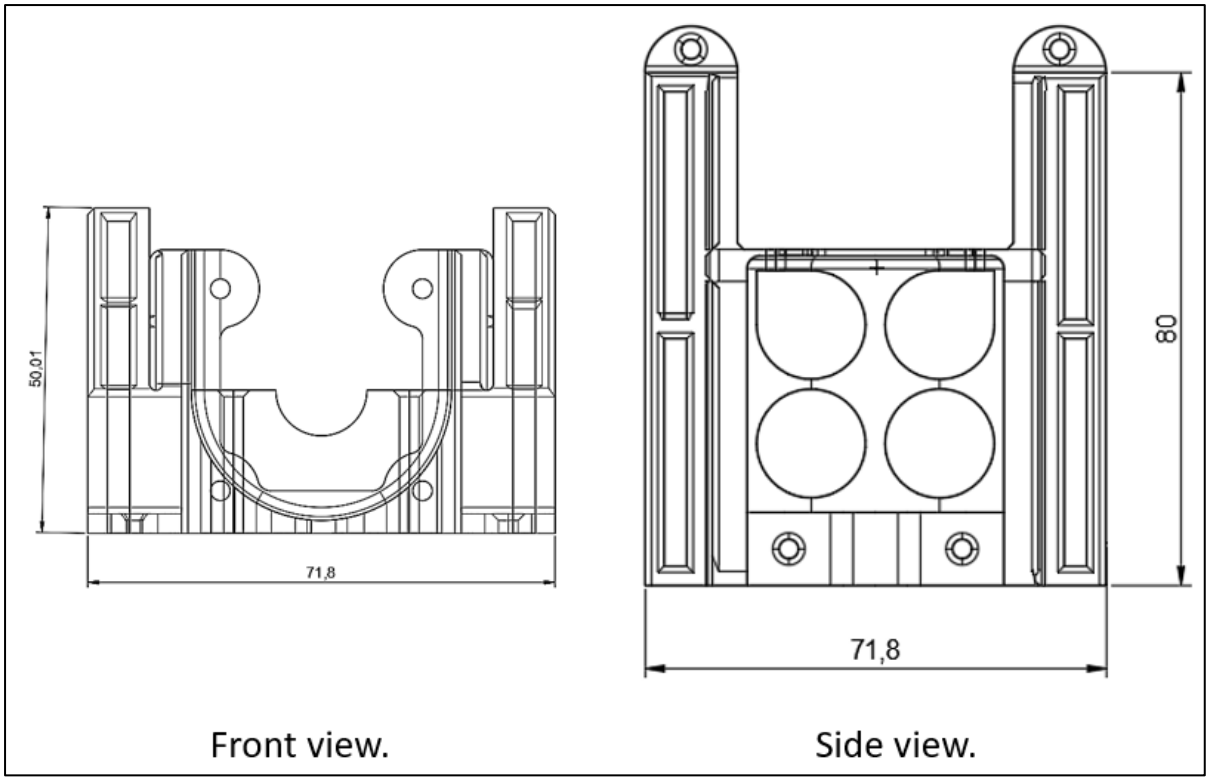

Figure 77: Stepper motor holder.

Figure 77 illustrates the stepper motor holder. The motor fits into a cube shape which its slightly squeezed in. The ends of the motors are bolted, and the motor rests against the base to reduce chances of rotating. Gaps were inserted such as the four circles, as seen in the side view, to reduce printing time and filament cost.

After testing, it was observed that a lot flexing occurred on the axis holders, therefore an external brace, which also functions as a stand, was built. The electronics as well as power supply was also attached.

2.2.4 Electronics design and manufacture

The electronics were also based on mass-produced parts. As in the reactor section, Arduino code was used to write the Graphic User Interface on the LED screen. To keep things as compact as possible, a shield, a stackable electronic unit will be designed. Fritzing is an open source software geared toward the rapid development of electronics. This software aided theshield design and provided the negative trace for the printed circuit board (PCB) etching. The entire system was designed on a breadboard originally, and a test code was written to see if each of the components work. A breadboard provides the use of the ability to make quick connections,

without soldering, to elucidate the wiring configuration. The protoype arrangement on the breadboard is directly entered into the software and then gets converted to traces.

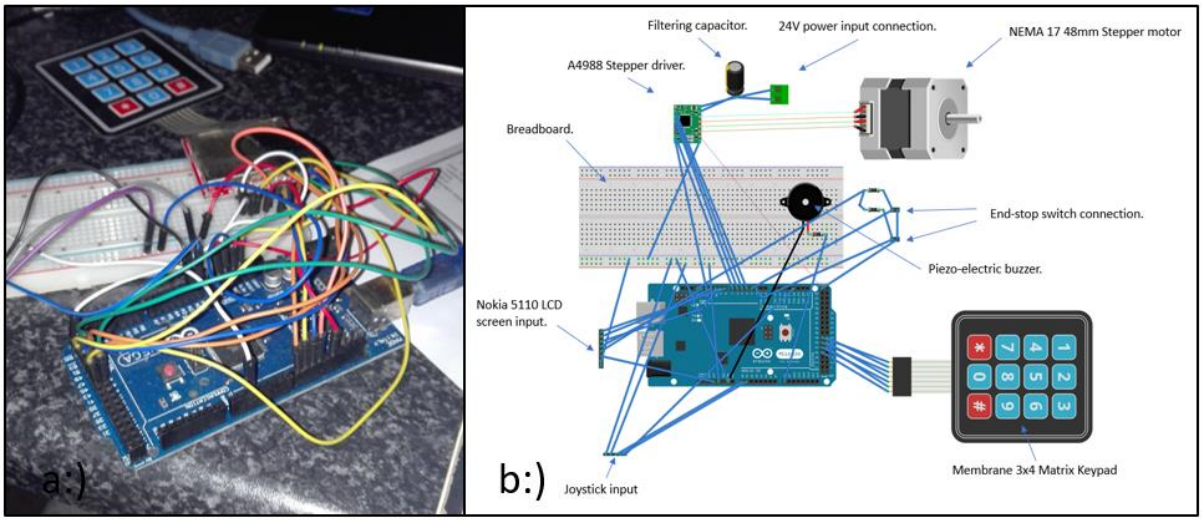

Figure 78:a:) Breadboarding and prototyping. b:) Breadboard input in Fritzing.

The system's arrangement can be seen above in Figure 78. Since a lot of traces can be incorporated onto a PCB, this would drastically organise the system. PCB's can be manufactured in multi-layered systems, but the manufacturing steps increase drastically. However, all traces could be fitted on a single level.

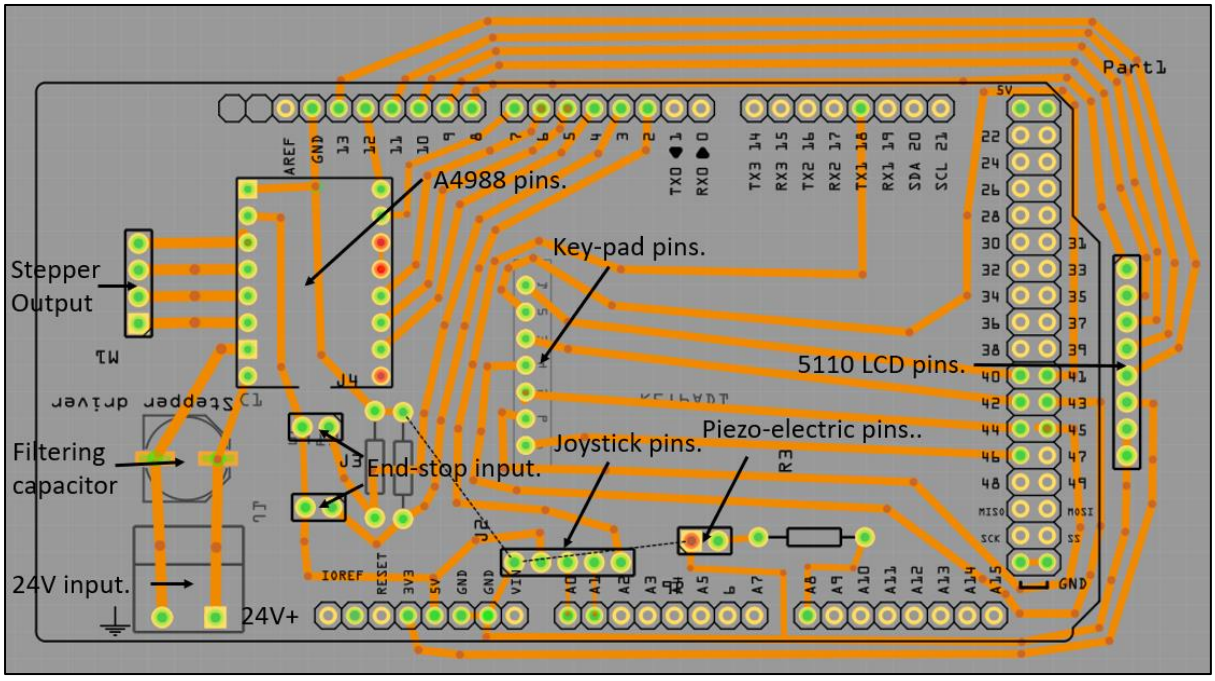

Figure 79:Illustration of PCB shield design for Arduino Mega.

Figure 79 shows the track design for the PCB. As mentioned, a single layer was obtained, which simplified the process significantly. The software generates a negative image which is printed, through a laserprinter, onto gloss paper. Laser printer toner consists of a polymer, which can be transferred, instead of a dye. The copper clad is finely sanded to remove any oxidised material. The cladding was washed afterwards with soap and rinsed to remove any oils. The gloss side with printed negative was place against the clean copper surface and the edges were taped to assure that no movement will take place. A clothing iron was used to melt the polymer from the paper to the copper. The piece was then soaked in water to dissolve as much of the paper as possible. The excess paper was removed carefully with a slightly abrasive cloth and washed.The tracks which did not transfer were fixed by drawing them with a permanent marker with multiple layers.

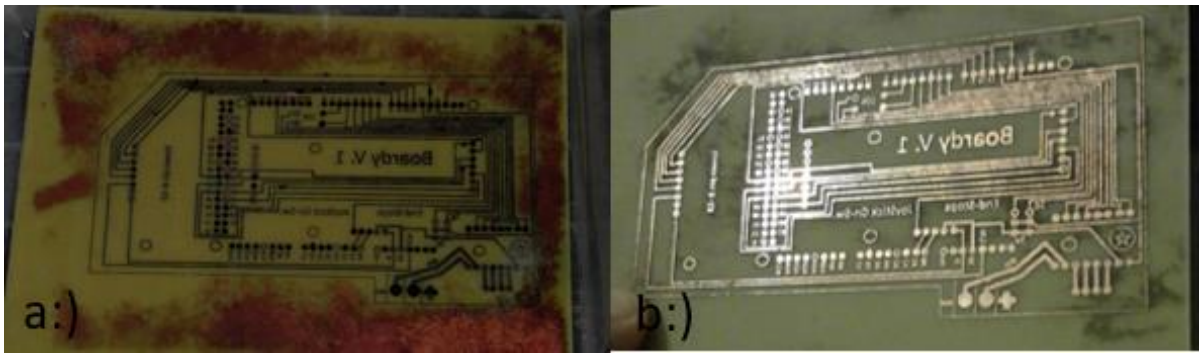

Figure 80:Etching of a previous PCB design of the pump. a:) Copper is being etched away while the negative mask protects the traces. b:) Protected traces are exposed by wiping the mask of with acetone.

A ferric chloride solution was prepared, which will be used as the etchant. The concentrations were not monitored, and small amounts were added every 5 minutes by stirring until the etching process was complete. The cladding with the negative imprint was submerged in the solution to begin the etching. The solution turned from a light blue to a slight green colour as the process occurred. The solution was stirred slowly until the process was complete. After all the visible copper was etched away, as seen in Fig 80 , the PCB was removed and washed. The mask was removed by wiping it with an acetone soaked cloth. 0.8mm Holes were drilled at the points were soldering was required. Generic components were soldered and obtained from E-bay. After some consideration it was decided that the addition of the joystick was redundant, because the user interface can be designed by using the keypad alone.

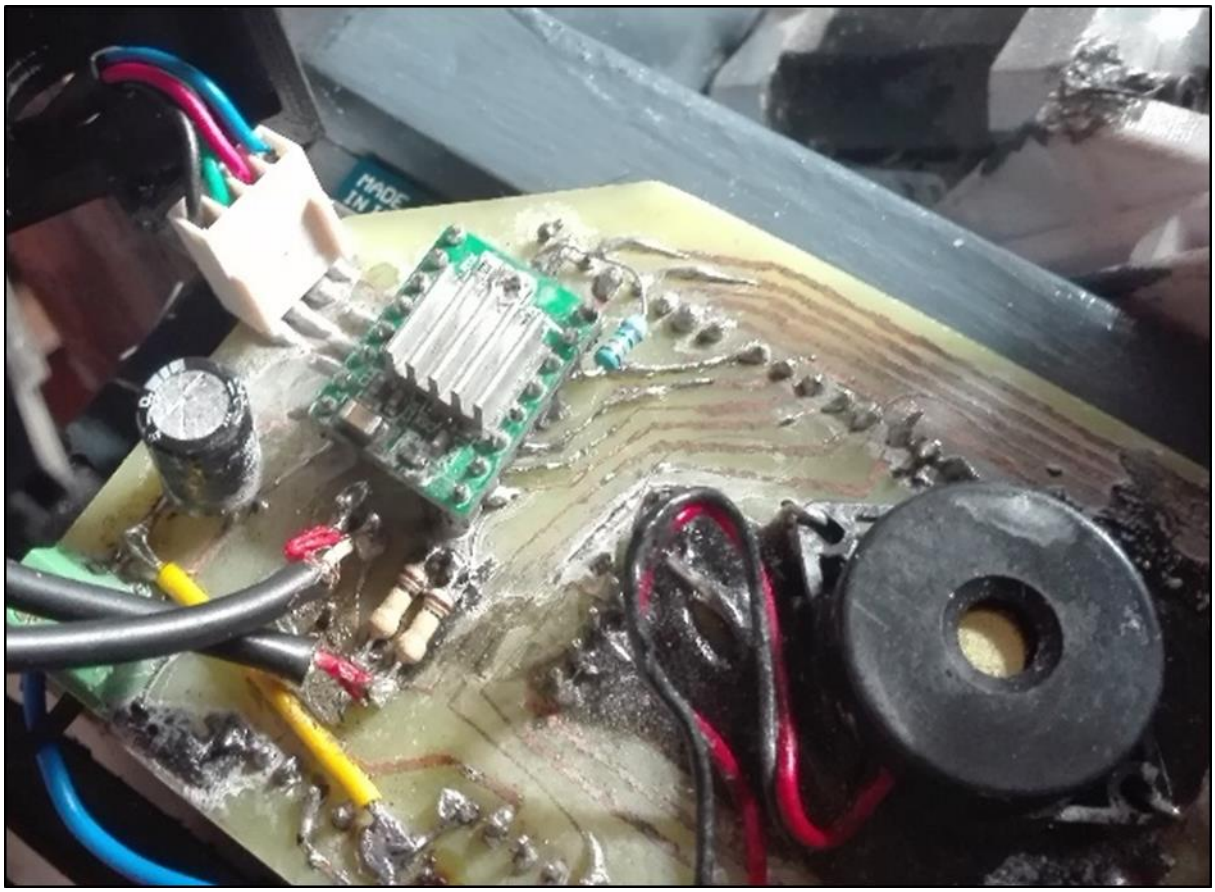

Figure 81:Track cross-over limitation of single layered PCB boards.

In Figure 81 the cladded side of the PCB was selected to be on top of the shield. This was to secure the header pins, which fit solidly into the Arduino Mega development board,. This resulted in weak mounting of header pins on top. After some investigation it was decided to solder the wires directly onto the tracks. The stepper driver was also soldered directly onto the PCB. Since these drivers are sensitive to high current and susceptible damage, it was not ideal to solder them directly, however the nature of the project was a proof of concept. Future designs would be double layered and milled instead of etched. The mask peeled off at some places during the etching, which required continuous repairing. Also, a double sided PCB would assure stronger mounting of pins and reduce the size of the board.

2.2.5 Programming of the pump

The programming code has been placed in the index in section 4.3. The code is explained after comment operators (//) within the code.

2.2.6 Electronics enclosure

There was no attachment to mount the electronic components therefore a 3D printed container was designed. The purpose was to protect the electronics as well as provide a mounting area for the peripheral parts such as the screen and keypad.

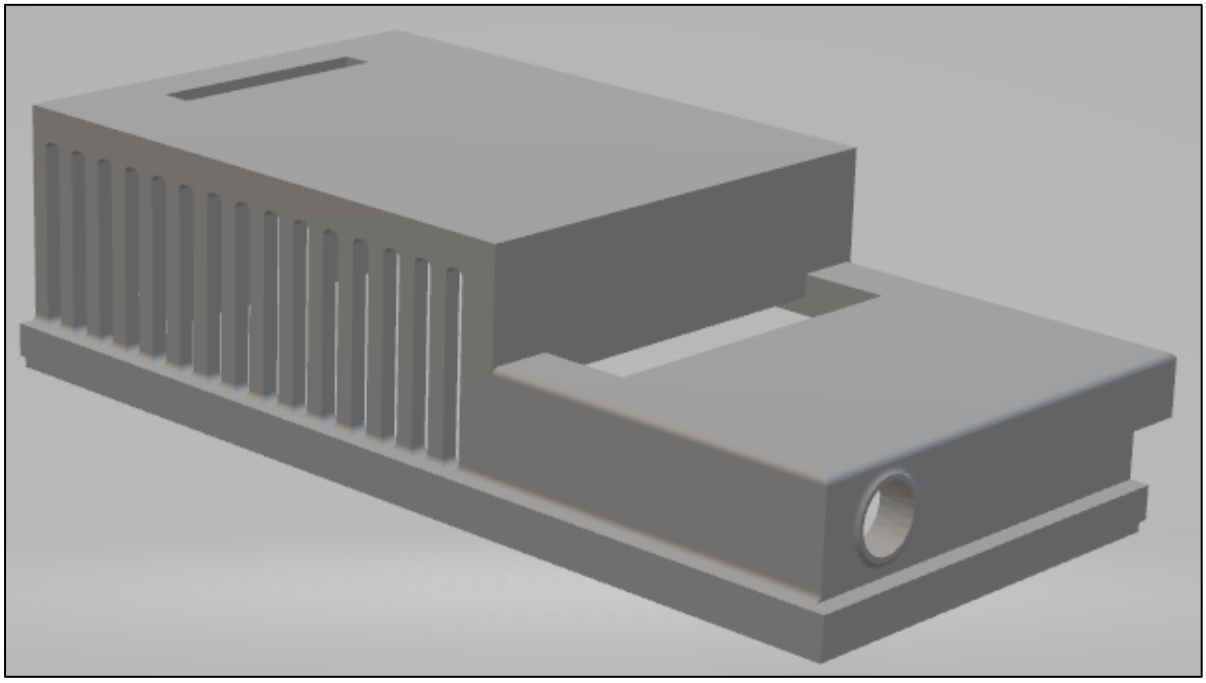

Figure 82: Top enclosure of the electronics enclosure for the pump.

Figure 82 shows the controller box developed for the pump's electronics. Slits had been placed on the sides to facilitate airflow for cooling the drivers. The screen is plugged onto the lower section and keypad above. The top section fits into a bottom section.

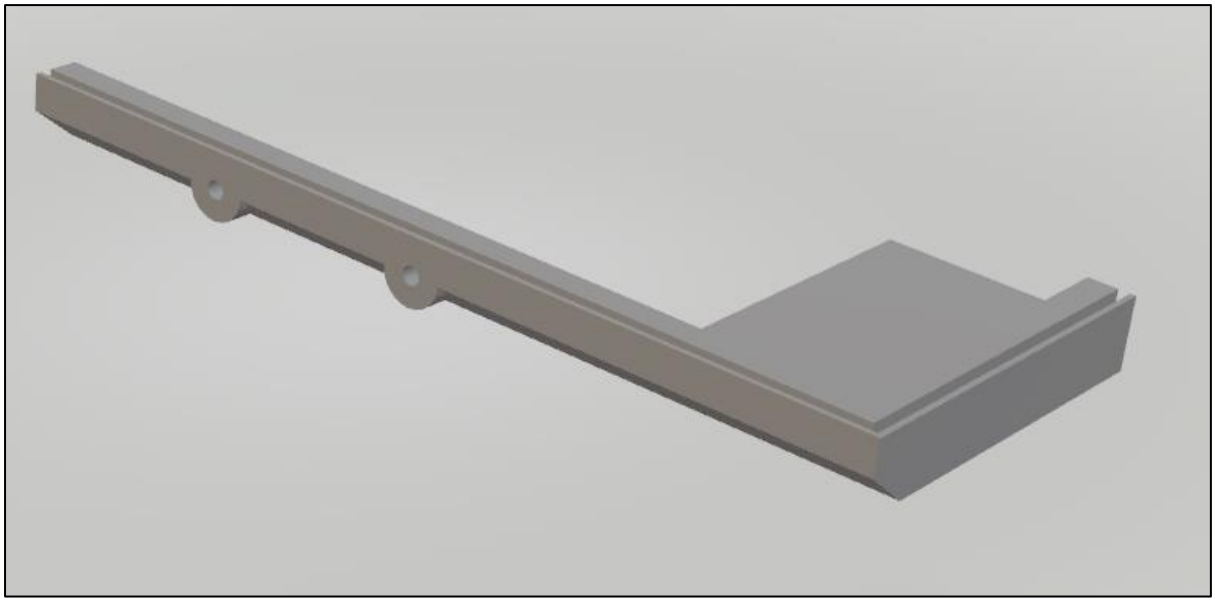

Figure 83: Bottom section of electronics enclosure for the pump.

The bottom fitted around a wooden base and had holes to screw the bottom part of the controller to the wooden base. The power supply was screwed to the back of the pump's brace where the bottom of the casing also acted as support. The top piece extends over the electronics base onto the pumps brace, which can be seen in Figure 83. This reduces stress on the bottom.

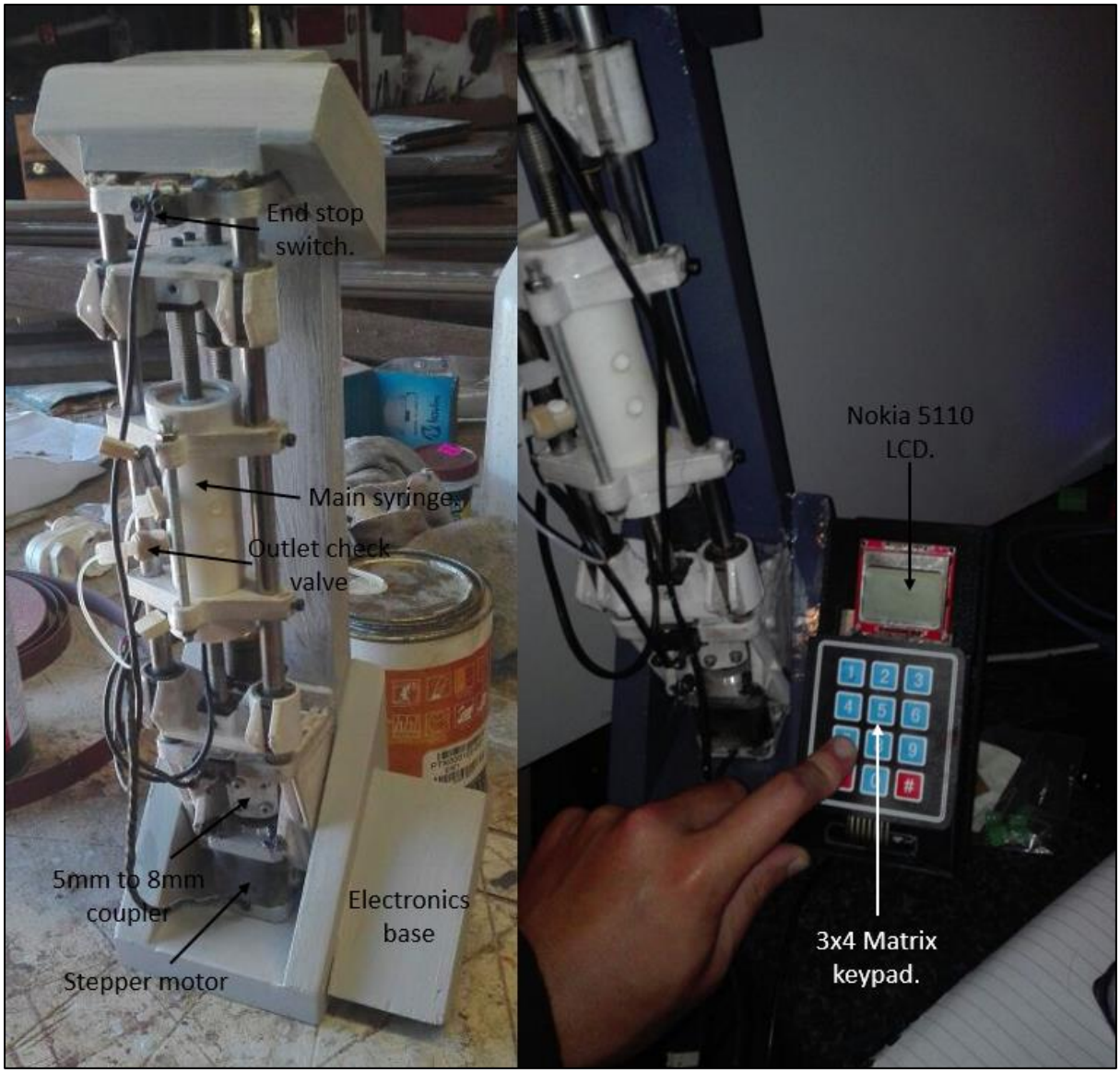

Figure 84: Base coating and final pump product.

As seen in Figure 84, the pump's scaffold was painted with an MS primer which seals the wood against moisture. After the primer was dry, the surface was painted with a battleship grey enamel coat. The stepper motor was connected to the threaded rod with a 5mm to 8mm coupler, which was also 3D printed.The edges of the LCD were covered with a 3D printed cap.

2.3 Cost of Manufacture.

A brief analysis of the cost of the project was done for comparative purposes. Personal labour was excluded since a lot of trial and error was undergone. This compounded the working time on the project. Therefore a lot of optimization may be developed for upscaling. The cost has been split into material cost and processing cost.

Table 9: Materials cost of reactor and reactor unit.

Materials	**Dimenions**	**amount**	**Price R**
Hastelloy C276	50mm x 40mm x 3.2mm	1	77.80
200Ω 50W Power resistor		2	55.92
Arduino UNO R3 Clone		1	57.55
Single Side Copper Clad	70mm x 100mm	1	11.53
Headers and Pins	40pin 2.54mm	3	9.20
Pt100 thermocouple	25mm x 3mm	1	637.58
PR4114		1	2436.00
PR4501		1	626.40
5mm Glass slide	40cm x 50cm x 5mm		20.00
		Total	**R3932**

Table 9 represents the materials and equiptment cost of the reactor and its reactor unit. The majority of the price was due to the PR Electronics components. Although these components are of excellent quality and simplified the design process, the price makes the equiptment much more expensive. Further investigation can be done to look for more affordable temperature control systems.

Table 10: Machining and process cost of reactor and reactor unit.

Process	**discription**	**Price R**
Laser cutting	Clamp cap cutting	288.6
3D printing of reactor parts	Based on R15/hour	120
Laser etching.	Done externally	1500
Manual labour	Not determined	
	Total	**R1908.6**

Table 10 shows the processing cost of the reactor and it's unit. The laser ablation/etching was the most expensive procedure. The main reason for this being that it has been done externally. Insourcing the procedure would significantly reduce

processing cost. Therefore it can be estimated that the cost of the reactor and it's unit will be R5840 excluding personal labour.

Table 11: Materials cost of pump.

Materials	**Dimenions**	**amount**	**Price R**
White Teflon Shaft	1m x 32mm	1	614.27
Arduino Mega R3 Clone		1	116.27
SilverSteel Rod	1m x 10mm	1	110
LM10UU bearings		1	68.27
Esun ABS filament 1kg	1.75mm	1	299
BS013 O ring	1.78mm cross section 10.83mm ID	2	80
BS018 O ring	1.78mm cross section 15.83mm ID	2	80
4x3 dot matrix keypad		1	9.15
Nokia 5110 Screen		1	54
Single Side Copper Clad	70mm x 100mm	1	11.53
Etchant	200g	1	58.71
1/4-28 inlet check valve		1	727.44
1/4-28 outlet check valve.		1	727.44
		Total	**R2956.08**

Table 11shows the cost of the pump's materials. Most of the pump's cost can be attributed to the two check valves. Reducing the price of these valves or finding an alternative would significantly reduce the price further. This problem often occurs with other low volume high pressure pumping technologies, such as HPLC and diaphragm pumps.

Table 12: Machining and process cost of pumping system.

Process	**Description.**	**Price R**
3D printing of reactor parts	Based on R15/hour.	610.00
Manual labour	Not determined	
Cylinder machining	Based on R90/hour.	360.00
	Total.	**R2470**

Table 12 represents the machining and processing of the pumping system. The bulk of the cost is due to the 3D printing of the plastic parts. A 0.5mm nozzle was used to print the parts. By increasing nozzle size to a 1mm nozzle, the printing rate may be increased 4 fold since a circular surface area has a exponential function. The

cylinder was initially attempted in Hastelloy. However Teflon proved to be an excellent compromise due to its machinability and chemical resistance. Therefore it can be assumed that the cost of the pump will be R5426.08 excluding personal labour.

Table 13: Price comparison of own system compared to commercial counterparts.

Component	**Own System**	**Chemtrix Labtrix**	**Uniqsis FlowSynth**
Pump	R5426.08	-	-
Reactor	R1577.8	-	-
Reactor unit.	R4462.2	-	-
Total cost.	R11266	R182777,00	R980487,54

Table 13 shows the price comparison between the manufactured system and it's commercial counterparts. It should be noted that the system is in it's prototype stage. Further, development, marketing, scaling up, logistics nor profits were included which will increase the price.However, a weaker local currency will increase the profit margin for international markets, which will most likely make the system affordable compared to other systems.

3. Testing equipment

3.1 Pump

3.1.1 Flowrate accuracy and reproducibility

3.1.1.1 Overview

For the pump to be usable, accurate flowrates must be attained at different flowrates. It is expected that the relationship between pulse rate and flowrate will be linear. However due to time constraints the correct check valves did not arrive in time. Therefore, the check valve which was selected for this pump was not ideal. Although the pump's intended use is geared towards microfluidics, it will also be beneficial to test it at higher flowrates, esepecially where larger volume meso-reactors are used. 0mL/min to 4mL/min will be tested for reproducibility. The cylinders were designed to be slightly larger to allow for a larger range flow rate. The reproducibility will also be tested by doing the tests in triplicate. Theoretical flow rates will be compared to the obtained flowrates, and deviations from the linear relationships will be discussed. Xiang et. al used a similar method, where the flowrate was compared to rotation and deviations from the linear relationships were observed. Instead of RPM on the X-axis, the set value will be used. (37) The literature cited for this study only showed a range of 0 – 300µL/min.

3.1.1.2 Aims and questions

- To assess the viability of the pump in its current state.
- Identify weaknesses for future studies.
- Is the pump suitable in its current state?
- What is causing the problems, if not suitable?

3.1.1.3 Materials

- Distilled water.
- 100mL graduated cylinder.
- Vacuum source.
- Stop watch.
- Cotton wool.

3.1.1.4 Methods

The cylinder did not have a purge valve to de-gas the cylinders. Therefore, a vacuum was used to suck out the air in the first cylinder through the first check valve. This was done by removing the larger cylinders fitting on the check valve side. The other side's tubing is submerged in liquid with piece of Parafilm covering the tip. A vacuum is pulled on the other side, where the check valve is removed. The vacuum was turned on to to suck out air. When the pressure was at its lowest the parafilm around the tip, which is submerged, was removed, and liquid flows into the cylinder and displaces the vacuum. This was repeated 3-times. The same was done for the smaller cylinder while the first cylinder was sealed with a check valve which was removed.

The pump had variations in its flow at the large cylinders charge to discharge cycle. Therefore, the volume that was pumped was kept constant at 30mL to account for the variation in flowrate. Possible reasons will be discussed below. The experimental domain was between 0 and 4mL/min. All the experiments are done in triplicate.

Table 14: Experimental parameters for flowrate reproducibility.

Experiment	**Flowrate (mL/min)**	**Time (min)**	**Volume(mL)**
1	0.25	120	30.0
2	0.50	60	30.0
3	1.00	30	30.0
4	2.00	15	30.0
5	4.00	7.5	30.0

The cotton wool was placed at the neck of the flask to minimize evaporation especially for longer runs. The observed flowrate vs the theoretical flowrate was plotted where the ideal flowrate is represented by a linear line with a gradient of 1.

3.1.1.5 Results

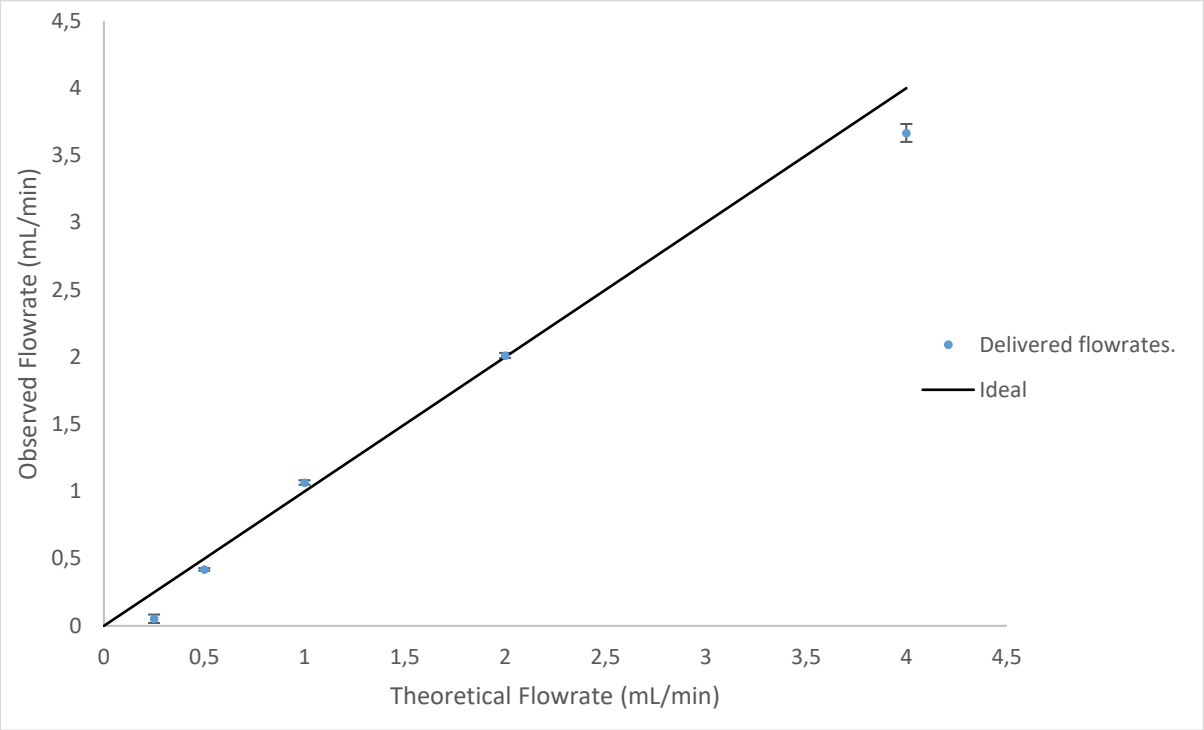

Figure 85: Delivered Flowrate vs Theoretical Flowrate in mL/min.

Figure 85 shows the results obtained from the flowrate accuracy and reproducibility experiments. At 0.25mL the flowrate was much lower than expected; at 0.5mL/min the flowrate was closer to the actual value and at 1mL/min the flowrate slightly exceeded the ideal value. The flowrate was ideal at 2mL/mL and at 4mL/min it was lower than expected. The relative standard deviation to flowrate size significantly decreased from 0.25mL/min to 4mL/min deviations. Therefore at higher flowrates it does not have such a large effect on volume. Figure 86 highlights the total volume expected vs delivered, which better illustrates the problem. Although it appears that the error bar does not exist for 0.5mL/min to 2mL/min, it was extremely small, and smaller than the width of the datapoint. So the datapoints for Figure 85 were reduced in size to illustrate the error bars.

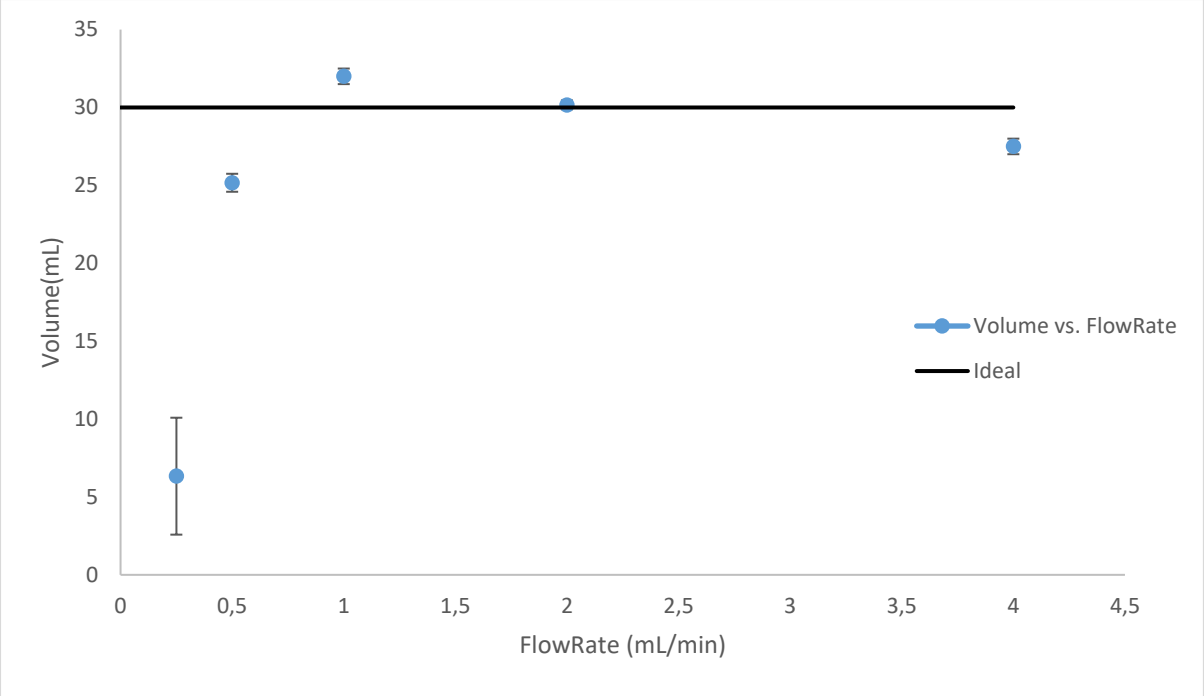

Figure 86: Dilivered volume vs Flowrate. Ideal volume at 30mL.

Figure 86shows the deviations in total volume delivery from the ideal volume at different flowrates for 30mL/min. As discussed under Figure 85 the lower flowrates show extreme deviations from the delivered volume. As the flowrate increases the volume is more accurately dispensed. When comparing the reproducibility between each flowrate point it is clear the 0.25mL/min had the highest standard deviation.

Some general observationsare show that some minor leaking did occur at the piston/cylinder seal interface, especially at higher flowrates. It appeared that piston holders flexed significantly. The two anti-backlash nuts did move in a synchronised way when the direction changed. However, one nut relaxed in the movements change of direction, which caused one of the piston holders to momentarily cease in motion. Possible results of these anomalies will be discussed below.

3.1.1.6 Discussion

There was a significant variation in the flowrate as well as deviation from the ideal values at the higher and lower end of the graphs. The dispensed volumes were fixed between each data point thus the variation in flowrate's effect was excluded. Although the flowrate increased with an increase in pulse rate, the relationship between the observed and theoretical was not linear, which would not allow for the use of microfluidics. Two factors probably influence the variation flowrate, with the first being the flexing in the piston holders, see Figure 73. Flexing of the piston holder plates caused a problem when the direction of the stroke changed. Before the piston switches stroke direction at the ends, the bend in the holder must first be relaxed, and tension in the opposite direction must build up sufficiently. This, in effect, creates variation in the flowrate. Some attempts were made to account for the flexing by incorporating bracing into the design. However, the flexing was still observed in both holders. This might be mitigated by increasing the amount of bracing. AMetallic holder would be ideal for the piston holder. The problem with metallic parts in the machining is more expensive and hence the production cost will rise. Other sources of flowrate variation are the anti-backlash nuts. As the direction changed, the one nut appeared to relax. A probable reason for this is the dislodging of the brass nut from its housing. Single part metallic anti-backlash nuts are available, which is commonly used in 3D printing, thus it is a more suitable option for this application.

Therefore, to reduce the variation in flowrate, the flexing must be eliminated, and the two piston holders need to be synchronised in its movement. A single metallic unit which houses both piston holders would most likely solve some of the flowrate variation.

Another problem which presented itself, is the total dispensed volume deviations at the lower and higher flowrates. It is suspected that the lower and higher deviations are not due to the same mechanism. The original inlet check valve, which was connected to the inlet of the larger cylinder's cracking pressure was too high, therefore the flow during the charge phase was severely limited. To solve this, a springless check valve was installed. The reverse flow causes a pressure spike which seals a membrane on the inlet side. At low flowrates the pressure spike was not sufficient to seal the check valve, hence the cylinder discharges in the opposite

direction. The reduced total volume to standard deviation ratio also exacerbated this problem. Proper check valve selection will therefore significantly improve the flowrate profile on the lower ends.

Deviations at the higher flowrates can be described by two mechanisms. The one is the increased pressure, due to flow rate, which stresses the seals, and leaking occurs. This was observed at higher flowrates. Improving the sealing will solve this issue. Another possibility is the restriction of flow into the charging of the first larger cylinder. The pressure driving the initial charge phase is the atmospheric pressure, which is limited to one Atmosphere. Backpressure is proportional to flowrate; hence the main cylinder does not have enough time to charge during faster flowrates. An inlet check-valve with a larger orifice will increase the maximum possible flowrate into the main cylinder, hence a larger range of pumping can be achieved. However, we have not investigated these answers further, but this would form part of a potential future study.

3.1.1.7 Conclusions

The pump did in fact work and displayed that there is viability to the proof of concept. However certain problems made the pump unsuitable in its current state, to be used for microfluidics. Proper check valve selection, improved structural integrity and improving the seal design, might make this pump suitable for the continuous flow and microfluidic industry.

3.2 Reactor

3.2.1 Reactor Volume Testing

3.2.1.1 Overview

To quantify the residence time in microfluidics, the volume of the reactor needs to be known. In chapter 2 it has been shown that there are slight variations in the channels' cross-sectional geometry when using the laser ablation method. Additionally, the compression of the Teflon gasket into the channel volume is not known. Therefore, accurate manual calculation is not feasible for this study. More uniform and reproducible dimensions would have shown an accurate theoretical value. However there was some variation which made calculations less reliable. The thin Teflon gasket enables the user to see inside the reactor. Consequently, the progression of flow can be easily monitored as it flows through the empty channels. Thus, the time the liquid takes to flow through the reactor can be used to calculate the reactor volume if the flowrate is known.

3.2.1.2 Aims and Questions

- To determine the reactor volume.
- Is the reactor volume reproducible at a fixed flowrate?
- Is the volume constant over different flowrates?

3.2.1.3 Materials

- Distilled water.
- Stop watch.
- Bright light source.
- Chemyx syringe pump.
- SGE 5mL glass syringe.

3.2.1.4 Methods

The whole reactor was filled with water to ensure that the non-tested regions do not compress its volume during testing. The non-tested regions are, inlets, piping and all pre-mixing areas, where non-compressionis sre required during testing. Compression in these areas will lead to larger readings. Therefore, these areas were filled with water which is non-compressible. All the filled non-compressible areas' openings were shut to insure the pump does not pump into these regions. For this method to work accurately, the reactor must be liquid free in the reaction region. This

was accomplished by flushing the region with compressed air from both sides, and a vacuum was also applied. This is to ensure that all the moisture was removed. Water was pumped and monitored as it flowed through the reactor region. The time it took to flow through was used to calculate the reactor volume. 10µL/min, 20µL/min, 30µL/min and 40µL/min were used to calculate the volume. Each flowrate had 4 experiments to test for reproducibility. Higher flowrates were investigated. However the reason for not including this will be discussed on the discussion page.

3.2.1.5 Results

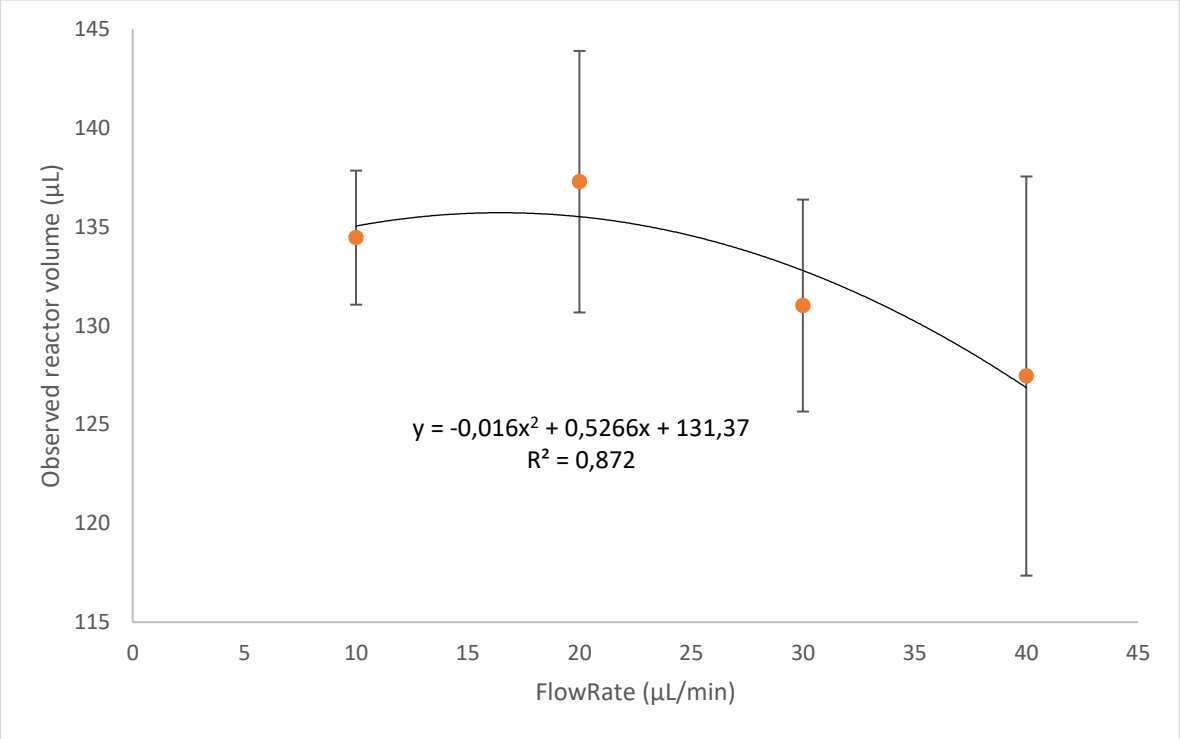

Figure 87: Observed reactor volume vs. Flow Rate (µL/min).

Figure 87 shows the average volume obtained at each flowrate, with its standard deviation. Since there is significant overlap of the standard deviations between the flowrates, a t-test was done which tests for the statistical differences between each of these values. The null hypothesis for this test is that there is no statistical difference between these values. The alternative hypothesis is that there is a statistical difference.The following table highlights the results obtained for the T-test.

Table 15: T-test for observed reactor volume at different flowrates.

flowrate data sets(n=4)	**10&20**	**10&30**	**10&40**	**20&30**	**20&40**	**30&40**
Result (P0.95)	0.781	0.292	0.259	0.094	0.092	0.216

Table 15 shows the results of the T-tests between each of the flowrates. A value of 0.05 and lower indicates that there is a statistical difference. None of the flowrates had a p value below that. Thus, there is insufficient evidence to conclude that there is a difference between the change in flowrate on the reactor's volume. (47) Overall, however, there was a decrease in the uncertainty of the volume as the flowrate increased.

Based on the trendline the maximum reactor volume was ~135µL. This value was used to calculate the residence time for the following experiments. Estimations from the design phase was 194,3µL. However that did not consider the compression of the Teflon that might displace reactor volume.

3.2.1.6 Discussion

Although precise data could not be obtained for the reactor, the values were within a reasonable region. It was decided to use 135µL. The disparity between the theoretical and what was achieved can be explained by the compression of the seal into the reactor volume. At higher flowrates it appeared that at two parallel channels the fluid runs over the surface into the adjacent channel. This created multiple plugs of fluid which complicated the volume determination. Blockages might have been the culprit. However at lower flow rates the liquid ran normally through the reactor, hence eliminating blockages as a cause. Another probable reason might be weak sealing on the surface. The back pressure required to flow down the channels exceeds the pressure to skip over the channels. Since the Teflon films were compressed over a wide surface, compression of the Teflon itself was not possible. However small air pockets between the layers might have compressed, causing the liquid to skip the channels. Having a single layer gasket might solve this issue. Another solution is to increase the clamping pressure, but this will cause other issues, such as the cracking of glass or bending of the clamp.

3.2.1.7 Conclusions

The reactor volume was estimated to be 135µL/min. As the flowrate increases the uncertainty of the measurement volume reading increases. Hence as the flowrate increases, the volume of the reactor becomes more unknown according to the method used. However the T-tests suggest there was not sufficient evidence to pronounce that the volume is constant over different flowrates. However lower flowrates generally afforded superior reproducibility. Thus the reactor's volume was chosen at lower flowrates.

3.2.2 Reactor kinetics comparison

3.2.2.1 Overview

For the reactor to have any commercial value the performance level is essential. Therefore,a model reaction is required which analyses the reactor kinetics. The kinetics of the tested reactor will be compared to two commercial microfluidic systems, namely Little Things Factory (1300µL) and Chemtrix Labtrix glass reactor (19.5µL). Since the volumes of these reactors are different from one another conversion will be used instead of chemical throughput. In a commercial setup number up can be used to account for the volume differences. A simple Fischer-esterification will be done whereby the conversion will be used to determine comparison of the kinetics. Ethyl acetate synthesis will be used as a model reaction.(48)

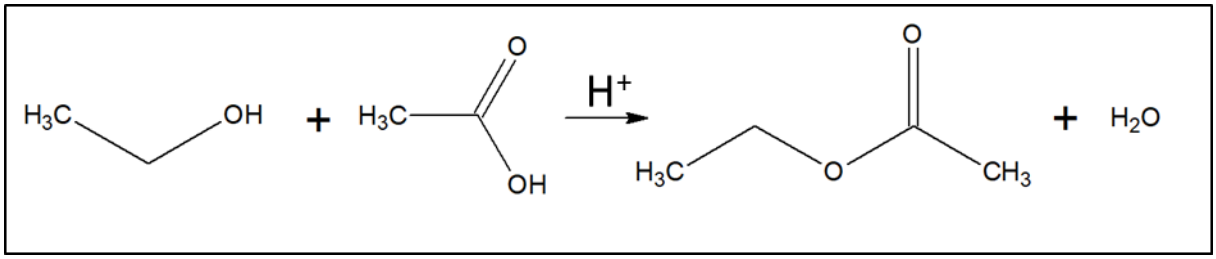

Figure 88: Reaction overview of ethyl acetate synthesis.

The reaction is acid catalyzed; hence the kinetics will also be determined by the acid content. Since the purpose of the study is comparative, pushing the reaction until completion for all the reactors won't give the necessary information to discern between the performance. Therefore, a miniscule amount of sulfuric acid was added as a catalyst (1mL H_2SO_4 in 200mL EtOH).

3.2.2.2 Aims and questions

- Determine chemical conversion profile for each reactor.
- Develop an accurate model for comparing the performance of different reactors.
- To determine which reactor has the highest conversion?

3.2.2.3 Materials

- Absolute ethanol Merck.
- 98% Sulfuric acid APC.
- Glacial acetic acid Merck.
- Micropipette. 1mL volume.
- 100mL graduated cylinder.
- 1000mL glass beaker filled with mineral oil.
- 2 x Chemyx syringe pump.
- Stirring hotplate with temperature probe.
- 2 x SGE 5mL glass syringe.
- Bruker Alpha FTIR with ATR unit.
- LTF-MS(0.2mL) + LTF-VS(1.1mL).
- Chemtrix3227(19.5uL) + Thermoelectric temperature control.
- Test reactor.
- GC cap.

3.2.2.4 Methods

The analysis method used was inline FTIR. The reaction was extremely time specific and this method provided rapid analysis. A multi-compound analysis standard curve was prepared which contained all the compounds in the reaction mixture but at different concentrations. This was done with a micropipette hence a high degree of accuracy was achieved. The software, QUANT 2 which forms part of OPUS, automatically identified the peaks using second order derivatives, hence manual peak selection was excluded. Standard curves were generated for each compound in the mixture and the software automatically gave the molar percentage composition of each compound in the solution. Molar percentage was used as a unit to access the composition. The conversion was obtained from the relative percentages, hence the need for yield calculations is omitted. The conversion for the

reactions was calculated by this method. The standard curves can be obtained from the Index.

Two different master solutions were prepared for the synthesis. One batch consisted of neat acetic acid anhydride and the other batch of ethanolwith; a concentration of 0.0938M sulfuric acid (1mL in 200mL EtOH). The flowrates varied in residence time and the ratio of the flow of acetic acid anhydride to ethanol solution was 1 to 1.88. The ethanol solution equivalent was 1.53 compared to the acetic acid. An excess of ethanol was used to attempt to slightly dissolve the acetic acid anhydride due to its corrosive nature. Initial trials with the reactor showed that the acetic acid rapidly dissolved the ABS clamp cap. Thus, if leaking occurred the corrosion damage might be mitigated. Since the purpose of the study was comparative in nature the same concentrations were used for each reactor.

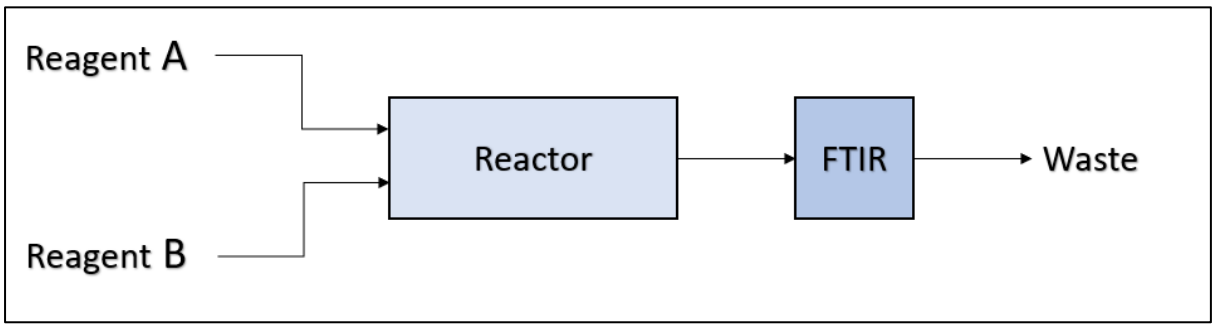

Figure 89: Reaction setup of comparative studies.

The neat acetic anhydride and 0.0938M H_2SO_4 ethanol solution both were pumped with the Chemyxwith 5mL syringes. At an equivalent flowrate of 1:1,53 acetic anhydride to ethanol. The residence times for each reaction is in Table 16:Reaction parameters for reactor comparison. The reactors with their auxiliaries were interchanged and the rest of the setup remained the same. Originally a Bruker inline flow cell was used. However,good reproducibility of the data was not possible. The internal volume of the cell was too large for the application. Since the residence time cannot be separated from the kinetics the reactors volume most probably added to the residence time and consequently there was a constant shift as time progressed. To account for the large volume a new miniature cell was constructed from a standard GC vial's cap.

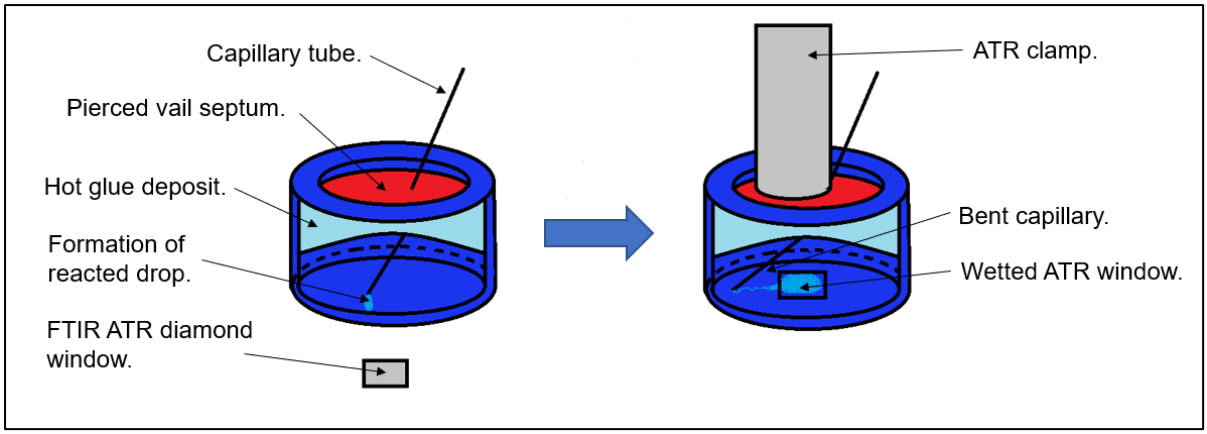

Figure 90: Alternative flow device for microliter scale FTIR analysis.

Figure 90 shows the gc-cap FTIR flow cell. The internal volume is filled with hot glue to minimize the internal volume, thus reducing the evaporation rate. The internal surface of the cap was wetted to further increase the vapour pressure in order to further reduce possible evaporation. The system first blanked with a clean diamond window. As the drop's volume built up the drop fell by itself onto the ATR window, and the cap was immediately clamped.The reading was also immediately taken to avoid further reactions. This afforded the best reproducibility when compared to the commercial flow cell. Multiple readings were taken in each run to confirm that the data for the specific experiment was reproducible. This counted as a single experiment, not as many. Thus, the whole heating process and reactor equilibration had to be redone to count as an experiment.

Table 16:Reaction parameters for reactor comparison.

Sample	**Residence time. (min)**	**Temperature C°**	**Experiments.**
1	1.8	35	4
2	1.8	50	4
3	1.8	65	4
4	2.7	35	4
5	2.7	50	4
6	2.7	65	4
7	3.89	35	4
8	3.89	50	4
9	3.89	65	4
10	5.4	35	4
11	5.4	50	4
12	5.4	65	4

The following parameters were used to generate the model and was done for each of the reactors. The reactors compared were LTF MS with LTF-VS (1300uL) and Chemtrix 3227. The temperatures were selected due to the glass temperature of the ABS plastic on the reactor. Future models would eliminate the need for polymer and have an all metal design. Higher temperatures might cause the fittings to shift and possibily increase leakage. Higher temperatures were obtained in the high yield experiments.

A regression model has been generated from the conversions on Statistica. An R^2 value of 0.979 was obtained, which means 97.9% of the data can be accounted for the by model. The following regression model was used.

Equation 6:

$$Conversion\% = int. + b_0T + b_1R + b_2T^2 + b_3R^2 + b_4RT + D_b b_5T + D_b b_6R + D_C b_7T + D_C b_8R$$

The constants can be found in Table 34 in the index, which also includes other statistical parameters. Settings D_b and D_c are the dummy variables. The test reactor excludes the dummy variable in its model while the Chemtrix 3227 includes

the D_b factors, and the LTF includes the differences. Therefore, these models can be compared. A surface plot of each reactor has also been prepared.

3.2.2.5 Results

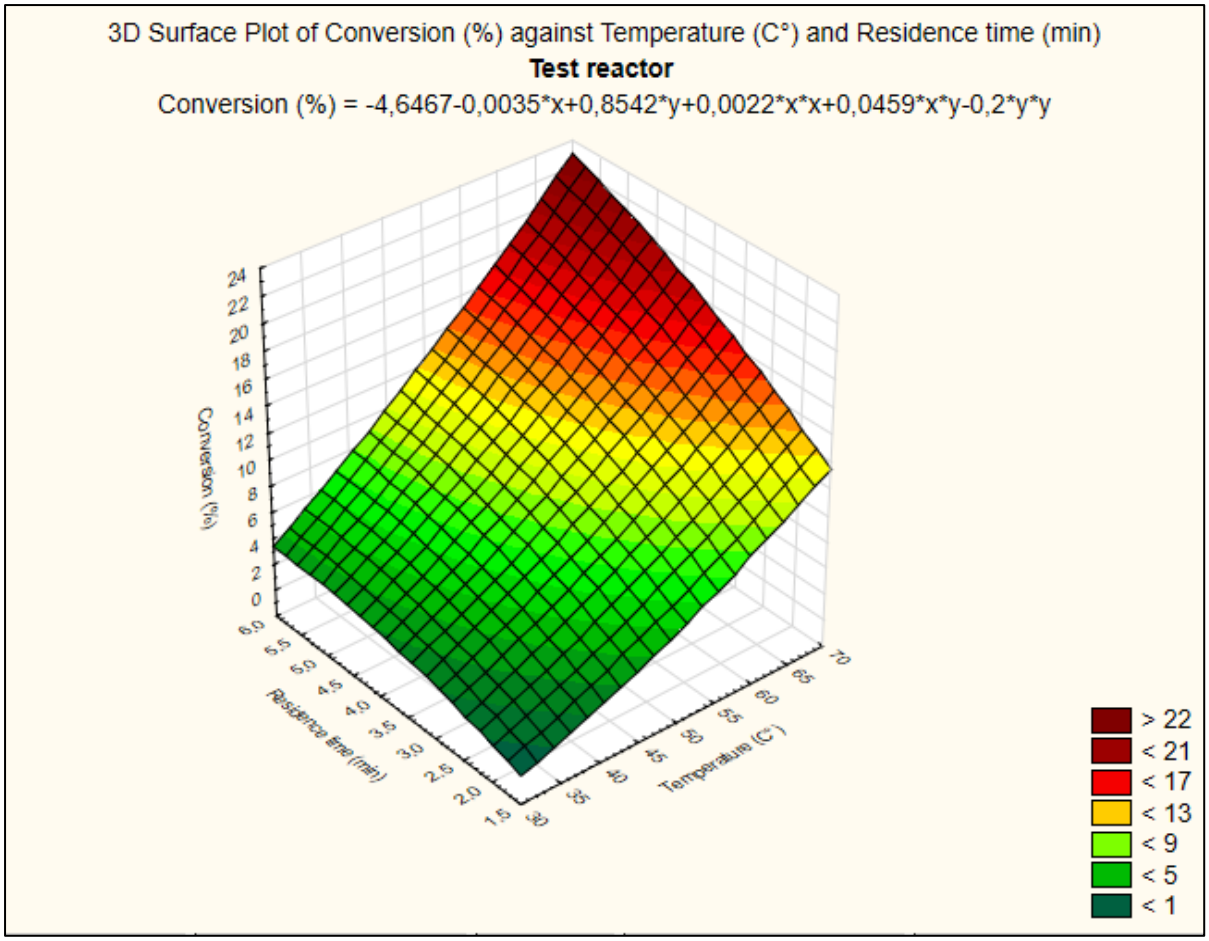

Figure 91:3D surface plot of the test reactor. Residence time and temperature was varied, and conversion was given as a response.

Figure 91 shows the surface response plot obtained for the test reactor. The Y-axis shows the residence time, the X-axis shows the temperature and the Z-axis is the response, namely, conversion. For the sake of efficiency, maximum throughput is preferred for industrial setups. Therefore conversion should be maximized to afford higher throughput. Due to the maximum conversion on the edge, optimum conditions could not be observed in Figure 91. Increasing the residence time as well as temperature will most likely increase the conversion. Increasing the temperature yields an exponential function, while the residence time's curve is more linear, thus increasing temperature would be more economic for industrial purposes.

It should be mentioned that the edges of this plot is outside of the experimental domain, therefore the profile plots, Figure 94 to Figure 96, were used as final

comparison. Something that was unique to this plot is that there was an exponential drop-off at lower residence times, which seems to be exacerbated at lower temperatures. Increasing the residence time does increase the conversion. However increasing the temperature has given the conversion a slight exponential response for the test reactor. Therefore,an elevated temperature reactor would be more beneficial than a high-volume reactor for this specific reaction.

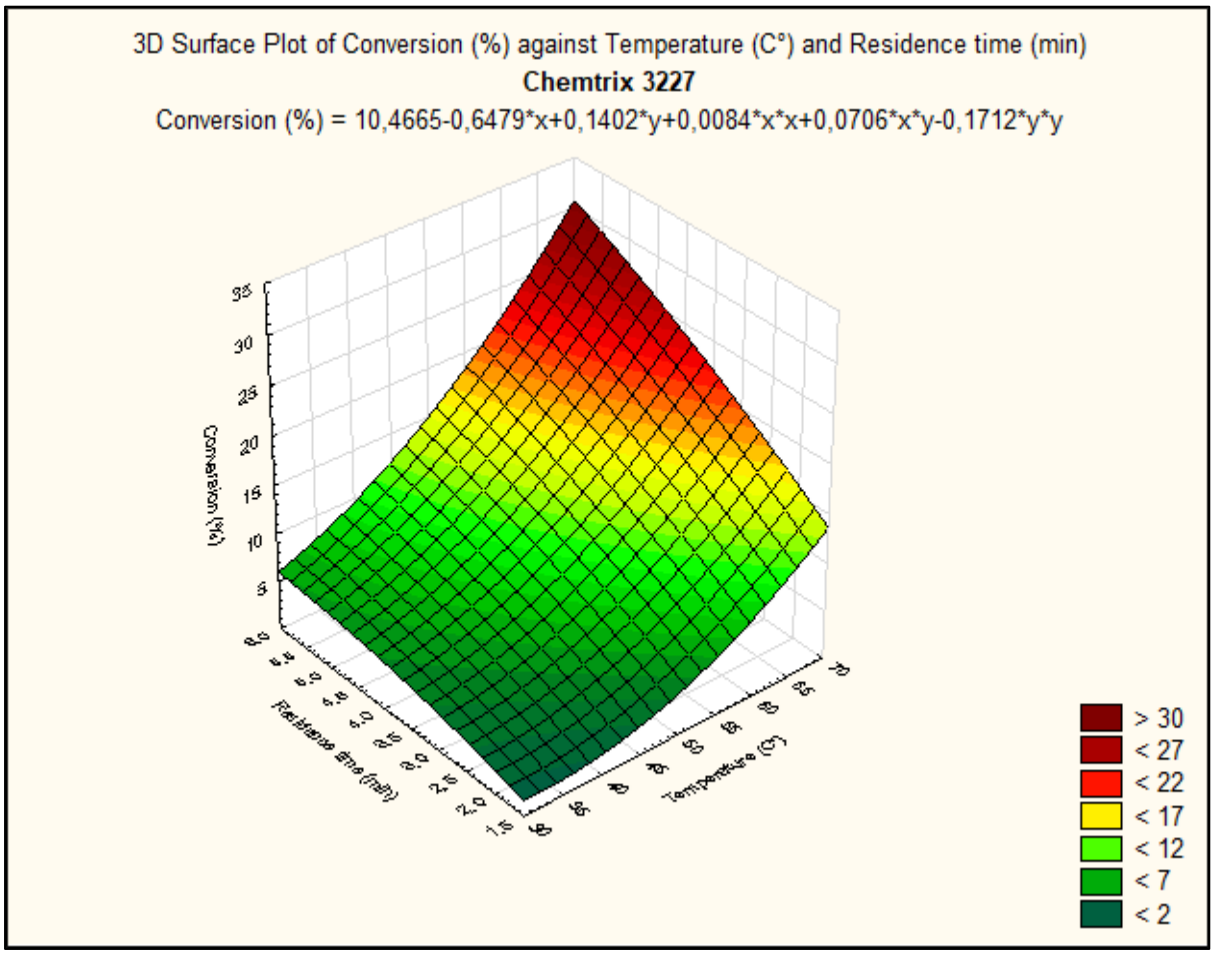

Figure 92: 3D surface plot of the Chemtrix3227 reactor. Residence time and temperature was varied, and conversion was given as a response.

Figure 92 shows the surface response obtained for the Chemtrix 3227 reactor. The Y-axis shows the residence time; the X-axis shows the temperature, and the Z-axis is the response, namely conversion. This reactor had the smallest volume of all the reactors. Comparing it with Figure 91 shows that there is a lot more bending in the slope, which indicates that the increase in temperature has a more exponential contribution to the conversion rate. At higher temperatures the resident time appears to have a more linear relationship. Comparing the maximum and minimum conditions it also appears that this reactor is more efficient than the test reactor.

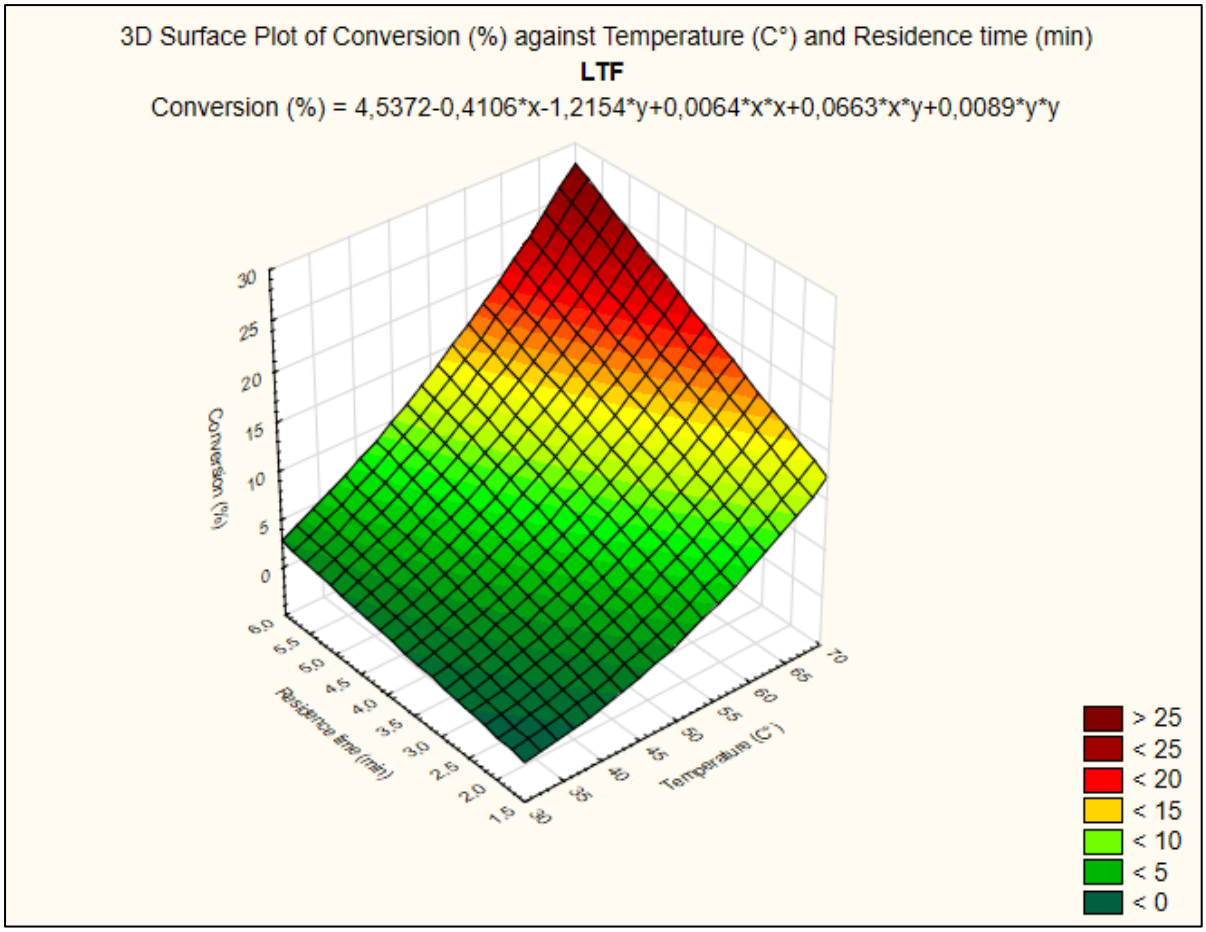

Figure 93: 3D surface plot of the Chemtrix3227 reactor. Residence time and temperature was varied, and conversion was given as a response.

Figure 93 shows the surface plot obtained for the LTF factor reactors. The Y-axis shows the residence time, the X-axis shows the temperature and the Z-axis is the response, namely conversion. This reactor had the largest volume of all reactors. This plot has a unique feature that the other two plots do not have. The residence time vs conversion rate was more linear especially at lower temperatures. The temperature vs. conversion profile still had an exponential increase. .

To compare the reactors more accurately, profile plots were generated. These plots are slices of the 3D surface plot that can be represented on a 2D plane.

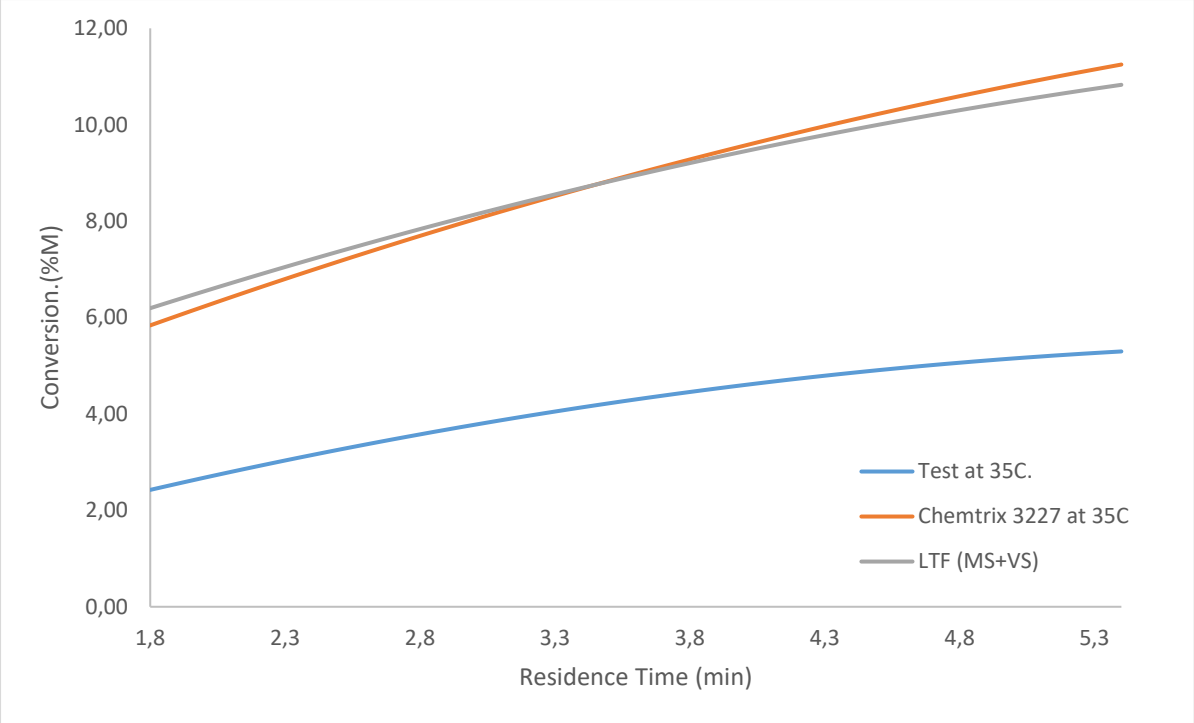

Figure 94: Profile plot of varying residence time at 35°C for all the tested reactors.

Figure 94 shows the profile plots obtained at the 35°C cross-sectional slice for each reactor. The test reactor under performed severely with its commercial counterparts. Comparing the magnitudes of the slopes, the test reactor loses its relative efficiency as the residence time increases. Possible reasons for this will be discussed in the discussion section. The chemtrix 3227 reactor provided the largest increase in efficiency as residence time increased at 35C°. The LTF reactor had the highest efficiency at the lowest residence time. At about 3.4 minutes residence time the Chemtrix overtook the LTF in conversion efficiency.

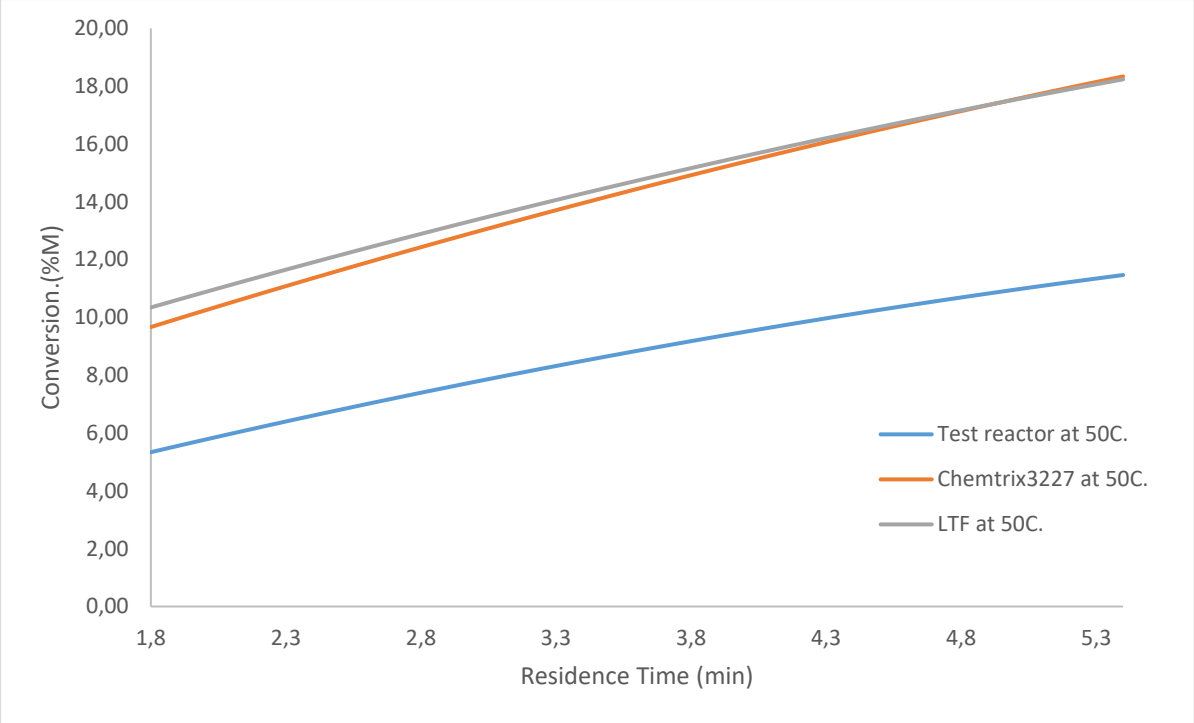

Figure 95: Profile plot of varying residence time at 50°C for all the tested reactors.

Figure 95 shows the profile plots obtained at the 50°C cross-sectional slice for each reactor. As in Figure 94 the test reactor underperformed significantly. However, when considering the relative conversion rate there is an improvement. The slope height compared to the previous figure is also higher. This suggests that higher temperature mitigates inefficiency as a function of residence time.

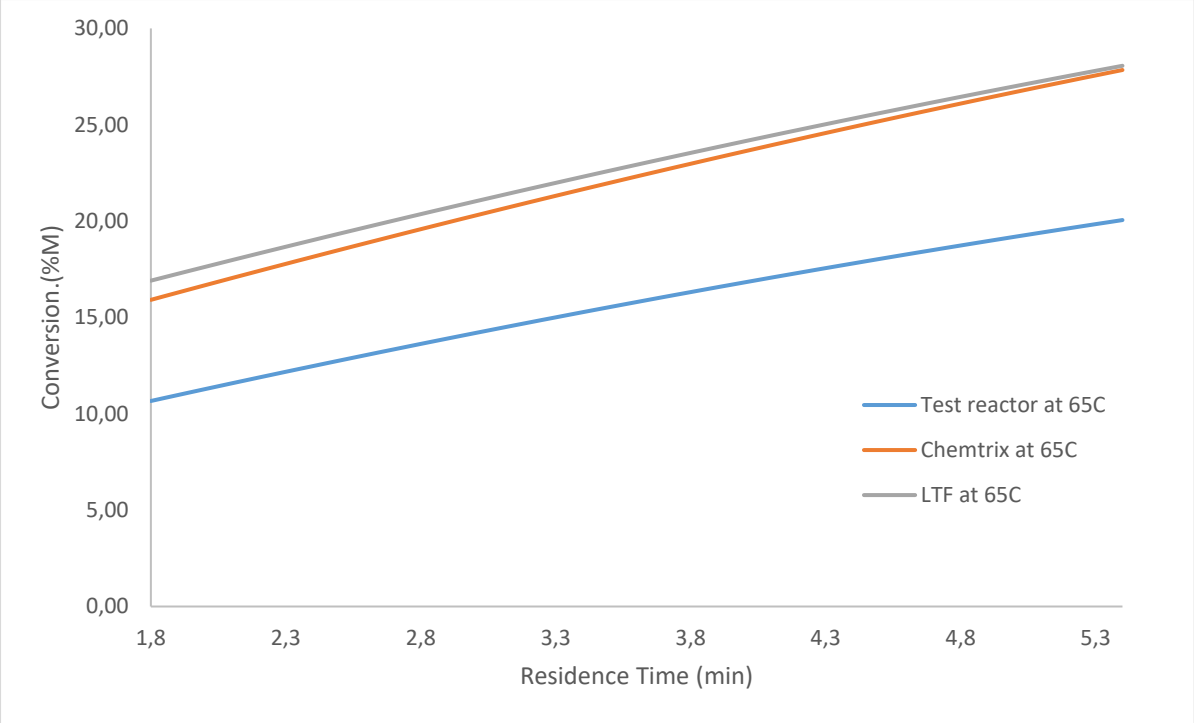

Figure 96: Profile plot of varying residence time at 65°C for all the tested reactors.

Figure 96 shows the profile plots obtained at the 65°C cross-sectional slice for each reactor. The same trend was observed where an increase in temperature normalises the change in the slope. Thus, the reaction is much more temperature specific than time specific. The LTF reactor outperformed all the reactors in this instance. The test reactors performance was the best relatively to the other reactors at higher temperatures.

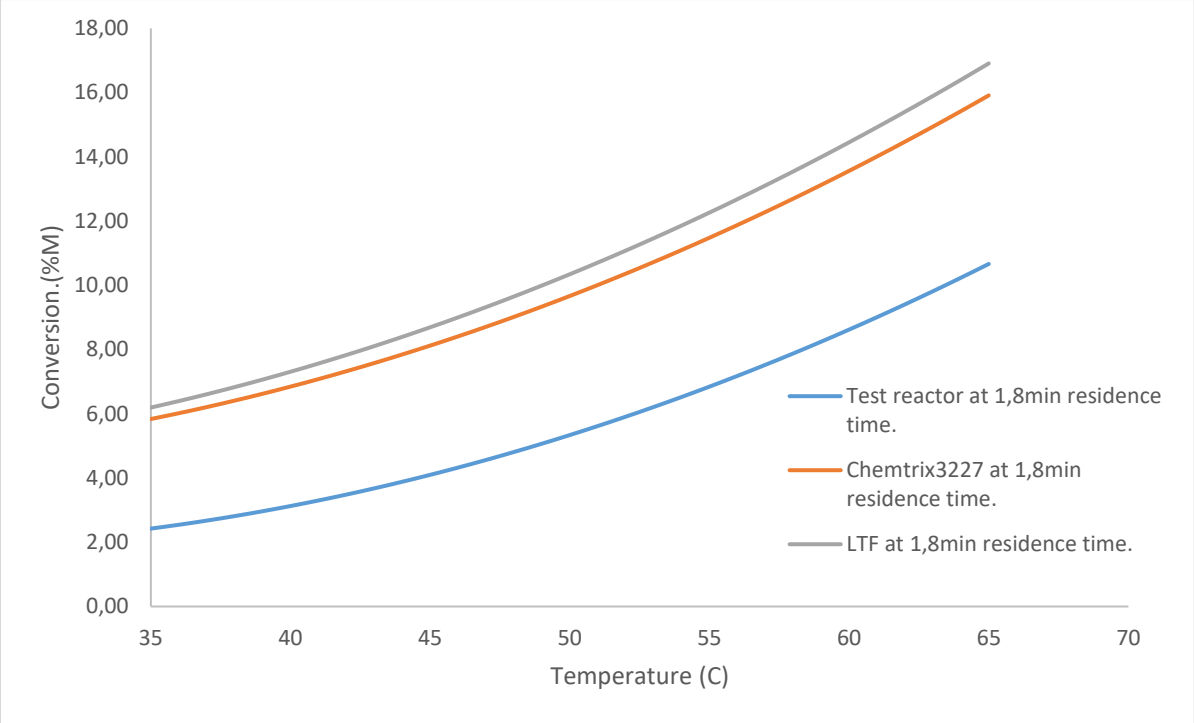

Figure 97: Varying temperature at 1,8min residence time for all the tested reactors.

Figure 97 shows the temperature variation from 35°C to 65 °C at 1.8 minutes residence time. The LTF reactor performed the most at this flowrate where the Test reactor performed the worst. As the temperature increased the LTF performance increased to a higher degree then the other reactors. Further explanation will be covered in the discussion section.

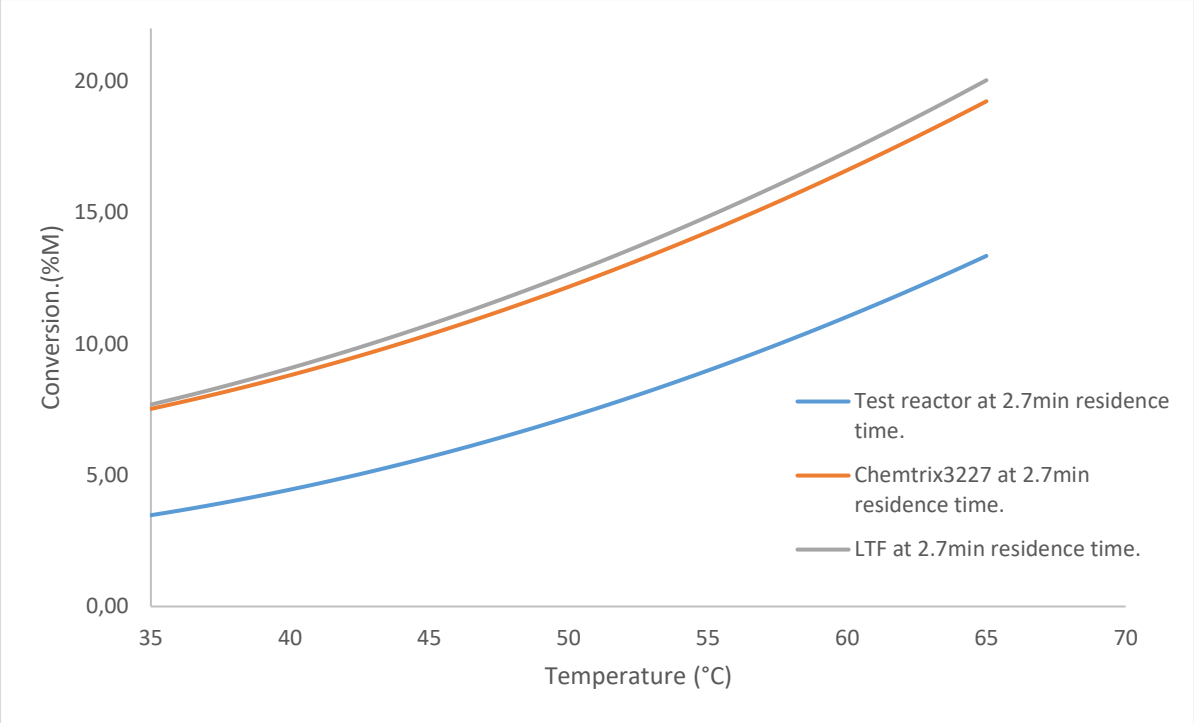

Figure 98: Varying temperature at 2.7min residence time for all the tested reactors.

Figure 98 shows the temperature variation from 35°C to 65 °C at 2.7 minutes residence time. As the residence time increased from 1.8 to 2.7 minutes the lower temperatures yielded the same conversion value. However, as before, the LTF performed better than the Chemtrix3227 at higher temperatures. The test reactor still had inferior conversion rates.

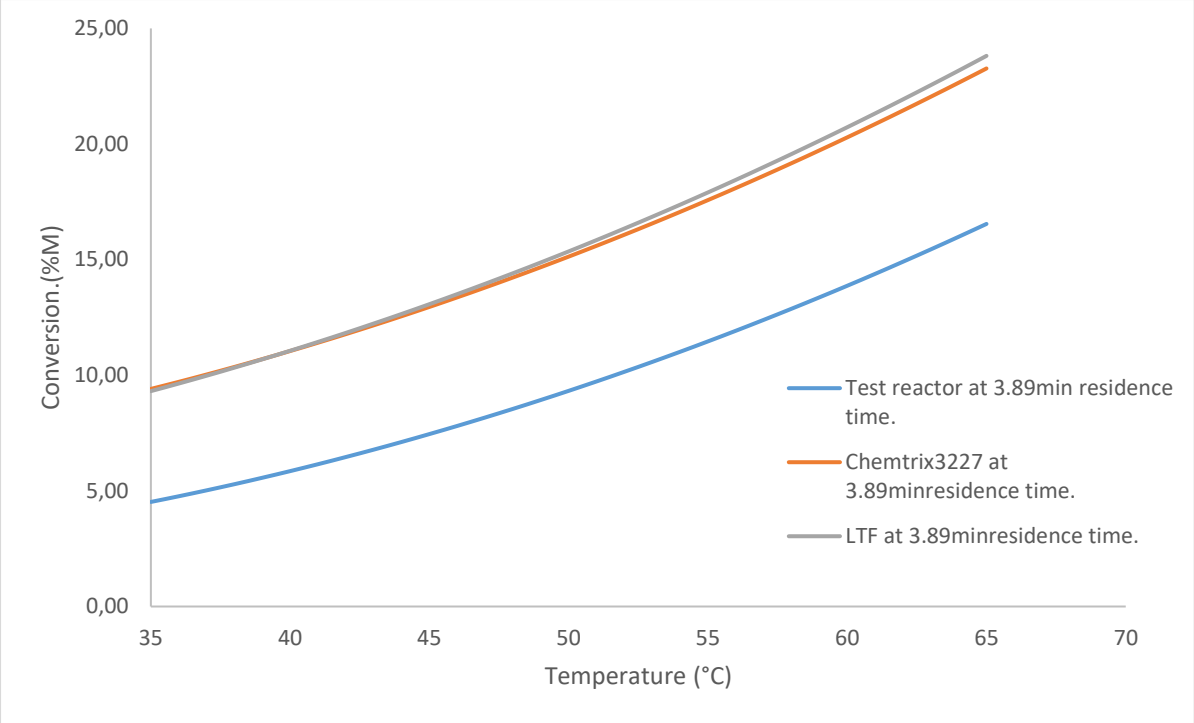

Figure 99: Varying temperature at 3.89min residence time for all the tested reactors.

Figure 99 shows the temperature variation from 35°C to 65°C at 3.89 minutes residence time. The Chemtrix reactor and LTF reactor's performance started to merge more at higher residence times.

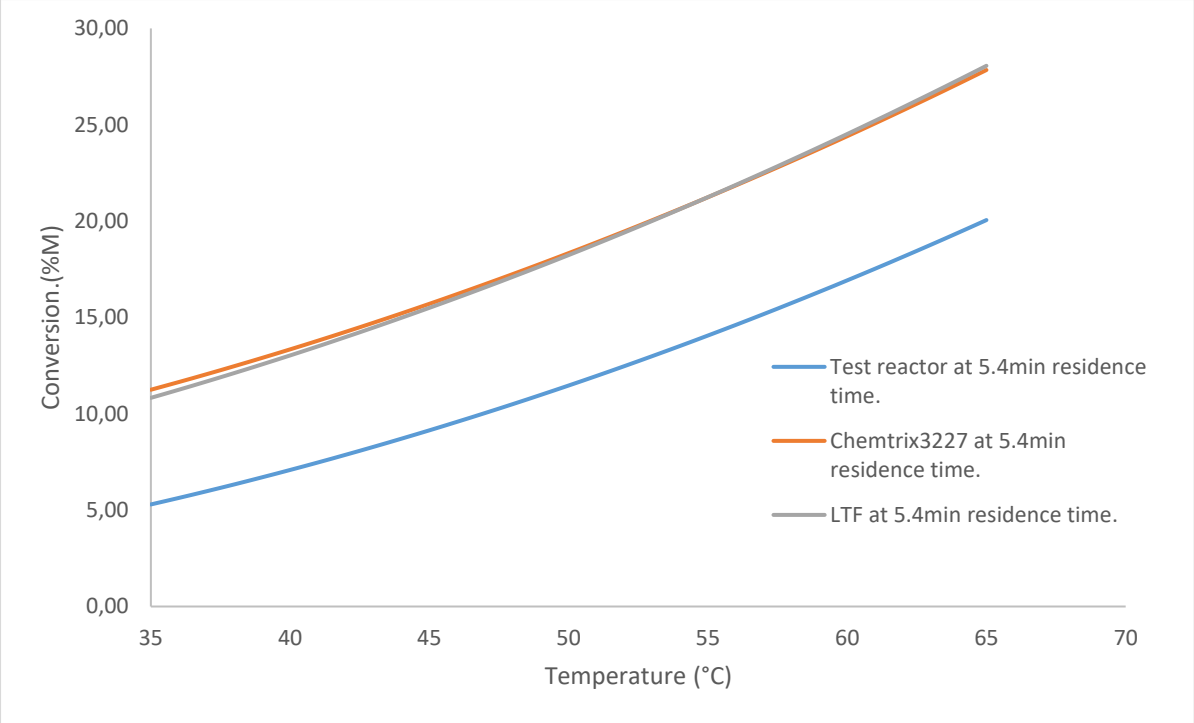

Figure 100: Varying temperature at 5.4min residence time for all the tested reactors.

Figure 100 shows the temperature variation from 35°C to 65°C at 3.89 minutes residence time. The Chemtrix and LTF at this flowrate essentially had the same profile plot.

3.2.2.6 Discussion.

The method used, afforded excellent results within the domain. About 98% of the data could be explained through the model. The commercial flow-cell was attempted although at first the internal volume was too large compared to the reactors internal volume, and the results were very unpredictable. The Little Things Factory and Chemtrix 3227 performed very similarly, but unfortunately the test reactor did not perform well at all when compared to the commercial reactors. Two factors are considered as the culprit. The first factor being considered is the sealing potential. Both the commercial counterparts were physically bonded, hence, no leaking could occur except at the fitting interfaces. To achieve the residence time's flowrates more than 40µL/min was used. In Figure 87 it was shown that there is a general increase in uncertainty as the flowrate increases. The largest flowrate that was used for this experiment was 75µL/min. The reason why the flowrate would be an issue is that the increased backpressure could cause the reagents to skip across the channel's

wall. If the reagent stream crosses one channel wall the residence time is decreased by 1.56%. This was observed in multiple areas in the reactor thus the residence time based on the flowrate is most probably not an accurate reflection of the residence time.

The second possible problem is the temperature control. The design of the test reactor had a large distance for the heat to travel through the metal. The PT100 probe was in the middle of these two regions. Stainless steel has a conductance of 16 W/m·K while Hastelloy C276 only has 9.8 W/m·K. The edges of the aluminium did touch on the clamping device, and the clamp device showed a significant temperature. It is suspected that the clamping device decreased the Hastelloy C276 reactor disc's temperature. The regression model obtained in this experiment suggests that an increase in temperature exponentially increases the conversion instead of linearly. Thus, the cooling by the clamping device, is exacerbated by this relationship. Measuring the temperature at the surface of the reactor was not possible due to the glass and Teflon film. Viable solutions to this problem may be to isolate the reactor disc and clamp thermally, as well as reducing the thickness of the heating block. A thinner reactor disc will facilitate the conduction of heat as well as decrease the price, since the material cost is high. Further an insulation material can be placed around the clamp device. This will limit heat loss as well as protect the user form potential burns.

As mentioned in the discussion of the volume determination section, very small air pockets were present between the Teflon sheets. Originally a 35µm sheet was used, however the reactors surface was not flat enough, so leaking took place. So multiple layers of the film were stacked on top of each other. The distance between the channels may be increased to increase the pressure threshold for jumping across the channel. Additionally, a thicker film would eliminate air-pockets that might compress and provide a pathway for the stream across the reactor well.

Comparing the LTF and Chemtrix the LTF had a slight advantage at higher flowrates (Low residence times). The reactor's internal diameter was much larger than the Chemtrix and test reactor, therefore the Reynold's number would be higher. Thus, it is most likely chaotic mixing which gave the reactor the advantage. The LTF reactor set had a total volume of 1300µL and the Chemtrix 3227 had a total volume of

19.5µL, therefore the throughput of the LTF is about 67 times more and occupies less desk space. Thus, the LTF system is the preferred system for this model reaction. Different temperature systems were used for both of these reactors. Slight deviations might also have influenced the conversion, especially with the LTF that used an oil bath. The oil was stirred to generate as uniform a temperature as possible.

3.2.2.7 Conclusions.

The test reactor did not perform in comparison with commercial units. However, some aspects of the design, which were named, may be improved to achieve more comparable yields. The method developed gave excellent reproducible data in a reasonable amount of time. Higher conversions are expected once the sealing and thermal problems are solved.

3.2.3 High yield reactions on test reactor.

3.2.3.1 Overview

Since the test reactor did not perform as well as hoped for in the previous experiment, the question still remains, is it suitable for flow chemistry? The previous experiments used lower temperatures as well as a very diluted sulfuric acid concentration. Although the reactor is not yet at a stage where it can compete with commercial competitors, it will be beneficial to see what it is capable of in more extreme conditions. Therefore, the same reaction will be done, using higher temperatures as well as higher concentrations of Sulfuric Acid.

3.2.3.2 Aims & questions

- To achieve a high yield reaction with the test reactor.
- Is it possible to handle more corrosive components through the reactor?
- What is the upper limit of the temperature?
- Is the method used with the reactor a comparable study, suitable for higher yields?

3.2.3.3 Materials

- Absolute ethanol Merck.
- 98% Sulfuric acid APC.
- Glacial acetic acid Merck.
- Micropipette. 1mL volume.
- 100mL graduated cylinder.
- 2 x Chemyx syringe pump.
- 2 x SGE 5mL glass syringe.
- Bruker Alpha FTIR with ATR unit.
- Test reactor.
- GC cap (Modified as described earlier).

3.2.3.4 Methods

The same analysis was applied as in the reactor comparison study, using Bruker's QUANT 2 package. Two stock solutions were prepared. Neat acetic anhydride was used in one, and an ethanol sulfuric acid mixture in the other. 4mL of Sulfuric acid

was pipetted to a 100mL half-filled graduated cylinder. The cylinder was topped with Ethanol. The contents were transferred to a Schottky bottle for storage. This equated to a 0.75M concentration of H_2SO_4in ethanol. The ethanol solution was pumped in a 1.06 ratio compared to the glacial acetic acid. The following parameters were screened.

Table 17: Reaction parameters for high yield reaction.

Sample	**Residence time. (min)**	**Temperature °C**	**Experiments**
1	1.8	70	4
2	1.8	80	4
3	1.8	90	4
4	1.8	100	4
5	2.7	70	4
6	2.7	80	4
7	2.7	90	4
8	2.7	100	4
9	3.89	70	4
10	3.89	80	4
11	3.89	90	4
12	3.89	100	4
13	5.4	70	4
14	5.4	80	4
15	5.4	90	4
16	5.4	100	4
17	10.8	70	4
18	10.8	80	4
19	10.8	90	4
20	10.8	100	4

Since the conversions were low in the previous experiment the resident time was increased, as well as the temperature to increase the conversion. The temperature was raised to just below the glass transition temperature of ABS plastic. The statistical model was omitted, due to reproducibility issues at higher conversions.

3.2.3.5 Results

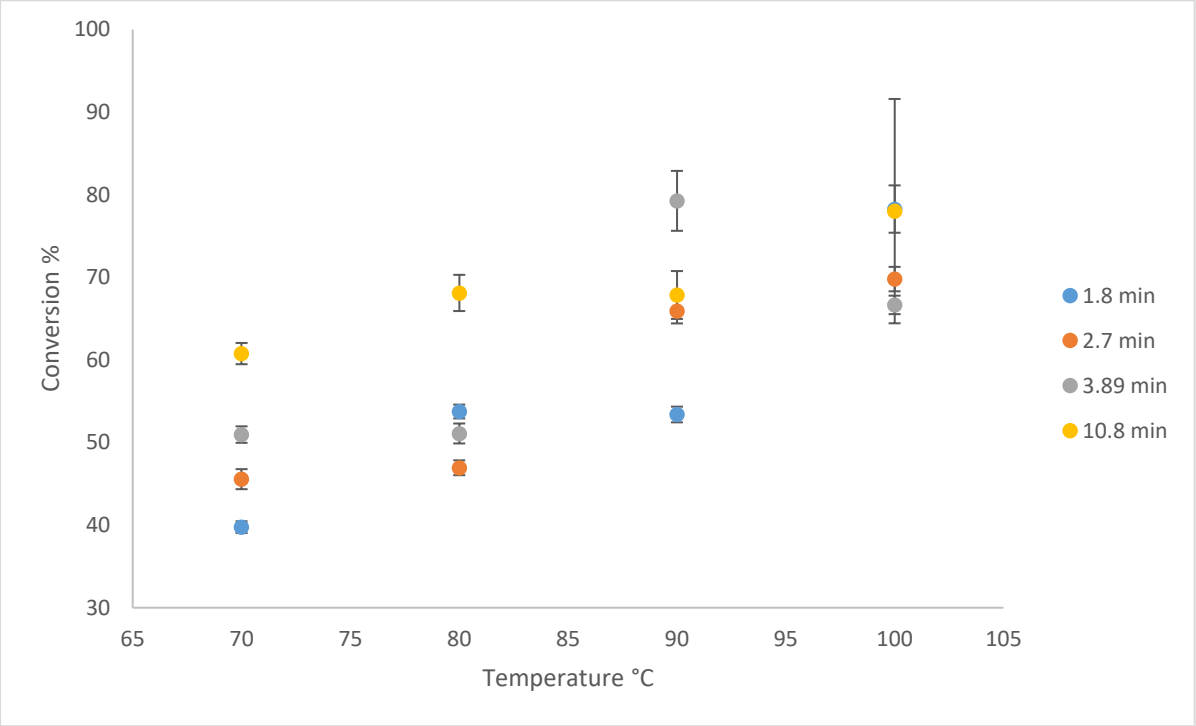

Figure 101: High conversion reactions in test reactor.

Figure 101 shows the conversion vs temperature plot of the high yield reaction. There was a general increase in conversion, with increased temperature and increasing residence time. However, the trend was not as clear as in previous experiments. It was also observed that the output stream was not homogenous. The IR spectra also showed a significant amount of water with ethanol and acetic acid and very little ethyl acetate. The method failed to accurately predict the conversion at higher yields. It appears that the threshold is just above 60% conversion where the data becomes unreproducible.

3.2.3.6 Discussion

The method worked well below ~60% conversion. The output stream was heterogenous with tiny balls of liquid. This is most likely the phase separation of ethyl acetate and water. It is thought that the reduction in ethanol and acetic acid reduced the miscibility of ethyl acetate in the water. Additionally, higher concentrations of sulfuric acid in the water might hydrolyse the ethyl acetate that is present. Since water's density is higher, the excess of the water was at the bottom of the ATR window. This accumulation of water is what distorted the data. No damage could be observed in the system, which suggests that it is able to operate at

100°C for extended periods. Higher temperatures were omitted due to the glass temperature of ABS plastic cap, which holds the tubing in place.

3.2.3.7 Conclusion

Although the reactor has some design flaws, it has been shown that the reaction can take place in conversions of more than 60% in less than 1.8 minutes, which is suitable for microfluidic applications. Also, no apparent damage was observed in the reactor after these reactions. The method was not suitable for accurately analysing the mixture above 60% due to phase separation of the solution.

3.2.4 Conclusion and future work

Although the commercial microfluidic and continuous synthesis systems are relatively expensive, the development and manufacture of a system would benefit the local pharmaceutical manufacturing economy. A proof of concept system has been constructed which has some functionality. The design was focused around open source technology, which makes any modification of the system non-proprietary. Since research is an adaptive field, this easy modification would benefit most labs as well as industry.

The cost analysis from page 104 has shown that the preliminary price of the system is far lower than it's European commercial counterparts, thus, it is economically feasible if pricing is kept within reason. The cost of the business model was also excluded and this might compound the price to offset the infrastructure cost. However if the price is low enough and the quality good the sales will offset the development cost.

The pump in principle did work, however some changes are needed to perfect it for it's intended design. Although 3D FDM printing was useful for quick prototyping of the parts, it did not provide enough rigidity for the mechanical parts which contributed to variation in flowrate. Proper check valve selection is also needed. The pump in it's current state only works between 1- and 3mL/min. The first inlet check valve did not close at lower flowrates and at higher flowrates it appears that the flow was not sufficient to fill the cylinder in time. Finally, there was also some leaking at the seals, which suggests that different seals, or a plunger type seal should be used. In summary, future work for the pump includes :

- Improving the structural rigidity to eliminate flexing, hence reducing flowrate variation.
- Design a single piece piston holder which eliminates the effect from variation between anti-backlash nuts.
- Investigate proper check-valve selection to extend the pump's functional range.
- Improve piston's seals or create an HPLC type plunger seal.

The metal disc reactor worked in principle, however some technical issues retarded the reactors performance. The seal did not work as anticipated, this is most likely

due to small air pockets that compress and weaken the pressure against the reactor surface. A feasible way to solve this is by using a thicker single sheet of Teflon. The heating system also needs to be compacted and isolated from the clamp system. It is suspected that the current design caused the unwanted cooling of the reactor during testing. Additionally, the ablation process took a lot of time, which would push up the price in a commercial setting. In summary, future work for the reactor includes.

- Improving sealing of reactor by; Improving the clamp device to increase pressure, using a thicker single layered membrane and byslightly increasing inter-channel distances.
- Provide isolation from the clamp to the reactor and isolated the heating system from the clamp.
- Reduce thickness of the reactor as well as the heating block to minimize thermal gradients.
- Design a thinner single layer heating block with the thermocouple closer to the disc.
- Determine the temperature offset from the thermocouple to reactor under different conditions.
- Investigate its viability as a block resistant reactor.
- Investigate stronger lasers for faster ablation rates.

The cost of development and construction of the entire project was less than one Chemtrix lab on a chip set. This can be attributed to open-source knowledge and using mass manufactured components where necessary. The author also was not trained in any engineering field; therefore a lot of improvements are possible. Although the project does not reach the standard of a commercial level, it can be concluded that the manufacturing of continuous flow equipment can be done at a local level.

4. Index

4.1 References

1. Geyer K, Codée JDC, Seeberger PH. Microreactors as Tools for Synthetic Chemists—The Chemists' Round-Bottomed Flask of the 21st Century? Chemistry – A European Journal. 2006;12(33):8434-8442.
2. DTI. Seventh United Nations Conference to review the UN Set on

Competition Policy. United Nations Conference Review. 2015.
3. Yoshida J, Nagaki A, Yamada D. Continuous flow synthesis. Drug Discov Today Technol. 2013;10(1):e53-59.
4. Kashid MN, Renken A, Kiwi-Minsker L. Gas–liquid and liquid–liquid mass transfer in microstructured reactors. Chemical Engineering Science. 2011;66(17):3876-3897.
5. Halder R, Lawal A, Damavarapu R. Nitration of toluene in a microreactor. Catalysis Today. 2007;125(1):74-80.
6. Martínez-Cisneros CS, Pedro SG-d, Puyol M, García-García J, Alonso-Chamarro J. Design, fabrication and characterization of microreactors for high temperature syntheses. Chemical Engineering Journal. 2012;211-212(Supplement C):432-441.
7. Kockmann N, Gottsponer M, Roberge DM. Scale-up concept of single-channel microreactors from process development to industrial production. Chemical Engineering Journal. 2011;167(2):718-726.
8. Bana P, Örkényi R, Lövei K, Lakó Á, Túrós GI, Éles J, et al. The route from problem to solution in multistep continuous flow synthesis of pharmaceutical compounds. Bioorganic & Medicinal Chemistry. 2017;25(23):6180-6189.
9. Bahrami M. Viscous Flow in Ducts: Simon Fraser University; 2009 [
10. Ferenc D. VH, György D. . Flow Chemistry- Fundamentals. Publishers DG, editor2014.
11. Bothe D, Stemich C, Warnecke H-J. Computation of scales and quality of mixing in a T-shaped microreactor. Computers & Chemical Engineering. 2008;32(1-2):108-114.
12. Kamholz A YP. Molecular diffusive scaling laws in pressure-driven microfluidic channels: deviation from one-dimensional Einstein approximations. Sensors and Actuators B: Chemical. 2002;82(1):117-121.
13. Knight JB, Vishwanath A, Brody JP, Austin RH. Hydrodynamic Focusing on a Silicon Chip: Mixing Nanoliters in Microseconds. Physical Review Letters. 1998;80(17):3863-3866.
14. Hsieh S-S, Lin J-W, Chen J-H. Mixing efficiency of Y-type micromixers with different angles. International Journal of Heat and Fluid Flow. 2013;44(Supplement C):130-139.
15. T T Veenstra TSJL, M C Elwenspoek and A van den Berg Characterization method for a new diffusion mixer applicable in micro flow injection analysis systems. Journal of Micromechanics and Microengineering. 1991;9(2).
16. Capretto L, Cheng W, Hill M, Zhang X. Micromixing within microfluidic devices. Top Curr Chem. 2011;304:27-68.
17. F. Schönfeld aVHaCH. An optimised split-and-recombine micro-mixer with uniform 'chaotic' mixing. 1. 2004(1).
18. H. Bing JB, B. Zhang, X. Zhang, R. Regnier, Fred. A Picoliter-Volume Mixer for Microfluidic Analytical Systems. Analytical chemistry. 2001;73:1942-1947.
19. Hossain S, Kim K-Y. Mixing Analysis of Passive Micromixer with Unbalanced Three-Split Rhombic Sub-Channels. Micromachines. 2014;5(4):913-928.
20. Dietrich T. FA. Production and Characteristics of Microreactors Made from Glass. Chemical Engineering Technology. 2005;28(4).
21. Xinghua Li TA, Masayoshi Esashic. Deep reactive ion etching of Pyrex glass using SF6 plasma. Sensors and Actuators A: Physical. 2001;87:139-145.

22. Nakamura A, Yoshida K, Kuwahara S, Katayama K. Photocatalytic organic syntheses using a glass-milled microchip. Journal of Photochemistry and Photobiology A: Chemistry. 2016;322-323:35-40.
23. Korkmaz E, Onler R, Ozdoganlar OB. Micromilling of Poly(methyl methacrylate, PMMA) Using Single-Crystal Diamond Tools. Procedia Manufacturing. 2017;10:683-693.
24. Suriano R, Kuznetsov A, Eaton SM, Kiyan R, Cerullo G, Osellame R, et al. Femtosecond laser ablation of polymeric substrates for the fabrication of microfluidic channels. Applied Surface Science. 2011;257(14):6243-6250.
25. McCann R, Bagga K, Groarke R, Stalcup A, Vázquez M, Brabazon D. Microchannel fabrication on cyclic olefin polymer substrates via 1064 nm Nd:YAG laser ablation. Applied Surface Science. 2016;387:603-608.
26. Kadimisetty K, Mosa IM, Malla S, Satterwhite-Warden JE, Kuhns TM, Faria RC, et al. 3D-printed supercapacitor-powered electrochemiluminescent protein immunoarray. Biosens Bioelectron. 2016;77:188-193.
27. Credi C, Levi M, Turri S, Simeone G. Stereolithography of perfluoropolyethers for the microfabrication of robust omniphobic surfaces. Applied Surface Science. 2017;404:268-275.
28. Sacristan M, Planta X, Morell M, Puiggali J. Effects of ultrasonic vibration on the micro-molding processing of polylactide. Ultrason Sonochem. 2014;21(1):376-386.
29. Masato D, Sorgato M, Parenti P, Annoni M, Lucchetta G. Impact of deep cores surface topography generated by micro milling on the demolding force in micro injection molding. Journal of Materials Processing Technology. 2017;246:211-223.
30. Nian S-C, Tsai T-H, Huang M-S. Novel inductive hot embossing for increasing micromolding efficiency. International Communications in Heat and Mass Transfer. 2016;70:38-46.
31. Pont. D. Teflon PTFE®fluoropolymer resin Properties Handbook.
32. Burris DL, Sawyer WG. A low friction and ultra low wear rate PEEK/PTFE composite. Wear. 2006;261(3-4):410-418.
33. Toolbox E. EngineeringToolbox 2017 [cited 2017 18 October.]. Online quick information website.]. Available from: http://www.engineeringtoolbox.com/.
34. Yilbas BS, Ali H. Laser texturing of Hastelloy C276 alloy surface for improved hydrophobicity and friction coefficient. Optics and Lasers in Engineering. 2016;78:140-147.
35. Togashi S, Miyamoto T, Asano Y, Endo Y. Yield Improvement of Chemical Reactions by Using a Microreactor and Development of a Pilot Plant Using the Numbering-Up of Microreactors. Journal of Chemical Engineering of Japan. 2009;42(7):512-519.
36. WorldPumps. Back to Basics With Centrifugal Pumps WorldPumps: Elsevier; 2010 [updated Summer 2001. Available from: www.worldpumps.com.
37. Xiang J, Cai Z, Zhang Y, Wang W. A micro-cam actuated linear peristaltic pump for microfluidic applications. Sensors and Actuators A: Physical. 2016;251:20-25.
38. Masnec S, Kalauz M. Cataract Surgery. INTECH. 2016.
39. Rodrigo M. Novel Pump for Flow Chemistry Applications with Increased Reliability: MIT; 2014.
40. Y. Kazakevich RL. Reciprocating Piston Pumps Seton Hall University2007 [Available from: http://hplc.chem.shu.edu/HPLC/Instrumentation/pmp_recp.html.
41. Summers J. Syringe Pump Mechanics 2014 [Available from: https://publiclab.org/notes/JSummers/12-30-2014/syringe-pump-mechanicals.
42. Paul Horowitz WH. THE ART OF ELECTRONICS. Press CU, editor. 32 Avenue of the Americas, New York2015.
43. Pipus G, Plazl I, Koloini T. Esterification of benzoic acid in microwave tubular flow reactor. Chemical Engineering Journal. 2000;76(3):239-245.
44. Wiles C, Watts P, Haswell SJ, Pombo-Villar E. Solution phase synthesis of esters within a micro reactor. Tetrahedron. 2003;59(51):10173-10179.

45. Berdys M, Koreniuk A, Maresz K, Pudło W, Jarzębski AB, Mrowiec-Białoń J. Fabrication and performance of monolithic continuous-flow silica microreactors. Chemical Engineering Journal. 2015;282(Supplement C):137-141.
46. de la Iglesia Ó, Mallada R, Menéndez M, Coronas J. Continuous zeolite membrane reactor for esterification of ethanol and acetic acid. Chemical Engineering Journal. 2007;131(1):35-39.
47. Dennis D. Wackerly WMI, Richard L. Scheaffer. Mathematical Statistics Seventh Edition: Brooks/Cole; 2008.
48. McMurry J. Organic Chemistry. Seventh Edition ed. Belmont, Calafornia, USA: Brooks Cole; 2008.

4.2 Reactor Code

Table 18: Setup code for reactor's heater microcontroller.

```
#include <PID_v1.h> //PID library included into compilation.
int RelayPin = 13; //Sets pin 13 on the Arduino as the relay output.
int SignalWire = 7; //Connects with relay on PLC which pulls down once desired temperature is reached.
double Setpoint, Input, Output; //Variables required in PID algorithm.
PID myPID(&Input, &Output, &Setpoint,80,0.38,200, DIRECT); //Instantiates PID object.
int WindowSize = 5000; //Sample period of input signal.
unsigned long windowStartTime;//Sets the time according to the internal clock.
int Signal; //Trigger pins variable.


void setup() //Sets the values the above mentioned objects and variables.
 {
   pinMode(RelayPin, OUTPUT); //Sets the pin for the relay as an output signal.
   pinMode(SignalWire, INPUT_PULLUP); //Sets the SignalWire pin as an pullup input. Triggered by voltage drop.


   Signal = digitalRead(SignalWire);//Reads the state of the signal wire. Either HIGH or LOW.
   windowStartTime = millis(); //Sets the start time based on the MCU's internal clock.
   Setpoint = 0; // Initial PID value before measurement set to 0.
   myPID.SetOutputLimits(0, WindowSize); //Output's set operation time.
   myPID.SetMode(AUTOMATIC); //Set PID on.
   myPID.SetSampleTime(3000); //Time that PID sets its equation on.
   Serial.begin(9600); //Allows for communication over the USB port.
}
```

The standard Arduino Library has been used with a common open-source PID library by Brett Beauregard. The code has been split into the setup and main section. Explanation of the code can be found by the comment (//) sign followed by italics within the code.

Table 19:Looping code for reactors heater's microcontroller.

```
void loop() //main loop structure for Arduino interpreter.
{  // Code to be looped within the bracket.
 delay(100); //Delays code by 100ms.
 Signal = digitalRead(SignalWire); //Reads the state of the relay in pin 23 and 24 of the PLC.
 While(Signal == LOW)  //loops the code below in brackets while the relay on the PLC is closed.
  {
   digitalWrite(RelayPin,HIGH); //Sets Solid State Relay high and Pulse LED.
   delay(200); //Wait 200 ms. while relay on.
Serial.println(String(Input));//Shows the input value of the PLC over USB.
  Signal = digitalRead(SignalWire); //Reads the state of the PLC's relay
   digitalWrite(RelayPin,LOW); //Switches off the Solid State Relay.
   if (Signal == LOW){Setpoint = analogRead(A0);} //Sets the signal for the PID into setpoint variable..
   delay(200);
   //Serial.println(String(Input)); //Sends serial commands to USB for troubleshooting purposes.
   Serial.println(Signal); //Sends the strength of the signal over USB.
   Signal = digitalRead(7); //Passes relays value into Signal variable.
  } //Closing bracket for loop. If Signal high the loop ends.

 Setpoint = analogRead(A0); //Sets the signal obtained into the Setpoint variable.

  while(1) //The signal has been obtained so the algorithm goes into an infinite loop.
  {
    Input = analogRead(A0); //Updates the input value from the PLC.
    myPID.Compute(); //Runs PID computations.
    Serial.println(String(Input)); //Sends input value over USB for troubleshooting purposes.
    unsigned long now = millis(); //sets the current time from the MCU's timer.
    if(now - windowStartTime>WindowSize)//Updates the windows size.
     { //time to shift the Relay Window
       windowStartTime += WindowSize;
     }
    if(Output > now - windowStartTime) digitalWrite(RelayPin,HIGH);//Switches relay on upon completion.
    else digitalWrite(RelayPin,LOW); //Keeps relay off until window's period is complete.
  }
}
```

This code is only applicable for a once off setup. For the temperature to be changed a built in hard reset has been incorporated on the control panel of the reactor. The button has been wired up to the ground pin and, if pressed the voltage falls and code resets.

4.3 Pump code

Table 20: Pump code part 1. (comments shown after // in italics)

```
#include <stdlib.h>

int MS1 = 4; //Microstepping pins.
int MS2 = 5;
int MS3 = 6;
char pin_Direction = 12;
char pin_Pulse = 7;
float cylinderArea = 1.5394; //cm^2
float ScrewPitch = 1.00; //mm The distance the thread progresses per rotation.
int StepsPerRev = 200; //How many steps per revolution of the screw. 1 : 1 if no gearbox is used. NEMA 17 bipolar drivers typically have 200 steps/rev.
int DesiredFrequency = 2500; //The desired pulserate. Lower numbers have higher torque but flowrate is not as smoothed.
```

The pump was programmed in the same language as the reactor's PID control. The stepper motor's driver works through a digital 5V pulse. The pulse from the microcontroller is expressed as a square wave signal. The driver can micro step, which splits the distance between each pole in a binary fashion. One example would be where a motor that has 200 steps/rev that undergoes half step mode would in effect have 400 steps/rev. The A4988 driver can go up to 1/16th micro step mode, therefore

3200 pulses are required for 1 revolution. A frequency library has been used to generate the tone which the driver will interpret as a signal. The code for the pump was significantly more complex compared to the reactor's due to a user interface that is required.

Table 21:Pump code part 2. (comments shown after // in italics)

```
char FlowRateChar[5]; //Character array for U8glib object
String FlowRateString; //Variable to expresses character array as a string.
String StepMode; //Stores the step mode variable.
float FlowRate; //Sets the flowrate in mL/min
int MenuPosition; //Keeps track of the menu number
bool ButtonState; //Keeps state of button as HIGH/LOW or  1/0.
char KeyPressed; //Stores character pressed.
char Buzzer = A8; //Stores pin buzzer is connected to.
char InitialPosition; //Stores the initial key pressed.
bool MenuActive; //Stores Boolean for the menu's activity.
bool InitialActivity; //Shows if there is initial activity.
bool PointPresent; //Keeps track if a point is present in a value to its not selected twice.
const byte interruptPin1 = 2; //Variable for interrupt routine for end-stop 1.
const byte interruptPin2 = 3;//Variable for interrupt routine for end-stop 2.
volatile byte PulseDirection = LOW; //Variable which dictates what direction pump should turn.
#include <Keypad.h> //Inclusion of KeyPad library.
const byte ROWS = 4; // Four rows
const byte COLS = 3; // Three columns
char keys[ROWS][COLS] = { //2D Array holds key values.
  {'1', '2', '3'},
  {'4', '5', '6'},
  {'7', '8', '9'},
  {'*', '0', '#'}
};
byte rowPins[ROWS] = { 40, 41, 42, 43 }; //Allocates the pins of the keypad into the Arduino
byte colPins[COLS] = { 44, 45, 46 };
Keypad kpd = Keypad( makeKeymap(keys), rowPins, colPins, ROWS, COLS ); //Instantiates the keypad object.
#include <U8glib.h> //Includes LCD library
U8GLIB_PCD8544 u8g(13, 11, 9, 10, 8); //Instantiates the LCD object, which handles LCD's code.
#include "PumpControl.h" //Loads pump control library. Library included after code.
PumpControl PumpControl(MS1, MS2, MS3, pin_Direction, pin_Pulse,  ScrewPitch, StepsPerRev, DesiredFrequency, cylinderArea); //Instantiates the pump object. Written to be universal for syringe pumps.
```

The above code sets the variables and the objects that will be used in the program. The following code will cover the loop cycles followed by the pump object's code.

Table 22:Pump code part 3. (comments shown after // in italics)

```
void setup(){ //Runs once before main loop is initialised.
  u8g.setFont(u8g_font_6x10);//sets the font of the LCD driver object.
  u8g.setColorIndex(1); // Instructs the display to draw with a pixel on.
  Serial.begin(9600); //Opens USB communications in case of debugging.
  MenuPosition = 0; //Keeps track of the menu position.
  ButtonState = LOW; //Sets button state LOW incase it is undefined.
  kpd.setDebounceTime(100); //Sets the time a key can't be pressed after pressing in ms.
  pinMode(Buzzer, OUTPUT); //Sets the piezo-electric connected pin as an output.
  MenuActive = HIGH; //Sets the Menu active Boolean to HIGH
  PointPresent = LOW; //Handles the comma separator in screen. Adjusted by menu change function.
  DrawEnterFlowRate(); //Calls subroutine which draws the EnterFlowRate screen on LCD.
  pinMode(interruptPin1, INPUT); //Sets the pin the end-stop is connected to as an interrupt.
  attachInterrupt(digitalPinToInterrupt(interruptPin1), Reverse, RISING); //Sets the interrupt conditions.
  pinMode(interruptPin2, INPUT); //Same as above just different end-stop.
  attachInterrupt(digitalPinToInterrupt(interruptPin2), Forward, RISING);
  pinMode(4, OUTPUT); //Sets pin 4 as output. MS1 pin (low impedance state)
  pinMode(5, OUTPUT); //Sets pin 5 as output. MS1 pin
  pinMode(6, OUTPUT);//Sets pin 6 as output. MS1 pin
  pinMode(7, OUTPUT);//Sets pin 7 as output. Direction pin as High.
  digitalWrite(4, HIGH); //MS1 set as HIGH.
  digitalWrite(5, HIGH); //MS2 set as HIGH.
  digitalWrite(6, HIGH); //MS3 set as HIGH. (3Pins HIGH = 16th step, thus 3200 steps/rev)
}
void loop()
{
  switch (MenuPosition) {
    case 0:
      PumpControl.StopPump();
      noTone(7);
      for (int z = 0; z < 5; z++)
      { FlowRateChar[z] = 00; }//empty array with null character.
      charArrayAdd();
      FlowRate = atof(FlowRateChar);
      Serial.println(String(FlowRate) + "this is entered flowrate");
      PumpControl.setFlowRate(FlowRate);
      delay(1);
      MenuPosition = 1;
      break;
```

Table 23:Pump code part 4. (comments shown after // in italics)

```
  case 1:
     noTone(7); //Switches off pulses if return back from menu position 2.
     while (MenuPosition == 1) //Loop the following code in brackets until MenuPosition 1 changes.
      { PumpControl.StopPump(); //Shuts down any activity on the stepper driver.
    MenuAssignment(kpd.waitForKey()); //Code stands still until a key is pressed, key value pass into
function.
     StepMode = PumpControl.serialAnalysis(); //Sets the step mode based on the flowrate.
   Serial.println(StepMode); //Sends the stepping mode over USB to the serial reader.
  DrawStartPumpScreen(); //Draws the pump starting screen.
 }
     break; //Breaks out of the case statement and run through until next condition is met.
   case 2:
     tone(7,PumpControl.determinePulse()); //Sets the pulses/s calculated from the PumpControl object.
     DrawPumpingScreen(); //Draws the screen which states the pump is active.
   while (MenuPosition == 2) {
  MenuAssignment(kpd.waitForKey(); //Breaks out of loop if 4(pause) or 6(reset) is pushed.
     }
     break;
  }
  delay(1); //delays code for 1ms. Done as a safety measure to minimise conflicting code.
}
//Mainloop ends here. Following code contains collections of code called as a function. Void indicates that
nothing //should be returned when the code is called.

void DrawEnterFlowRate() //Combines code below as a single function that can be called above.
  u8g.firstPage(); //Clears the LCD of previous menu.
  do {   //Do the following code until while condition is satisfied.
    u8g.setFont(u8g_font_5x7); //Set the font for the next text to be drawn.
    u8g.drawStr( 6, 9, "Enter Flow Rate"); //Writes “Enter flowrate” on the specified position of the LCD.
    u8g.setPrintPos(0, 25); //Sets area where the character array should be printed.
    u8g.print(FlowRateChar); //Prints the character array.
    u8g.drawStr( 20, 45, "Submit #"); //Gives instruction to the user.
  }
  while (u8g.nextPage());//Condition until above code is complete.
  u8g.setColorIndex(0);//Refreshes the LCD screen.
  u8g.setColorIndex(1);
  delay(5); //Slight delay to stabilise the code.
}
```

The code in table 15 can be explained as function “void DrawEnterFlowRate”. The whole code within the brackets is called by one function, hence it drastically reduces the size and clutter of the code.

Table 24: Pump code part 5 (comments shown after // in italics)

```
void DrawStartPumpScreen()
{
  u8g.firstPage();
  do {
    u8g.setFont(u8g_font_5x7);
    u8g.drawStr( 6, 9, "FlowRate(mL/min)");
    u8g.setPrintPos(0, 25);
    u8g.print(FlowRateChar);
    //u8g.print(FlowRateChar);
    u8g.drawStr( 1, 45, "Submit #, Re-Enter 4");
  } while (u8g.nextPage());
  u8g.setColorIndex(0);
  u8g.setColorIndex(1);
  delay(5);
}

void DrawPumpingScreen()
{
  u8g.firstPage();
  do {
    u8g.setFont(u8g_font_5x7);
    u8g.drawStr( 6, 9, "Pump is active.");
    u8g.setPrintPos(0, 25);
    u8g.print(FlowRateChar);
    u8g.drawStr( 2, 45, "*:Pause #:Reset");
  } while (u8g.nextPage());
  u8g.setColorIndex(0);
  u8g.setColorIndex(1);
  delay(5);
}
```

Table 25:Pump code part 6 (comments shown after // in italics.)

```
void MenuAssignment(char ButtonState) //Changes the Menu Position variable to vary in the case statement to change the menus.
{
  delay(1);


  if (ButtonState != NO_KEY) {//if some button is pressed the code in the brackets will start. The following code test's      for the key that was pressed.
    if (ButtonState == '4' || ButtonState == '*') // ||indicates or. If 4 or '*' is pressed the following code will run.
    {
      MenuPosition = abs((MenuPosition - 1) % 3); //Modulus used to keep the menus within the limits in main loop.
      digitalWrite(Buzzer, HIGH); //Activates the piezo if the button is pressed.
      delay(30); //Keeps piezo buzzer on for 30ms.
      digitalWrite(Buzzer, LOW); //Turns of Piezo buzzer.
      delay(1);
    }
    else if (ButtonState == '6' || ButtonState == '#') //6 or '#" takes the menu forward and resets if end of menu reached
    {
      MenuPosition = abs(MenuPosition + 1) % 3; Modulus used to keep the menus within the limits in main loop.
      delay(1);
      digitalWrite(Buzzer, HIGH);Activates the piezo if the button is pressed.
      delay(30);//Keeps piezo buzzer on for 30ms.
      digitalWrite(Buzzer, LOW);//Turns of Piezo buzzer.
    }
    else if (ButtonState == '6') //Activates the pump active menu.
    {
      MenuActive = HIGH;
      delay(1);
    }
  }
}
```

The code above is written defensively so that the looping of the menu's stays within the case statement in the main loop. If the menu assignment falls outside of the menu numbering system there is no code to bring it back into the loop, which is why a modulus function was used.

Table 26: Pump code part 7 (comments shown after // in italics.)

```
String AssignKey(String InputString) { //Returns a string (String instead of void in beginning)
  KeyPressed =  kpd.waitForKey(); //Waits until a key is pressed and pass into KeyPressed variable.
  delay(10);
  switch (KeyPressed) //Depending on what KeyPressed contains the matching case's code will run.
  {
    case '#': //if # is pressed code runs until break;
      MenuActive = LOW;  //Breaks out of active menu loop in main code.
      PointPresent = LOW; //Sets the period present to low for when updated values are required.
      digitalWrite(Buzzer, HIGH); //Turn buzzer on for 30ms.
      delay(30);
      digitalWrite(Buzzer, LOW);
      delay(1); //safety technique to ensure registers are updates.
      break;
    case '*' : //Inserts a period to initiate the decimal value insertion.
      if (PointPresent == LOW) //Only proceeds with code if Point present is low, else it skips the code in the
bracket.
      {
        InputString = InputString + '.'; //Adds the period after the numbers.
      }
      PointPresent = HIGH; //Sets PointPresent high so above code cannot re-run.
      delay(1);
      return (InputString); //Returns the value into the variable it has been called in the main code.
      delay(1);
      break;
    default : InputString.concat(KeyPressed); //Adds key the key that's pressed to the previous keys.
      delay(1);
      digitalWrite(Buzzer, HIGH);//Turn buzzer on for 30ms.
      delay(30);
      digitalWrite(Buzzer, LOW);
      return (InputString); //Returns the concatenated string variable.
      delay(1);
      break;
  }
}
```

Table 27: Pump code part 8 (comments shown after // in italics.)

```
void charArrayAdd() { //Adds the character to a character array. U8Glib uses C which cannot interpret a string.
  DrawEnterFlowRate(); //Calls function which draws the EnterFlowRate screen.
  PointPresent = LOW; //Removes period in array.
  for (int z = 0; z < 5; 0) //Repeats the code for 5 times while Z increments from 0 to 4.
  {
    delay(1);
    KeyPressed =  kpd.waitForKey();//Code stalls until key pressed. When pressed passes key into KeyPressed.
    if (KeyPressed == '#') //Signals the values are completed.
    { z = 4; //Causes for loop to break
      FlowRateChar[z] = 00;
      break;
    }
    if (KeyPressed == '*' && PointPresent == HIGH)
    {
      continue; //Skips the following expressions hence point is not inserted.
    }
    if (KeyPressed == '*')
    {
      PointPresent = HIGH; //Says the point has been used in case its pressed again.
      FlowRateChar[z] = '.';
      z++;
      DrawEnterFlowRate();
      digitalWrite(Buzzer, HIGH);
      delay(30);
      digitalWrite(Buzzer, LOW);
      continue;
    }
    if (KeyPressed == '0' && z == 0)(z = -1);
    FlowRateChar[z] = KeyPressed; //Sets the character in position z in the character array to key pressed.
    digitalWrite(Buzzer, HIGH);
    delay(30);
    digitalWrite(Buzzer, LOW);
    DrawEnterFlowRate(); Updates the screen to the new button pressed.
    z++;
  }
  MenuPosition = 1;
```

Table 28: PumpControl Header file.

```
void Forward() //Called when end stop switches opened. Stops current code and runs code below.
{
  digitalWrite(12, HIGH); //Sets the direction pin on the motor driver to high. Changes direction of rotation.
  delay(2);
}
void Reverse()
{
  digitalWrite(12, LOW);// Sets the direction pin on the motor driver to low. Changes direction of rotation.
  delay(2);
}
```

The code in table 19 is called when an interrupt sequence is initiated. Thus, the current code is paused, and the interrupt code is run. This allows actions to be performed without testing the state of each input. This improves the codes performance significantly. The code from table 11 to table 19 is for the main loop. The following code is the pump object. The code is bundled into an object which organises and encapsulates it, hence the object handles its own code, which is called externally. Multiple objects can be called which will each will be its own unit. This greatly simplifies code, especially when code becomes long.

Table 29:Pump code part 9 (comments shown after // in italics.)

```
//Header of PumpControl Object.
#ifndef PumpControl_h //Skips code if its already included in the code.
#define PumpControl_h
#include "Arduino.h" //Loads Arduino library for general functions.
class PumpControl //The name of the object library.
{
  public:
   PumpControl(int pin_MS1, int pin_MS2, int pin_MS3, char pin_Direction, char pin_Pulse, float pitch_mmprev, int stepsPRev, int DesiredFreq, float cylinderArea); //Sets the object instantiating function up to call for new objects.
   String StartPump(); //Starts the pump after code is set up.
   String StopPump(); //Stops the pump.
   void setFlowRate(float flowRate);//Complete
   String serialAnalysis();
   int determinePulse();
};
#endif
```

Table 30:Pump control header file part 2.

```
  private:  // internal variables and functions goes here. Use specific identifier for internal varaibals eg. int _state;
   void fullStep(); //Sets the pins connected to the drivers for fullstep.
   void halfStep();//Sets the pins connected to the driver for halfstep.
   void quarterStep();//Sets the pins connected to the driver for quarterstep.
   void eighthStep();//Sets the pins connected to the driver for eightstep.
   void sixteenthStep();//Set the pins connected to the driver for sixteenth step.
   String determineStepMode(); //Determines and set the step mode.
    //Uses determineStepMode() //function to calculate the frequency of the pulse at the step mode. Complete
   int _MS1;  //Pin MS1 is connected to.
   int _MS2;//Pin MS2 is connected to.
   int _MS3;//Pin MS3 is connected to.
   int _Direction; //Pin Dir on A4988 is connected to.
   int _PulsePin; //Pin Pulse on A4988 is connected to.
   float _FlowRate; //Holds the flowrate.
   float _TheoreticalFlow; //Holds a hypothesized flowrate for micro step testing.
   float _mLperRev; //How many mL is dispensed in one revolution.
   float _Pitch; // How far the pistons move per stepper revolution.
   float _RevPSec;
   float _mLPMin; //A variable that holds the flowrate.
   float _RevPMin;
   float _Area;
   float _PrevDifference;
   float _CurrentDifference;
   float _Volume;
   int _StepsPRev;
   int _DesiredFrequency; // Micro step should select output frequency close to this frequency.
   int _PulseRate; //The frequency based on the microstepping value calculated from determine stepmode function
   int _StepSelect; //Stores which step is selected for acquired frequency
 String _prevStep; //Forms part of step selection algorithm.
   String _StepMode; //Stores step mode in string.
};
```

These variables cannot be controlled externally. Only the public variables can be controlled by code external to the object. This protects the code in the object from external interference that might destabilise the code.

Table 31: PumpControl CPP file part 1.

```
#include "arduino.h"
#include "PumpControl.h" //Links header file's content with below code.
PumpControl::PumpControl(int pin_MS1, int pin_MS2, int pin_MS3, char pin_Direction, char pin_Pulse,  float pitch_mmprev, int stepsPRev, int DesiredFreq, float cylinderArea)
{
  _MS1 = pin_MS1; //sets public variables to private.
  _MS2 = pin_MS2;
  _MS3 = pin_MS3;
  _Direction = pin_Direction;
  _PulsePin = pin_Pulse;
  _Pitch = pitch_mmprev;
  _FlowRate = 2.00;
  _prevStep = "";
  _StepsPRev = stepsPRev;
  _DesiredFrequency = DesiredFreq;
  _Area = cylinderArea;
  //pinMode(_PulsePin, OUTPUT); //Sets pins to low impedance state for higher current output.
  pinMode(_Direction, OUTPUT);
  pinMode(_MS1, OUTPUT);
  pinMode(_MS2, OUTPUT);
  pinMode(_MS3, OUTPUT);
}
void PumpControl::fullStep() //Sets micro step mode to full-step mode.
{
  pinMode(_MS1, LOW);
  pinMode(_MS2, LOW);
  pinMode(_MS3, LOW);
}
void PumpControl::halfStep()//Sets micro step mode to half-step mode.
{
  pinMode(_MS1, HIGH);
  pinMode(_MS2, LOW);
  pinMode(_MS3, LOW);
}
void PumpControl::quarterStep()()//Sets micro step mode to quarter-step mode.
{
  pinMode(_MS1, LOW);
  pinMode(_MS2, HIGH);
  pinMode(_MS3, LOW);
}
```

The same was done for the eight step and sixteenth step, which was left due to redundancy.

Table 32: PumpControl CPP part 2.

```
String PumpControl::determineStepMode() //Returns the stepMode as an string (FullStep; HalfStep; QuarterStep; EighthStep; SixteenthStep)
{
  _RevPMin = (_DesiredFrequency / _StepsPRev) * 60; // Calculates current rev/p minute for desired frequency
  _mLPMin = _RevPMin * (_Pitch / 10) * _Area; //Calculates flow rate based on ideal values.
  for (int i = 0; i == 4; i++) //Runs following code for all the step modes to see what is the best.
  {
    _TheoreticalFlow = (_mLPMin/((pow(2, i)))); //Cycles the steps per rotation to test for theoretical vs given.
    delay(1);
    _CurrentDifference = abs(_FlowRate - _TheoreticalFlow);
    delay(1);
    if (i == 0)
    {_PrevDifference = _CurrentDifference; }
    if (_PrevDifference < _CurrentDifference)
    {_StepSelect = i - 1;}
    if (_PrevDifference > _CurrentDifference)
    {_StepSelect = i; }
    else if (i == 4 && _PrevDifference > _CurrentDifference)
    {_StepSelect = i; }
  }
  _StepSelect = i; //correspond to the step mode with the least difference.
  switch (_StepSelect) //Selects the step mode that correspond to I obtained above.
  {
    case 0 : _StepMode = ("FullStep");
      fullStep();
      break;
    case ( : _StepMode = ("HalfStep");
      halfStep();
      break;
    case 2 : _StepMode = ("QuarterStep");
      quarterStep();
      break;
    case 3 : _StepMode = ("EighthStep");
      eighthStep();
      break;
    case 4 : _StepMode = ("SixteenthStep");
      sixteenthStep();
  }
  return (_StepMode);
```

Table 33:PumpControl CPP part 3.

```
void PumpControl::setFlowRate(float flowRate) //Sets the flowrate to be calculated inserted from user.
{_FlowRate = flowRate;}
int PumpControl::determinePulse() //Needs to be called after determineStepMode()
{ PumpControl::determineStepMode(); //Internal object function being called by a function.
  _StepMode = determineStepMode();
  PumpControl::sixteenthStep(); //Changed after testing. FlowRate always at highest microstep for desired freq.
  _PulseRate = (int)(round((((_FlowRate / 60) * 200 * (pow(2, 4)) / (_Area * (_Pitch / 10))))));
  _PulseRate = _PulseRate * 2.0; //Was calculated for the large cylinder.
  return(_PulseRate); //Returns the value through the int. above into main loop.
}
String PumpControl::StartPump()
{
  Serial.println("Starting pump");
  determinePulse();
  delay(5);
  setStartTime();
  if (_PulseRate != 0 && _PulseRate < 7500)
  {
    tone(_PulsePin, _PulseRate);
    return ("Running");
    Serial.println(_PulseRate);
  }
  else {
    Serial.println("Error");
    return ("Error");
  }
}
String PumpControl::StopPump() //Ceases all pulse communication to the pump.
{
  Serial.println("Pump Stopped");
  pinMode(_PulsePin, LOW);
  _PulsePin = 0;
  noTone(_PulsePin);
  return ("Stopped");
}
```

The code above was compiled using the Arduino compiler and the files were uploaded via USB. The graphical user interface did not have any noticeable error's during operation. Since the controller did not have a direct output to the motor's current, the stepper motor had to be tuned in. The only factor that might affect the torque is the micro stepping mode, where a high micro stepping mode loses torque. The amount of current has to be balanced with the amount of heat generated, too much heat will burn out the electronics. Fortunately the A4988 has a failsafe, where

the driver shuts down if excess heat is generated. Additionally, a heat sink has been installed which reduces the concentration of heat.

4.4 Analysis Method Information

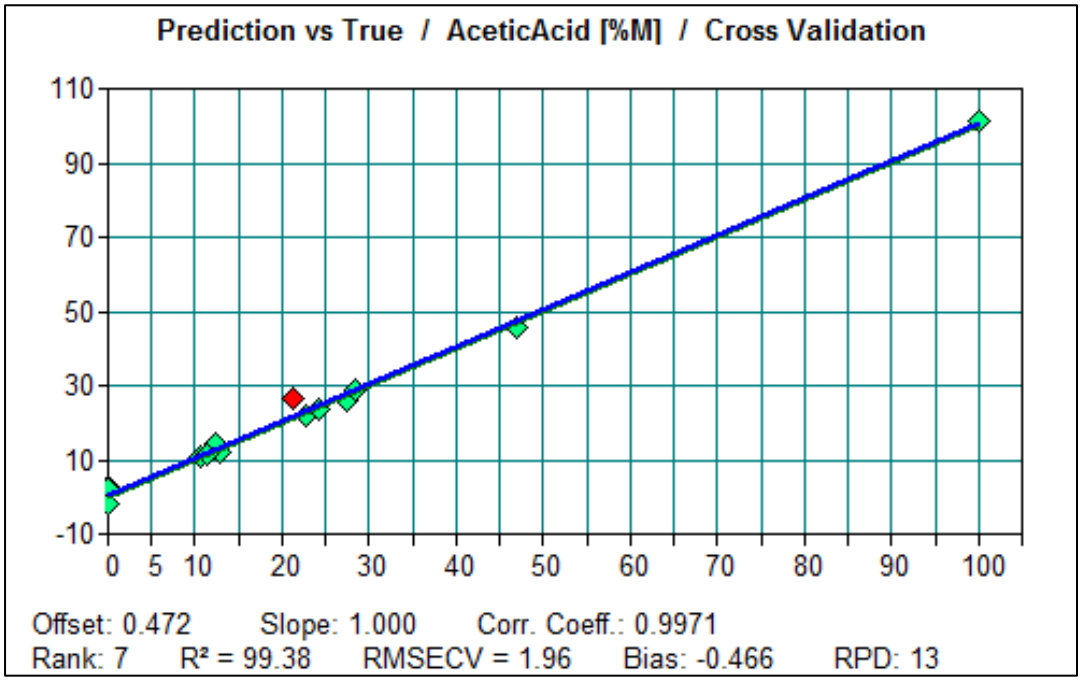

Figure 102: Acetic acid IR method's standard curve.

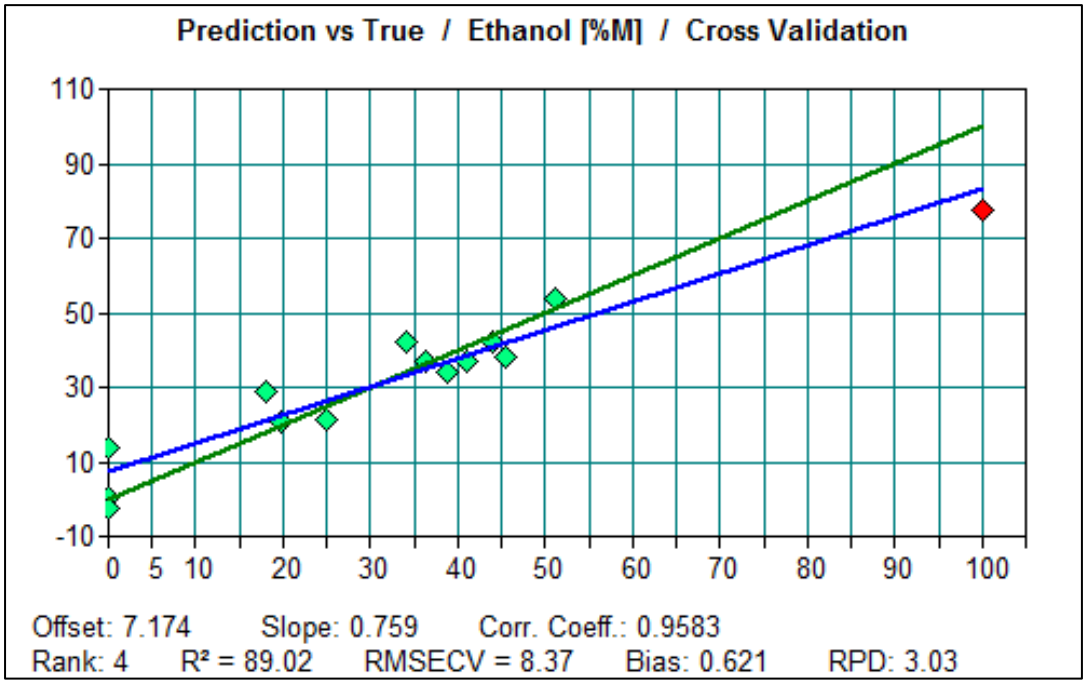

Figure 103: Ethanol IR method's standard curve.

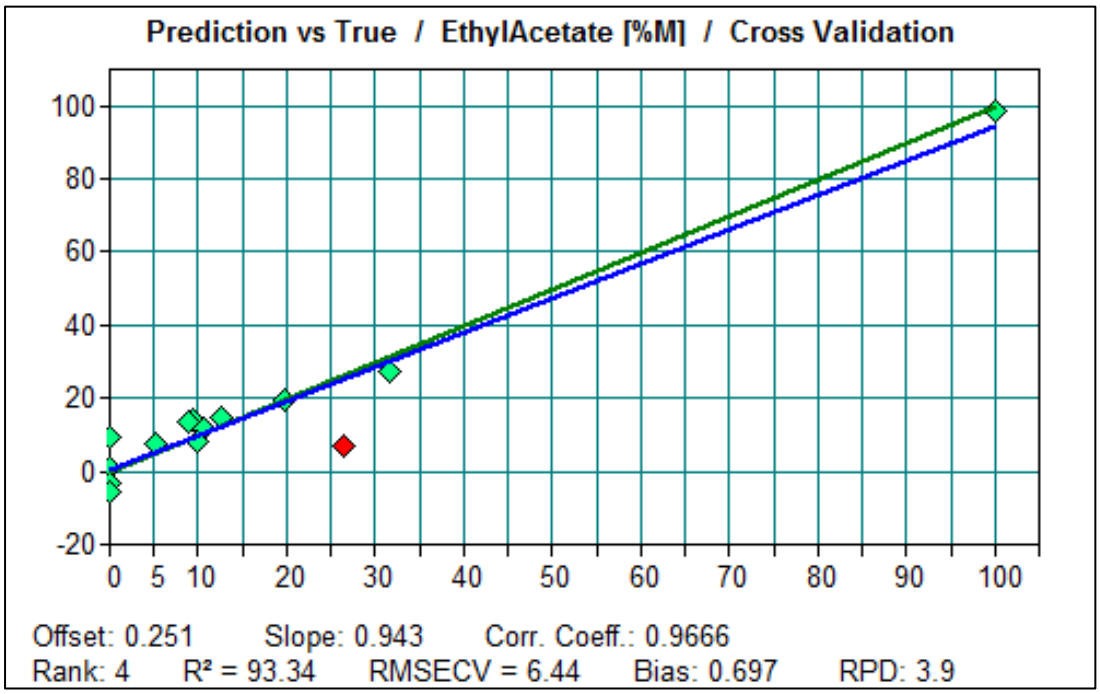

Figure 104:Ethanol IR method's standard curve.

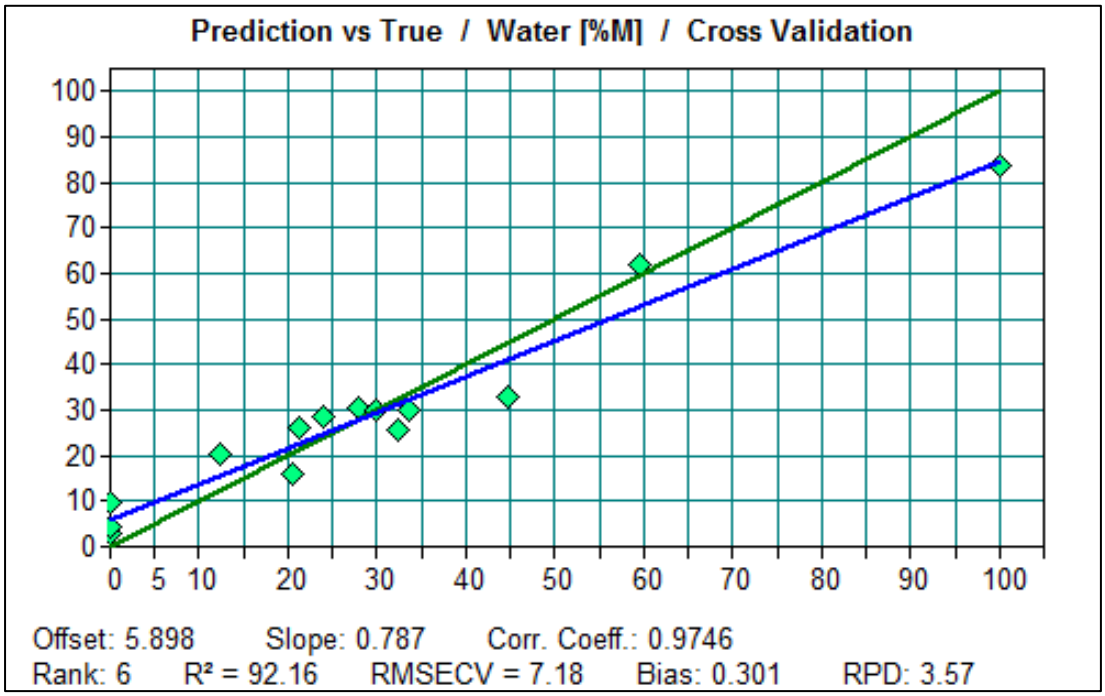

Figure 105: Water IR method's standard curve.

4.5 Reaction conversion model's statistics

Table 34:Regression model's constants.

	b	Std.Err.	t(183)	p-value
Int.	6.05834	1.673979	3.61912	0.000382
b_0	-0.37033	0.059820	-6.19070	0.000000
b_1	-0.33494	0.367435	-0.91156	0.363201
Db	-3.93942	0.725424	-5.43051	0.000000
Dc	-6.65880	0.748413	-8.89723	0.000000
b_2	0.00536	0.000579	9.26018	0.000000
b_3	-0.13601	0.044432	-3.06118	0.002537
b_5	0.06120	0.012303	4.97448	0.000002
b_7	0.08251	0.012583	6.55776	0.000000
b_6	0.70564	0.106418	6.63081	0.000000
b_8	0.48957	0.114753	4.26632	0.000032
b_4	0.06034	0.003831	15.74897	0.000000

Regression Summary for Dependent Variable: Conversion (%) (Spreadsheet3) R= ,99040841 R^2= ,98090882 Adjusted R^2= ,97976126 F(11,183)=854,78 p<0,0000 Std.Error of estimate: ,85747

Table 34 shows the regression models constants for the model used in the comparative studies. Db and Dc are the dummy variables which are responsible for adjusting the changes from the test reactor. Therefore, if Db is the Chemtrix3227 dummy variable all the factors having the Db variable will be included and Dc ignored.

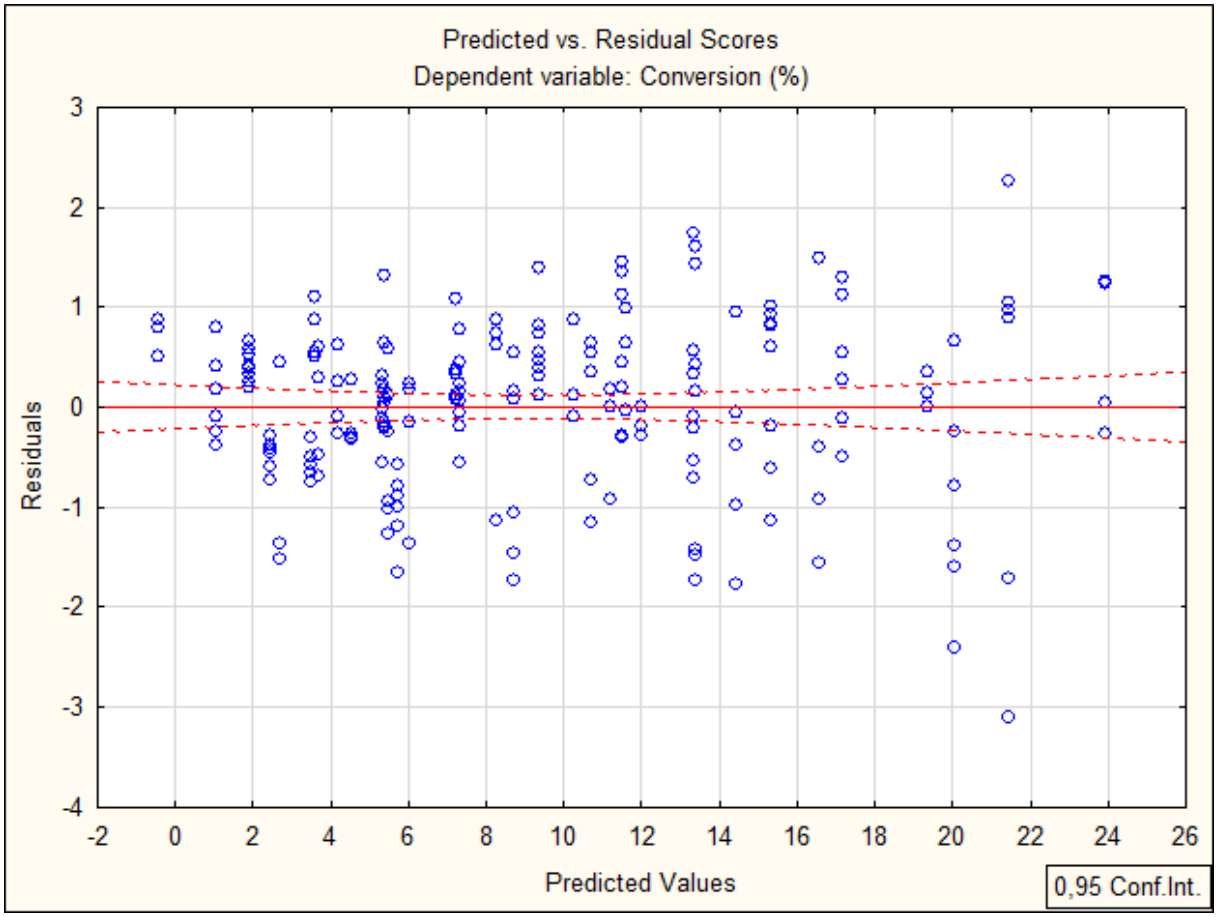

Figure 106: Predicted vs. Residual Scores of the model in .

Predicted vs residuals show the variation of the ideal to observed values. An equalized distribution of points indicates that random error is responsible for the deviation. A residual value outside of 3 is considered as an outlier. Only one value was an outlier for this model. See Figure 108 for an alternative representation.

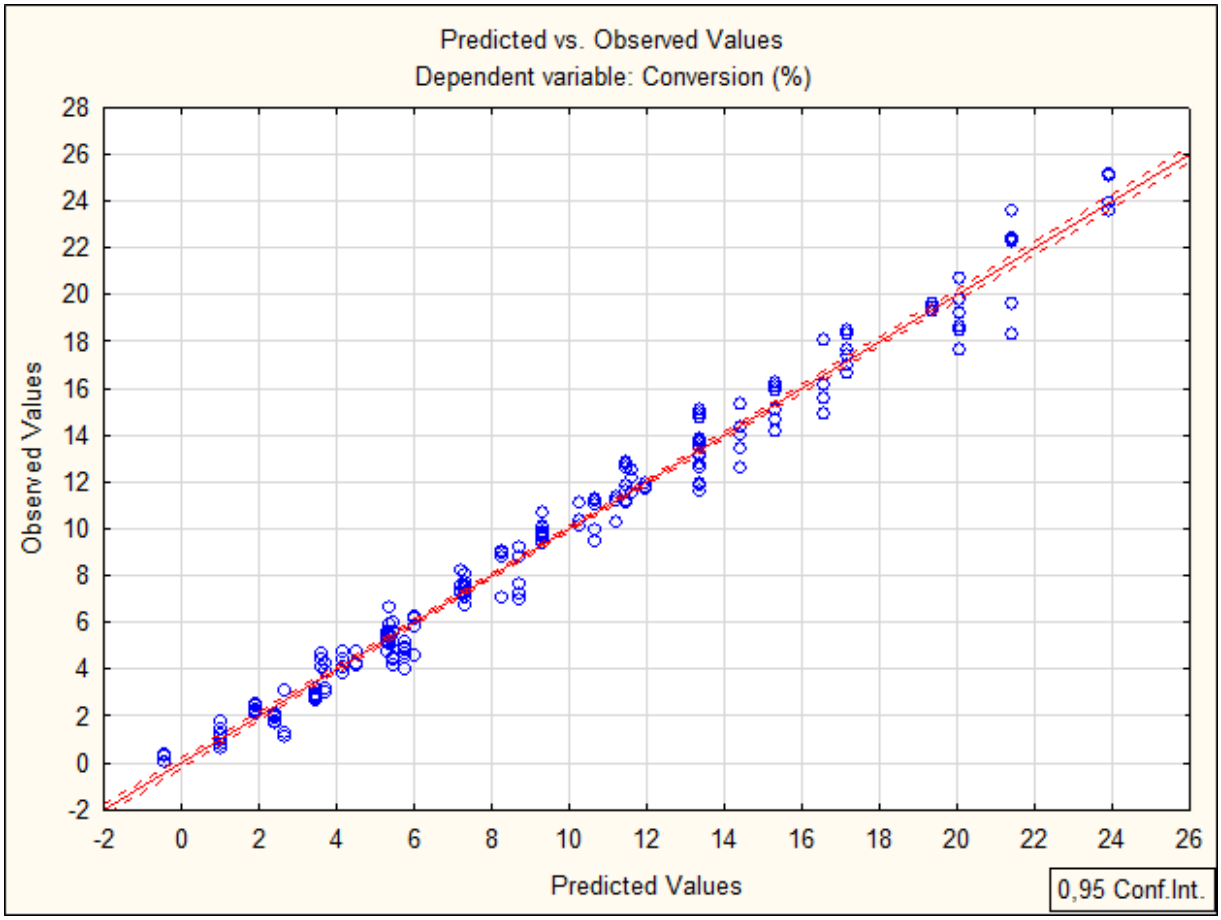

Figure 107: Predicted vs Observed values of the FTIR flow method.

Deviation from the diagonal line indicates the variation. However the variations appear constant in Figure 107. Most of the data sets also sliced the diagnol line therefore making the set statistically relevant.

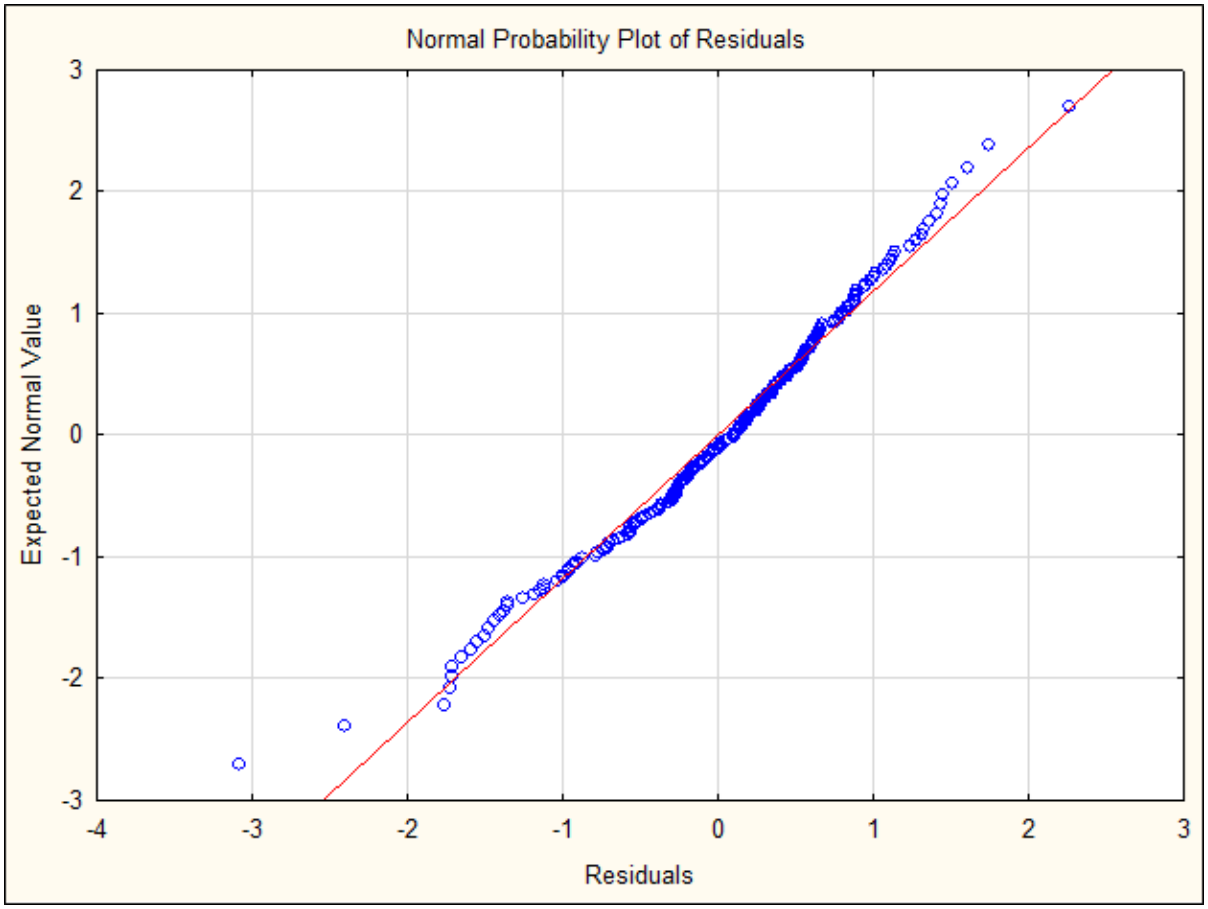

Figure 108:Normal Probability Plot of Residuals for the method.

Figure 108 is the normal probability plot of the residuals. At 0 on the residual axis the peak of the bell curve fits. Therefore the datapoint density would be the most dense there. As the points depart from the 0 residual value the density decreases.